Journal of Research

of the

National Bureau of Standards

U. OF MICHIGAN
NOV 10 1955
CHEMISTRY LIBRARY

OCTOBER 1955

VOLUME 55 NUMBER 4

U. S. DEPARTMENT OF COMMERCE
Sinclair Weeks, Secretary
NATIONAL BUREAU OF STANDARDS
A. V. Astin, Director

OCTOBER • 1955
VOLUME • 55
NUMBER • 4

JOURNAL OF RESEARCH

of the

NATIONAL BUREAU OF STANDARDS

PERIODICALS OF THE NATIONAL BUREAU OF STANDARDS

(Published monthly)

The National Bureau of Standards is engaged in fundamental and applied research in physics, chemistry, mathematics, and engineering. Projects are conducted in fifteen fields: electricity and electronics, optics and metrology, heat and power, atomic and radiation physics, chemistry, mechanics, organic and fibrous materials, metallurgy, mineral products, building technology, applied mathematics, data processing systems, cryogenic engineering, radio propagation, and radio standards. The Bureau has custody of the national standards of measurement and conducts research leading to the improvement of scientific and engineering standards and of techniques and methods of measurement. Testing methods and instruments are developed; physical constants and properties of materials are determined; and technical processes are investigated.

JOURNAL OF RESEARCH

The Journal presents research papers by authorities in the specialized fields of physics, mathematics, chemistry, and engineering. Complete details of the work are presented, including laboratory data, experimental procedures, and theoretical and mathematical analyses. Annual subscription: domestic, $4.00; $1.25 additional for foreign mailing.

TECHNICAL NEWS BULLETIN

Summaries of current research at the National Bureau of Standards are published each month in the Technical News Bulletin. The articles are brief, with emphasis on the results of research, chosen on the basis of their scientific or technologic importance. Lists of all Bureau publications during the preceding month are given, including Research Papers, Handbooks, Applied Mathematics Series, Building Materials and Structures Reports, Miscellaneous Publications, and Circulars. Each issue contains 12 or more two-column pages; illustrated. Annual subscription: domestic, $1.00; 35 cents additional for foreign mailing.

BASIC RADIO PROPAGATION PREDICTIONS

The Predictions provide the information necessary for calculating the best frequencies for communication between any two points in the world at any time during the given month. The data are important to all users of long-range radio communications and navigation, including broadcasting, airline, steamship, and wireless services, as well as to investigators of radio propagation and ionosphere. Each issue, covering a period of one month, is released three months in advance and contains 16 large pages, including pertinent charts, drawings, and tables. Annual subscription: domestic, $1.00; 25 cents additional for foreign mailing.

Order all publications from the Superintendent of Documents,
U. S. Government Printing Office, Washington 25, D. C.

The printing of this publication has been approved by the Director of the Bureau of the Budget, May 12, 1953.

Journal of Research of the National Bureau of Standards Vol. 55, No. 4, October 1955 Research Paper 2617

Infrared Absorption and Emission Spectra of Carbon Monoxide in the Region from 4 to 6 Microns[1]

Earle K. Plyler, Lamdin R. Blaine, and Eugene D. Tidwell

The infrared absorption and emission spectra of carbon monoxide and carbon dioxide have been measured with high resolution in the region from 4 to 6 microns. The measurements of the $C^{12}O^{16}$ fundamental band were carried out to a high precision, and a set of molecular constants were calculated from the experimental data. In emission the 1—0 and 2—1 bands of CO were measured in the P branch. Twenty lines of $C^{13}O^{16}$ were measured in absorption, and the molecular constants were calculated for this molecule. The fundamental band of CO_2 was found to have its center at 2,349.16, $B_0=0.39026 \pm 0.00005$, and $D_0=12.6 \pm 0.8\times10^{-8}$ cm^{-1}.

The complete emission spectra of CO and CO_2 from 4 to 6 microns are shown in two figures.

1. Introduction

The infrared absorption spectra of CO and CO_2 have been measured by many observers in the region from 4 to 6 μ [1].[2] The previous results showed the rotational properties of the bands, but the individual lines were not measured with sufficient precision for an accurate determination of the band's centers or the other molecular constants. The emission spectra of CO and CO_2 have also been the subject of a brief report [2], but a precise measurement of the rotational lines was not made.

The present work was carried out for the purpose of making a more precise determination of the wavelengths of the fundamental bands of these two molecules in emission and absorption, so that both sets of data could be used in the determination of the molecular constants. The improvement in the precision of the measurements was made possible primarily by the use of a Fabry-Perot interferometer for a comparison spectrum and by further calibration with standard atomic lines from enclosed arcs of xenon and krypton.

2. Experimental Method

An infrared grating spectrometer was used for the resolving instrument. Measurements were made with two gratings, one with 4,572 lines/in. and another one with 7,500 lines/in. Each grating had a surface with rulings about 5½ in. high and extended over 8 in. From 4 to 5.5 μ better resolution was obtained with the 7,500 lines/in. grating. In the absorption measurements lines separated by 0.2 cm^{-1} were resolved and in emission lines separated by 0.3 cm^{-1} were resolved. By the use of a synchronous motor and a precision gear drive, the grating is slowly turned so that the spectral region from 4 to 5.8 μ is scanned.

The details of the optical system and the arrangement of the interferometer, absorption cell and sources have been previously described [3]. A cooled PbTe photoconducting cell was used as the detector for the infrared radiation. A 1P28 photomultiplier was used as a detector of the visible fringe system produced by the Fabry-Perot interferometer. One amplifier is used with the photomultiplier, and a second one is used to amplify the signal changes of the PbTe cell. The output of the amplifiers are recorded on a two-pen recorder, and the recorded fringe system superimposed on the absorption spectrum throughout the band. In order to relate the fringe system is to definite wave numbers for measuring the absorption spectrum, higher orders of standard lines of xenon and krypton, which are detected by the PbTe cell, are superimposed on the chart.

By having the standard lines detected along the same optical path as the absorption spectrum, any errors that would be produced by a different optical path of the interferometer are avoided. By this method the fringe system is used for the determination of equal intervals of wavenumbers, and the absolute position of the band is determined by the standard lines.

In the measurements of this region the spacer of the interferometer was about 2 mm in thickness, and the separation of maxima of the visible fringe system, observed in the tenth order, was equal to 0.28 cm^{-1} in the 5 μ region.

3. Experimental Results

The observed spectra are shown in figures 1 through 4. In figure 1 is shown the 4.26 μ absorption band of CO_2 present in 6 m of laboratory air. On account of the low transmittance in the center of the band for about the first 15 lines in both the P and R branches, accurate measurement could not be made in that region. The 4.26 μ band of CO_2 is also overlapped by the two isotopic molecules, $C^{13}O_2^{16}$ and $C^{12}O^{16}O^{18}$. In addition a higher state, or hot band, of normal CO_2 should have appreciable intensity for this quantity of gas. With a vacuum instrument and measurements at reduced pressures of the CO_2 gas, it would be possible to resolve many rotational lines of the three molecules. The extra lines seen in the region from 2,290 to 2,330 cm^{-1} are

[1] This research was supported by the Office of Naval Research.
[2] Figures in brackets indicate the literature references at the end of this paper.

in most part due to the $C^{13}O_2^{16}$ molecule. The P branch of the band of $C^{13}O_2^{16}$ is not so strongly overlapped, and a number of the lines have been measured. In the use of the lines of CO_2 from 2,290 to 2,330 cm^{-1} for calibration, it is necessary to take into consideration the spectral slitwidth of the instrument employed, as the lines will change their position with varying resolution. In table 1 is given a list of the measured lines and the calculated and observed wavenumbers; the molecular constants calculated from these measurements are given in the last section of this report.

In figure 2 is shown the emission spectrum of CO_2. The spectrum in emission was observed from the flame of a glass blower's torch. A rich mixture of methane gas and oxygen was burned, as this type of flame gave good intensity for the emission bands of CO and CO_2. The two bandheads, 001–000 and 01^11–01^10, of the CO_2 emission spectrum are very prominent at the high frequency part of the spectrum. In between these two band heads are a number of the emission lines of the R branch of the CO_2 band. In the region beyond the two band heads there is overlapping of the emission spectrum of the flame and the absorption spectrum of atmospheric CO_2. The atmospheric absorption is so great that very few lines or other band heads are observed in the region from 2,310 to 2,375 cm^{-1}. The spectral lines, which are prominent in the region from 2,250 to 2,310 cm^{-1}, are produced by the absorption of $C^{12}O_2^{16}$ and $C^{13}O_2^{16}$. Twenty lines of the P branch of $C^{13}O_2^{16}$ were measured in absorption and are given in table 2. The band center, ν_0, was found to be 2,285.056 ± 0.014 cm^{-1}.

From 2,220 to 2,250 cm^{-1} several emission lines of the R branch of the 1–0 band of CO have been identified. They are overlapped by other lines and could not be measured to as high a precision as in absorption.

Figure 3 is a continuation to 1,940 cm^{-1} of the emission spectrum shown in figure 2. The rotational lines in this region primarily belong to the 1–0, 2–1, and 3–2 transitions of CO. Seventeen of the rotational lines of the 1–0 band of CO have been measured to a high precision and were included with the absorption data in calculating the molecular constants of CO. Twenty lines of the 2–1 band were also measured, and the observed and calculated values are listed in table 2, $\nu_0 = 2{,}116.80$ cm^{-1} for 2–1 transition. In the region from 1,860 to 2,050 cm^{-1}, some of the emission lines of the H_2O molecule appear in the spectrum.

TABLE 1. *Observed and calculated rotational lines of* $C^{12}O_2^{16}$ *and* $C^{13}O_2^{16}$

	$C^{12}O_2^{16}$				$C^{12}O_2^{16}$		
	Observed	Calculated	Deviation Obs−calc		Observed	Calculated	Deviation Obs−calc
	cm^{-1}	cm^{-1}	cm^{-1}		cm^{-1}	cm^{-1}	cm^{-1}
P 58	2293.762	2293.764	0.002−	P 48	2304.785	2304.774	0.011
56	2295.984	2296.014	.030−	46	2306.911	2306.904	.007
50	2302.645	2302.620	.025	2	2347.569	2347.593	.024−
R 30	2370.310	2370.274	.036	R 60	2384.958	2384.962	.004−
32	2371.431	2371.430	.001	62	2385.741	2385.738	.003
34	2372.602	2372.561	.041	64	2386.498	2386.489	.009
36	2373.662	2373.666	.004−	66	2387.211	2387.214	.003−
38	2374.741	2374.747	.006−	68	2387.923	2387.914	.009
40	2375.778	2375.802	.024−	70	2388.591	2388.588	.003
42	2376.823	2376.832	.009−	72	2389.273	2389.236	.037
44	2377.828	2377.837	.009−	74	2389.862	2389.859	.003
46	2378.810	2378.816	.006−	76	2390.444	2390.456	.012−
48	2379.751	2379.770	.019−	78	2391.049	2391.069	.020−
50	2380.691	2380.699	.008−	80	2391.556	2391.574	.018−
52	2381.600	2381.602	.002−	82	2392.105	2392.094	.011
54	2382.462	2382.480	.018−	86	2393.043	2393.057	.014−
56	2383.335	2383.333	.002	88	2393.503	2393.500	.003
58	2384.163	2384.160	.003	90	2393.905	2393.917	.012−

	$C^{13}O_2^{16}$				$C^{13}O_2^{16}$		
	Observed	Calculated	Deviation Obs−calc		Observed	Calculated	Deviation Obs−calc
	cm^{-1}	cm^{-1}	cm^{-1}		cm^{-1}	cm^{-1}	cm^{-1}
P 44	2245.610	2245.613	0.003−	P 24	2264.960	2264.969	0.009−
42	2247.660	2247.658	.002	22	2266.759	2266.771	.012−
40	2249.682	2249.678	.004	20	2268.547	2268.549	.002−
38	2251.671	2251.675	.004−	18	2270.313	2270.303	.010
32	2257.521	2257.518	.003	14	2273.744	2273.738	.006
30	2259.420	2259.417	.003	10	2277.076	2277.076	.000
28	2261.286	2261.282	.004	8	2278.708	2278.708	.000
26	2263.144	2263.143	.001	6	2280.314	2280.316	.002−

TABLE 2. *Observed and calculated rotational lines of* $C^{12}O^{16}$ (2–1), $C^{13}O^{16}$, $C^{12}O^{18}$

	$C^{12}O^{16}$(2–1)				$C^{12}O^{16}$(2–1)		
	Observed	Calculated	Deviation obs−calc		Observed	Calculated	Deviation obs−calc
	cm^{-1}	cm^{-1}	cm^{-1}		cm^{-1}	cm^{-1}	cm^{-1}
P 38	1948.66	1948.672	0.012−	P 22	2025.06	2025.069	0.009−
33	1973.40	1973.381	.019	21	2029.61	2029.582	.028
32	1978.24	1978.233	.007	17	2047.32	2047.312	.008
31	1983.05	1983.054	.004−	16	2051.65	2051.664	.014−
29	1992.63	1992.607	.023	15	2055.99	2055.984	.006
28	1997.34	1997.338	.002	10	2077.10	2077.093	.007
27	2002.02	2002.037	.017	9	2081.22	2081.216	.004
26	2006.71	2006.706	.004	8	2085.31	2085.305	.005
25	2011.32	2011.343	.023−	7	2089.36	2089.360	.000
23	2020.50	2020.525	.025−	5	2097.36	2097.370	.010−

	$C^{13}O^{16}$				$C^{13}O^{16}$		
	Observed	Calculated	Deviation obs−calc		Observed	Calculated	Deviation obs−calc
	cm^{-1}	cm^{-1}	cm^{-1}		cm^{-1}	cm^{-1}	cm^{-1}
P 13	2045.77	2045.788	0.018−	P 7	2069.63	2069.661	0.031−
12	2049.84	2049.845	.005−	4	2081.20	2081.173	.027
10	2057.88	2057.866	.014	3	2084.95	2084.946	.004
9	2061.85	2061.830	.020	2	2088.68	2088.687	.007−
8	2065.78	2065.761	.019	1	2092.40	2092.395	.005
R 0	2099.69	2099.714	.024−	R 10	2134.33	2134.320	.010
3	2110.43	2110.447	.017−	11	2137.60	2137.594	.006
4	2113.94	2113.958	.018−	13	2144.05	2144.040	.010
5	2117.43	2117.436	.006−	17	2156.51	2156.516	.006−
7	2124.31	2124.291	.019	18	2159.54	2159.547	.007−

	$C^{12}O^{18}$				$C^{12}O^{18}$		
	Observed	Calculated	Deviation obs−calc		Observed	Calculated	Deviation obs−calc
	cm^{-1}	cm^{-1}	cm^{-1}		cm^{-1}	cm^{-1}	cm^{-1}
R 4	2109.94	2109.940	0.000	R 11	2133.52	2133.536	0.016−
5	2113.44	2113.437	.003	12	2136.76	2136.739	.021
6	2116.84	2116.847	.007−	14	2143.11	2143.118	.008−
10	2130.27	2130.263	.007				

In figure 4 is shown the absorption spectrum of carbon monoxide. Some of the lines arising from the two isotopic molecules can be seen between the stronger lines of $C^{12}O^{16}$. Several lines of water vapor are superimposed on the spectrum in the region from 2,010 to 2,050 cm^{-1}. Because of the low intensity of the isotopic bands, many of the lines of $C^{12}O^{16}$ were not appreciably distorted and could be measured with high precision. A total of 10 sets of observations were used in obtaining the values of the wavenumbers of the lines. Great emphasis was placed on making precise measurements of the CO absorption spectrum, so that molecular constants of high precision could be obtained. Many lines of the bands, arising from $C^{13}O^{16}$ and $C^{12}O^{18}$ are present in the spectrum. Some of these have been measured, and the values are given in table 2. The wavenumbers of the calculated and observed values for the rotational lines of the 1–0 band of $C^{12}O^{16}$ are not given in this report, as they have previously been published [3].

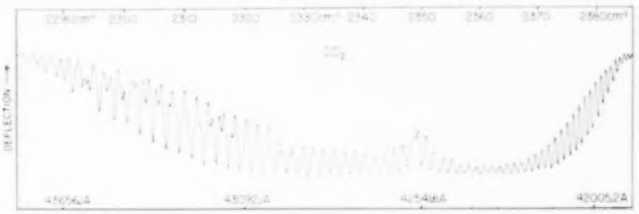

FIGURE 1. *The fundamental band of* CO_2 *at 4.26 μ.*
The absorption spectrum was measured in an air path of 6 m.

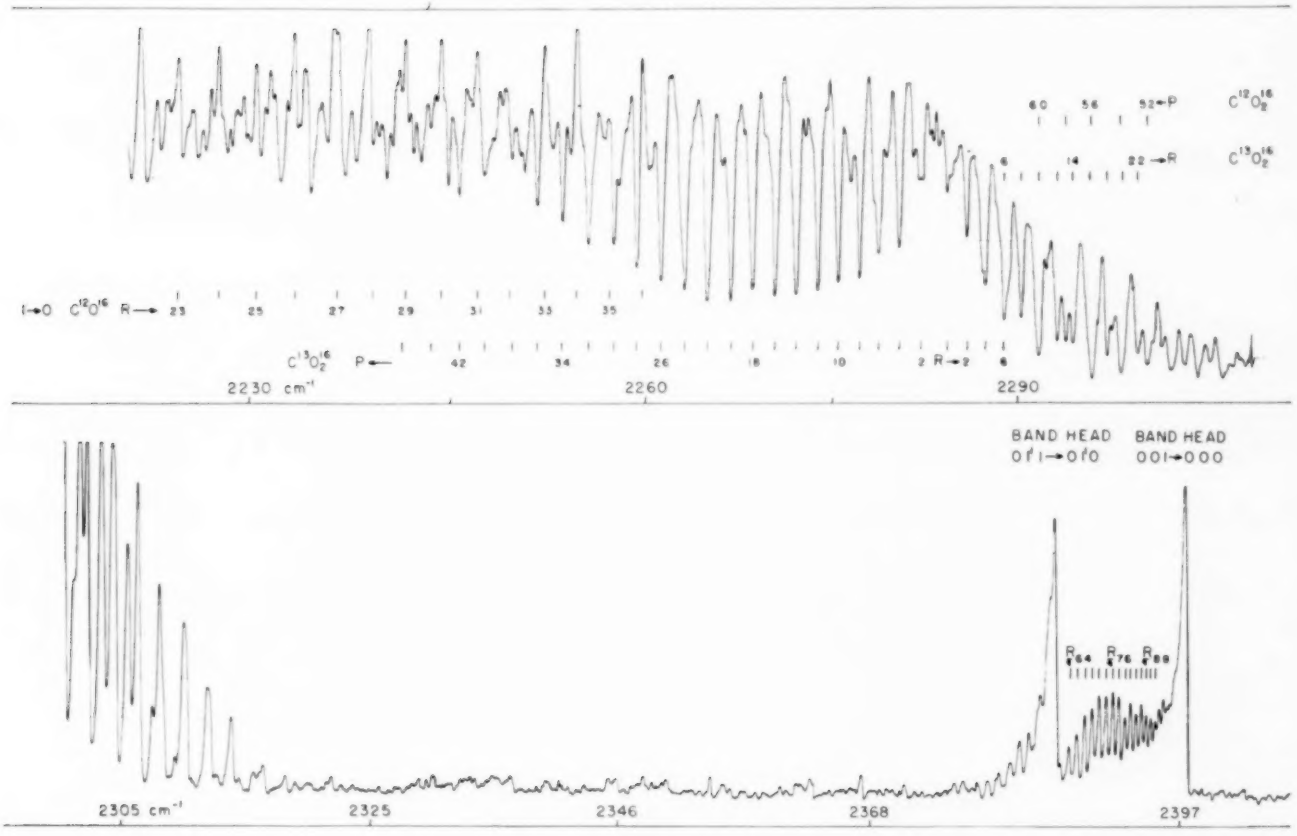

FIGURE 2. *The infrared emission spectrum of* CO_2 *from a rich methane-oxygen flame.*
From 2,250 to 2,280 cm^{-1}, the atmospheric absorption of $C^{13}O_2^{16}$ gives rise to an intense group of lines.

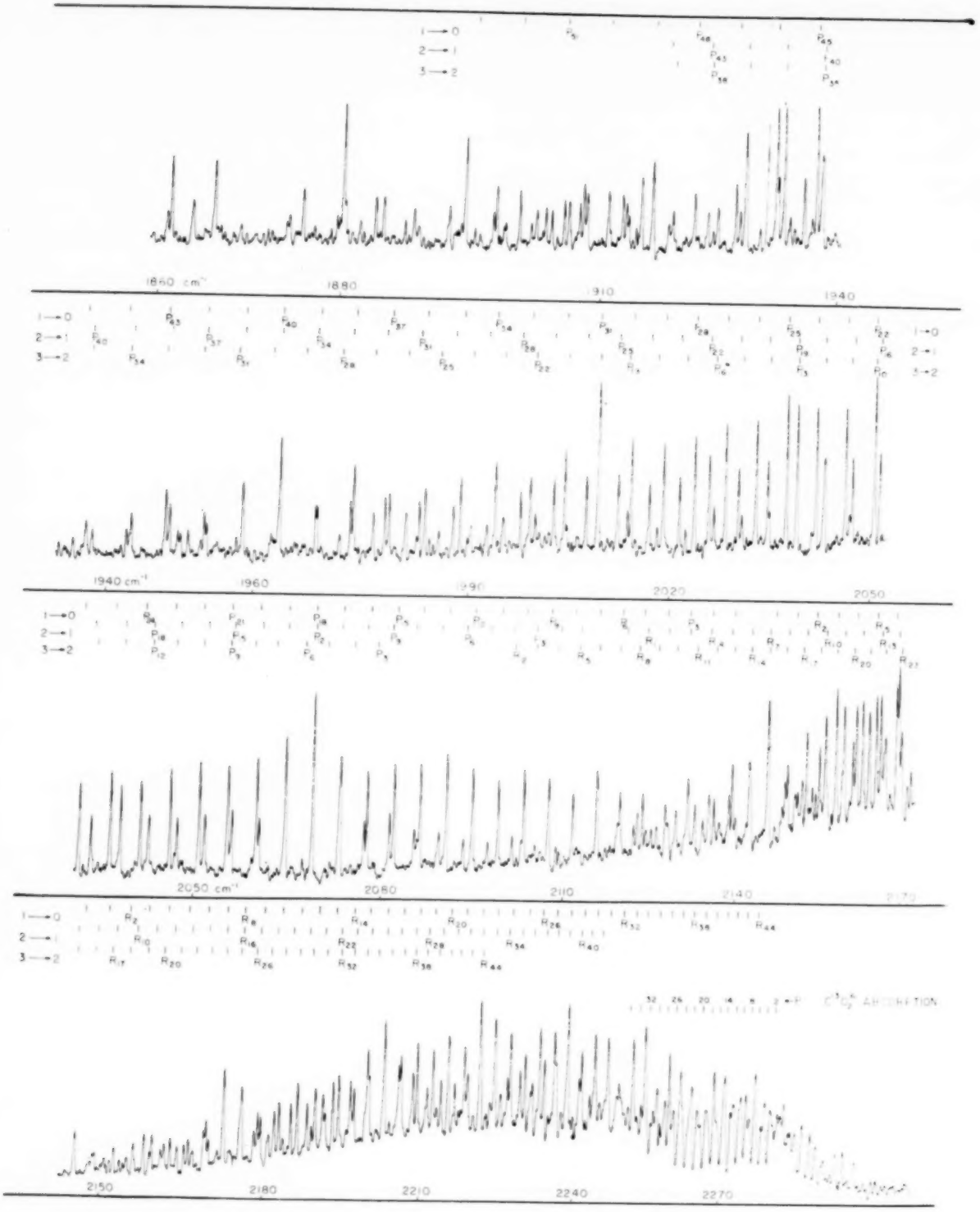

FIGURE 3. *The emission spectrum of* CO *from 1,860 to 2,170 cm⁻¹.*
Many of the lines are identified as belonging to the 3—2, 2—1, and 1—0 transitions.

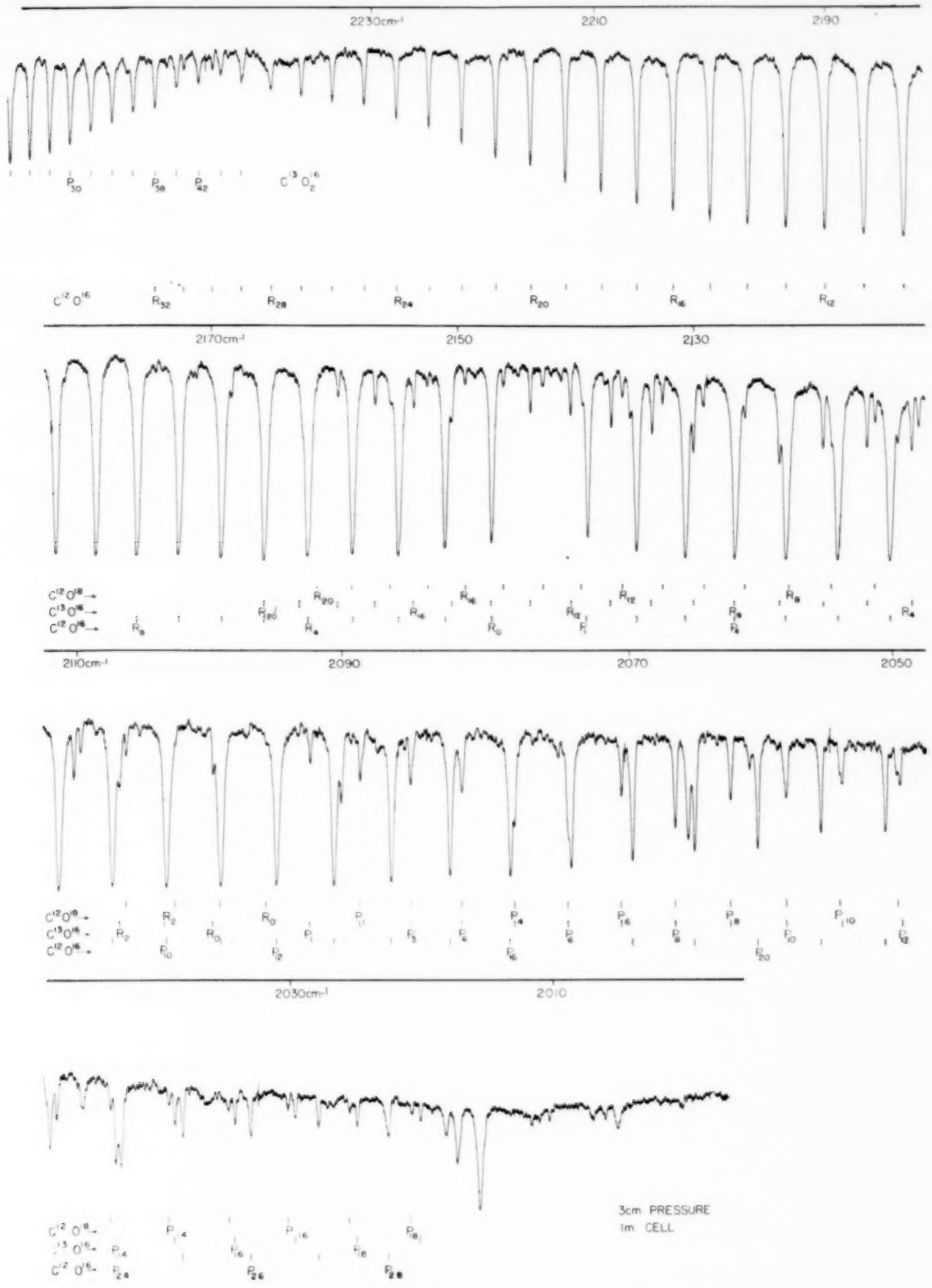

FIGURE 4. *The absorption spectrum of* CO *in the region from 4.5 to 5 μ.*
Lines arising from $C^{12}O^{16}$, $C^{13}O^{16}$, and $C^{12}O^{18}$ can be seen in this region. A cell of 1-m length was used, and the gas pressure was 3 cm of Hg.

4. Discussion of Results

From the measurements of the bands, which are shown in the figures, molecular constants have been obtained for the carbon monoxide and carbon dioxide molecules. Due to the overlapping of many lines in the emission spectrum, precise measurement could not be made of a sufficient number of the rotational lines in the R branches of the 2–1, 3–2, and 4–3 transitions of the CO bands to obtain the molecular constants for these states to a high precision.

From the measurements of the fundamental band, it has been possible to calculate the molecular constants of $C^{12}O^{16}$ to a high precision. The first important attempt to determine the constants of CO precisely was by Rao [4]. In 1952 Plyler, Benedict, and Silverman [5] made a study of the first overtone bands of CO in emission and absorption and obtained a set of constants which were not in accord with the results of Rao. These constants were obtained from measurements of the first overtone bands (2–0, 3–1, 4–2, and 5–3) of CO and were of good precision. The present work, however, shows that the values for ω_e, $\omega_e x_e$, and $\omega_e y_e$ were all slightly in error. The error was caused by the inaccuracy of the ν_0 for 3–0 band of CO. The band center was found to be 6,350.47 ± 0.05 cm^{-1}, but the present measurements show this band center should be 6,350.42 cm^{-1} which is at the limit of our estimated precision. This error of 0.05 cm^{-1} was large enough to create a perceptible difference in our molecular constants. More recently Goldberg and Müller [6] have made a study of the CO spectrum from the sun. Because of the high temperature of the sun, they were able to observe 6 bands in the first overtone region which had their origin in transitions from the higher energy levels. In addition, the high temperatures made it possible to observe lines with large J values in both the R and P branches. The lines of large J values are very important in the determination of those molecular constants which depend on cubic or quartic powers of the rotational quantum number. A comparison of their values and those obtained in the present work will be discussed later.

In the measurement of the lines in the fundamental band of $C^{12}O^{16}$, a Fabry-Perot interferometer was used in determining the wavenumbers of 43 lines which were measured in the absorption spectrum extending from R_{23} to P_{28}. Fifteen lines between P_{32} and P_{52} were measured in emission. By least squares the lines were fitted to the equation

$$\nu=\nu_0+(B_1+B_0)m+(B_1-B_0-D_1+D_0)m^2 -2(D_1+D_0)m^3-(D_1-D_0)m^4 \quad (1)$$

where B_0 is proportional to the reciprocal of the moment of inertia in the ground state, and D_0 is proportional to the centrifugal distortion. B_1 and D_1 are the same type of constants for the excited state. The constants obtained are as follows

$$\nu_0=2143.274 \pm 0.003 \text{ cm}^{-1},$$
$$B_1=1.904994 \pm 0.000036 \text{ cm}^{-1},$$
$$B_0=1.922523 \pm 0.000037 \text{ cm}^{-1},$$
$$D_0=6.26 \pm 0.025\times 10^{-6} \text{ cm}^{-1}, \text{ and}$$
$$D_1-D_0=-2.99\times 10^{-9} \text{ cm}^{-1}.$$

The values obtained for B_0 and D_0 are in excellent agreement with the same constants determined by microwave measurements [7] if the velocity of light is, $c=299{,}792$ km/sec. From the measurements on the fundamental band and the previous measurements of the first overtone, a new set of constants have been determined on the basis of the present work. These constants and those obtained by Müller and Goldberg are listed in table 3. In the calculation of ω_e, $\omega_e x_e$, and $\omega_e y_e$ the 7–5 and 6–4 harmonics, measured by Goldberg and Müller, have been used in addition to the 1–0, 2–0, 4–2, and 5–3 transitions measured in this laboratory. A comparison of the constants of Goldberg and Müller with those obtained in this work, shows that there is excellent agreement. The value of B_e obtained by Goldberg and Müller is 1×10^{-4} larger than the value calculated from our results. The small differences in γ_e and β_e are unimportant. Only under the best circumstances can these constants be determined with any degree of accuracy. Often the data are not sufficiently accurate to obtain the correct sign for these constants. On account of the use of a large range of quantum numbers of rotation and of vibration, the values of Goldberg and Müller for γ_e and β_e should be more accurate than the ones obtained from the present measurements, and they are in better agreement with the theoretical values.

McCulloh and Glockler [8] have measured the emission bands of $C^{13}O^{16}$ in the region from 1900 to 6500 A and from these results have calculated the ω_e, $\omega_e x_e$, and $\omega_e y_e$ for $C^{13}O^{16}$ and $C^{12}O^{16}$. Their values for $C^{12}O^{16}$ are $\omega_e=2{,}169.84$ cm^{-1}, $\omega_e x_e=13.301$ cm^{-1}, and $\omega_e y_e=0.0123$ cm^{-1}. These values are in good agreement with those listed in table 3, but they are slightly larger than the same constants calculated from the infrared bands.

In addition to the fundamental band of $C^{12}O^{16}$ at 4.67 μ, there are two weak bands which overlap it produced by $C^{13}O^{16}$ and $C^{12}O^{18}$. The rotational lines of these bands are in some cases superimposed on the lines of $C^{12}O^{16}$. Mills and Thompson [9] have made

TABLE 3. *Molecular constants, derived for carbon monoxide* ($C^{12}O^{16}$)

Constants	Goldberg and Müller	Present work
	cm^{-1}	cm^{-1}
ω_e	2169.83	2169.830 $\pm$0.004
$\omega_e x_e$	13.297	13.297 $\pm$0.017
$\omega_e y_e$	0.0115	0.01150 $\pm$0.00014
B_e	1.93141	1.93130 $\pm$0.00005
α_e	0.017520	0.017520
γ_e	2.96×10^{-4}	4.5×10^{-4}
D_e	6.18×10^{-6}	6.26×10^{-6}
β_e	-1.76×10^{-9}	-2.99×10^{-9}

a measurement of 33 lines of the $C^{13}O^{16}$ isotopic band. They used the calculated position of the fundamental band of $C^{12}O^{16}$ for calibration. The fundamental band was calculated by them from the measurements in this laboratory of the first overtone band. The agreement of the measurements of Mills and Thompson, compared with measurements on 20 lines in this laboratory, are excellent. It indicates that with proper calibration high precision measurements can be made on infrared bands.

The constants obtained from the two sets of data are in good agreement and are shown in table 4. Seven lines of the R branch of the fundamental band of $C^{12}O^{18}$ were found to be in close agreement with the values obtained by Mills and Thompson for this band. These lines are listed in table 2.

On account of the intense absorption of the CO_2 in the 6-m path, the lines near the center of the 001–000 band could not be measured. A total of 36

TABLE 4. *Molecular constants* $C^{13}O^{16}$

Constants	Mills and Thompson	Present work
	cm^{-1}	cm^{-1}
B_1	1.8218	1.8216
B_0	1.8382	1.8380
γ	0.01645	0.01633
D	5.4×10^{-6}	5.8×10^{-6}
ω_e	2141.41	2141.41
$\omega_e x_e$	12.67	12.67
ν_0	2096.07	2096.071

lines, however, were measured, and the constants were calculated by least squares using a cubic degree equation.

The agreement between the observed and calculated wavenumbers for the lines is shown in table 1. The position of any line can be obtained from the equation

$$\nu = 2{,}349.16 + 0.77743\ m - 0.0030926\ m^2 - 0.000000504\ m^3 \qquad (2)$$

where $m = J+1$ for the R branch and $m = -J$ for the P branch.

$$\nu_0 = 2{,}349.16 \pm 0.01\ \text{cm}^{-1}$$

$$B_0 = 0.39026 \pm 0.00005$$

$$D_0 = 12.6 \pm 0.8\times10^{-8}$$

B_0 was previously calculated from $3\nu_3$, and a value of 0.3902 cm^{-1} was found from that band. This is in good agreement with the present results [10]. These measurements are not as precise as those made on CO. The lines were broadened by the atmospheric pressure, and in many cases the absorption was too large, making it impossible to obtain the center of the line with precision.

Sixteen lines in the P branch of $C^{13}O_2^{16}$ have been measured. These lines are listed in table 1. The value of ν_0 was found to be 2,285.056 cm^{-1}. The estimated standard deviation of the lines from the calculated values is 0.006 cm^{-1}. The other molecular constants were not determined.

Because of overlapping it was not felt that sufficient lines of the 3–2 transition of CO could be measured with good accuracy so that reliable molecular constants could be obtained. This band can be obtained with greater precision by calculation from the other levels.

The authors express their appreciation to Joseph M. Cameron of the Statistical Engineering Section of this Bureau for assistance in making the least squares computations on the electronic computer, SEAC.

5. References

[1] G. Herzberg, Molecular spectra and molecular structure I diatomic molecules; II polyatomic molecules (D. Van Nostrand Co., Inc., New York, N. Y.).
[2] Earle K. Plyler and Joseph J. Ball, J. Chem. Phys. **20,** 1178 (1952).
[3] Plyler, Blaine, and Connor, J. Opt. Soc. Am. **45,** 102 (1955).
[4] K. N. Rao, J. Chem. Phys. **18,** 213 (1950).
[5] Plyler, Benedict, and Silverman, J. Chem. Phys. **20,** 175 (1952).
[6] Leo Goldberg and Edith A. Müller, Astrophys. J. **118,** 397 (1953).
[7] Gilliam, Johnson, and Gordy, Phys. Rev. **78,** 140 (1950). Bedard, Gallaghen, and Johnson, Phys. Rev. **92,** 1440 (1953).
[8] K. E. McCulloh and G. Glockler, Phys. Rev. **89,** 145 (1953).
[9] I. M. Mills and H. W. Thompson, Trans. Far. Soc. **49,** 224 (1953).
[10] Norman M. Gailar and Earle K. Plyler, J. Research NBS, **48,** 392 (1952) RP2327.

WASHINGTON, April 22, 1955

Journal of Research of the National Bureau of Standards Vol. 55, No. 4, October 1955 Research Paper 2618

Specific Heats of Collagen and Leather

Joseph R. Kanagy

Determinations of the specific heats of collagen, vegetable-tanned leather, chrome-retanned leather, chrome leather, and these materials containing varying percentages of moisture were made at 25° C. The same determinations were also made on dry chestnut and quebracho tanning extracts and on a stuffing grease and an animal oil. The results obtained with the collagen and leather containing various percentages of moisture show abrupt breaks in the curves, which indicate phase changes. These changes are explained on the basis of changes in the vibrational activity of the polar groups in the collagen molecule.

Lubricating materials, added to leather, increase the specific heat. This affects the comfort of the leather adversely during cold weather.

1. Introduction

In connection with the heats of wetting of collagen and leather [1],[1] interest arose with regard to the specific heats of these materials. For highly accurate calorimetric measurements, a knowledge of the specific heats of all components is necessary.

Although specific heat is a fundamental physical property, little information with regard to its values for leather or collagen is available in the literature. An examination of the literature located only one study of the specific heat of leather. A. Cheshire and N. L. Holmes [2] give a value of 0.263 cal/g for dry leather and 0.321 cal/g for leather containing 16.28-percent of water. The Handbook of Chemistry and Physics [3] gives a value of 0.36 cal/g/deg C for the specific heat of dry leather.

An important study related to leather was made by Hampton and Mennie [4]. They determined the specific heats of gelatin gels over a temperature range of 25° C to −180° C, in an effort to obtain some information on bound water. They found that the specific heats of water and dry gel were not additive, and their studies yielded no reliable information on the percentage of so-called bound water in these materials.

Specific heat is an important factor in determining the comfort of wearing materials. Although not as important as the rate of conduction of heat, the amount of heat required to maintain temperature equilibrium will depend upon the heat capacity of the materials worn. This is especially noticeable in cold weather when shoes are changed.

A study of the property of specific heat is most important in the elucidation of some of the fundamental properties of a material. A determmation of the specific heat of leather containing varying amounts of moisture may yield information with regard to the manner in which the two components combine. The comparison of the specific heat of collagen with that of leather may yield similar information with regard to the tanning agent and collagen.

In the present study, the specific heats of collagen and three different tannages of leather were determined at 25° C. Determinations of specific heats were made on the dry material and on the materials containing various percentages of water ranging from 0 to 17 percent. Specific heats were also determined for two types of tanning agents and for oils and greases used to lubricate leather.

2. Apparatus and Procedure

The calorimeter used in this work was the same as the one used in a study of the heats of wetting of collagen and leather [1]. This calorimeter was originally developed by Newman and Wells [5] to study the heats of hydration of cements.

An attempt was made, in the initial experiments, to make the determinations by suspending the materials in carbon tetrachloride. Carbon tetrachloride was used as the suspending liquid and heat transfer medium because it has a low specific heat (approximately 0.2 cal/g/deg C) and because it is a nonpolar liquid, which should not react with leather or collagen. A liquid of low specific heat was desired, so that the accuracy of the measurement would be improved by having a greater percentage of the total heat absorbed by the sample under test.

However, the determination of specific heats by suspending the specimens directly in the liquid medium used for thermal transmission was found to be unsatisfactory. The apparent specific heats obtained in this way were quite variable and sometimes negative, which is impossible. The medium apparently reacted with the materials to take up energy, or a slow solution process occurred.

In order to obtain reliable data, it was necessary to place the test specimens in a container where no direct contact was made with the heat-conducting medium. The specimens were placed in small copper tubes 11 cm in length and 1 cm in diameter. About 2.5 g of sample was contained by each tube. A series of ten tubes was used for a determination on each sample, making a total specimen size of about 25 g. The ten tubes were wired together to form a raft, and then submerged in the heat-conducting

[1] Figures in brackets indicate the literature references at the end of this paper.

356420—55——2

medium of carbon tetrachloride. This procedure proved to be very satisfactory. The small diameter of the tubes, and the intimate contact will all the tubes by the medium, gave rapid thermal equilibrium.

Determinations were made at 25° C on each sample at various concentrations of moisture. The copper tubes were filled with the leathers or collagen conditioned at 50-percent relative humidity and 73° F. After the specific heat was determined on each specimen, the caps on the tubes were removed, the tubes and contents were placed in a desiccator, and part of the moisture was removed by means of a vacuum pump. After pumping for several hours, the tubes were removed from the desiccator, the caps were replaced, the tubes and contents were weighed, and the specific heat was determined. This procedure was continued until there was no further loss in weight on evacuation. Six to eight determinations on each specimen with varying amounts of moisture were made in this way. Finally the specimen was completely dried by heating in an oven at 100° C for 24 hr and a specific heat determination made.

Determinations in the calorimeter were made in pairs. The runs were started slightly below 25° C. After thermal equilibrium was reached, heat was added by passing a measured current from a battery through a coil having a known resistance. The temperature rise in a definite time was determined, and when thermal equilibrium was again reached, the procedure was repeated. This gave two determinations of the heat capacity of the system for each run, one slightly below 25° C, the other slightly above 25° C. If the two determinations did not check within 0.5 percent, the run was repeated. The average of the two determinations was used to calculate the specific heat.

The average deviation from the mean of a single determination of specific heat was about 3 percent. This is equivalent to a standard deviation of ± 0.01 in the specific heat.

3. Results

The results of determinations of specific heats of collagen, chrome-retanned leather, vegetable-tanned leather, and chrome-tanned leather are given in table 1. These results include measurements made on the materials containing varying percentages of moisture, and also determinations on the materials dried by heating for 24 hr. at 100° C. Chemical analyses of the collagen and leathers are given in table 2.

In order to obtain some information on the specific heats of materials used in leathermaking, determinations were made on chestnut and quebracho tanning extracts. These materials were dried at 100° C for 24 hr before the determinations were made. Measurements were also made of the specific heats of stuffing grease and of animal oil (neat's foot). The stuffing grease was obtained by extracting it from a sample of chrome-retanned upper leather. The values obtained for the specific heats of the tanning materials and the lubricating materials are given in table 3.

TABLE 1. *Specific heats of collagen and leather samples at 25° C*

Collagen		Chrome-retanned leather		Vegetable-tanned leather		Chrome-tanned leather	
Moisture content	Specific heat	Moisture content	Specific heat	Moisture content	Specific heat	Moisture content	Specific heat
%	cal/g/deg C	%	cal/g/deg C	%	cal/g/deg C	%	cal/g/deg C
0	0.3723	0	0.3404	0	0.3334	0	0.3045
1.02	.3490	1.52	.3287	1.15	.3202	1.98	.2918
1.96	.3659	2.12	.3266	1.32	.3274	3.69	.3631
4.56	.4014	4.23	.3448	2.59	.3280	7.59	.3576
6.49	.4061	7.23	.3458	3.85	.3844	9.39	.3737
17.03	.4280	9.23	.3474	6.20	.3730	11.07	.3893
.....	.....	11.29	.3606	7.83	.3835	13.46	.3841
.....	.....	.....	.....	9.31	.3844	14.96	.4098
.....	.....	.....	.....	10.81	.4129	.....	.....

TABLE 2. *Chemical analysis of the leathers (moisture- and grease-free bases)*

Leathers	Hide substance	Ash	Cr_2O_3	Vegetable tannin by difference
	%	%	%	%
Collagen	100.7	.....	.....	.....
Vegetable-tanned leather	52.06	0.24	.....	47.70
Chrome-retanned leather	59.87	2.20	1.80	[a]34.82
Chrome-tanned leather	88.85	....	4.25	.....

[a] Calculated by using the conversion factor 2.73 to convert Cr_2O_3 to the basic chromium sulfate tanning agent and the value for the difference between percentage ash and percentage Cr_2O_3 [12].

TABLE 3. *Specific heats of leathermaking materials at 25° C*

Material	Specific heat
	cal/g/deg C
Chestnut tannin extract (powder) dry	0.2889
Quebracho tannin extract (solid) dry	.3152
Stuffing mixture (extracted from upper leather)	.5162
Animal oil	.5191

4. Discussion

The variation of the specific heat with moisture content for collagen, chrome-retanned leather, vegetable-tanned leather, and chrome-tanned leather is shown in figure 1. As the moisture content of the sample increases from 0 to 1 or 2 percent, the specific heat passes through a minimum. This behavior occurs with all of the samples. After the minimum, there is a sharp increase in the specific heat as the moisture content increases. After the sharp rise, the curves reach a plateau where the specific heat is nearly constant until the moisture content reaches about 9 percent. Beyond this point, the specific heat increases further with increase in moisture content. The plateau region occurs for each of the three leathers. For collagen, the number of determinations in this area was insufficient to establish the exact shape of the curve.

Breaks in the curves showing the increase in a physical property with moisture content are not unexpected. However, studies on moisture adsorption [6], heats of wetting [1], and dielectric constants

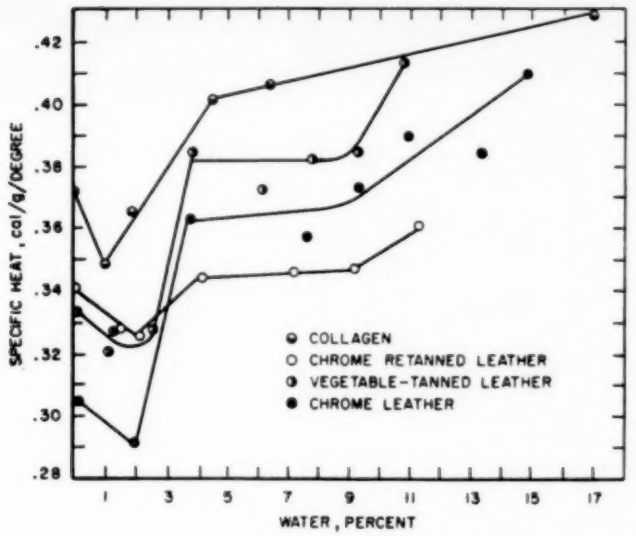

FIGURE 1. *Variation of the specific heat with the percentage of water in the materials.*

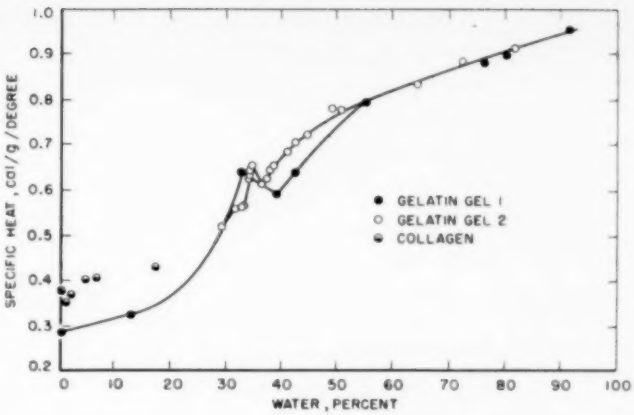

FIGURE 2. *Variation of the specific heats of collagen and of gelatin with the percentage of water in the samples.*

Data for gelatin from Hampton and Mennie.

[7, 8] have failed to reveal any abrupt changes with increase in moisture content. The sorption of moisture by a protein is undoubtedly similar to the formation of hydrates in inorganic compounds. The sorption of moisture over a wide range of relative humidities would be expected to form a series of hydrates. This series of hydrates should correspond to different compounds having different properties. From studies of the moisture relations of leather and other proteins by the above-mentioned procedures, it has been found that the energy of combination of moisture decreases as the amount of moisture is increased. The rate of decrease has, however, in all instances been characterized by a smooth curve indicating that the precision of the measurements was not great enough to detect a discontinuity which would be characteristic of a change in phase.

Studies of the heats of wetting [1] show that the greatest amount of heat is evolved in the adsorption of the initial amounts of water by the dry materials. The adsorption of this amount of moisture apparently lowers the activity of some of the atoms, decreasing the magnitude of their vibrations, so that they absorb less energy. This would produce a minimum in the specific heat. The addition of moisture, beyond about 2 percent, apparently forms additional vibrational sites, for an abrupt increase in the specific heat occurs.

It has been suggested [9] that the first water molecules adsorbed by a protein are taken up between two polar groups. This would definitely lower the activity of the two groups, and might correspond to the minimum for specific heat at about 2-percent moisture adsorption. In further addition of moisture, it was assumed that each group would adsorb a molecule of water. The abrupt rise in specific heat would then correspond to the point where the bridge between atoms formed by one molecule of water was broken, and the vibrational freedom of the atoms, was again increased. The plateau region in the curve from 3 to 9 percent may correspond to the adsorption of one molecule of water per polar group in the protein molecule, to complete a monomolecular layer. Pauling [9] gives data to show that approximately 9 percent of water is required for a monomolecular layer in collagen. Beyond 9 percent of moisture, the polar groups may be saturated with one water molecule per group, and possibly a second layer, with two molecules per polar group, is begun. This corresponds to the addition of more energy-adsorbing vibrational sites, and the specific heat shows a further increase.

Hampton and Mennie [4] determined the specific heats of gelatin gels containing varying percentages of water at temperatures ranging from 25° C to −180° C. Their mean results over the temperature range 0° to 25° C are shown in figure 2, together with the results obtained in the present study for collagen. The specific heat of dry collagen is higher than that of dry gelatin. When collagen is hydrolyzed to form gelatin by heating in water, a shrinkage reaction occurs with rearrangement and internal compensation of active polar groups. It is, therefore, expected that gelatin would have a more inactive structure, with fewer free polar groups to absorb vibrational energy, than collagen. For this reason the specific heat of collagen would be expected to be higher.

The results on gels by Hampton and Mennie, as shown in the curve in figure 2, show a break, which indicates a phase change at a moisture content of approximately 32 percent. There are not sufficient determinations with the gels at low concentrations to indicate whether there are any discontinuations in the curve at exactly the same points where they occur with collagen and leather. The gel-water system also does not exactly parallel the collagen or leather-water system. The former system borders on solution, whereas the latter represents a system of a solid and a vapor at low concentration.

Many attempts have been made, in studies of protein-moisture systems, to derive conclusions with

regard to the amounts and properties of the so-called bound and unbound water present. This is sometimes done by subtracting the calculated value for a physical property, based on that for the dry material, from the total value for the constant when water is present, with the assumption that the difference can be attributed entirely to the water content. By the application of this procedure to the results obtained for the specific heats of collagen and leather in this study, the values shown in table 4 were obtained.

These calculated results obviously have no significance, except to show that the specific heats of the dry leather and the water present are not additive to give the specific heat of the conditioned material. A negative apparent specific heat is obtained for water when the concentration in the collagen or leather is low. At higher concentrations, the apparent specific heat of water is positive, but varies with the type of leather. The actual specific heat of water at 25° C is 0.998 cals/g/deg C.

Determinations of bound and unbound water in a protein-water system are questionable. The so-called protein-water system is probably a hydrate that behaves as a compound, differing in properties from that of either the dry protein or the pure water. As the percentage of water increases, the properties of the compound change; the activity of the water increases, but it remains restricted in mobility, as would be expected in multilayer formation. The fact that water is adsorbed by a material is sufficient basis to conclude that its mobility has been restricted. There is apparently no sharp boundary line between bound and unbound water.

Specific heats of the dry leathers are lower than that of dry collagen. In table 3, values for the specific heat of chestnut and quebracho extracts are given. The specific heat of vegetable-tanned leather is approximately midway between that of the vegetable extracts and collagen. As shown in table 2, percentage of tannin in vegetable-tanned leather is approximately 50 percent. It therefore appears that the influence of the tannin on the specific heat of the leather is additive. Chrome leather has a lower specific heat than that of the other leathers. The Handbook of Chemistry and Physics [3] gives a value of 0.200 cal/g/deg as the specific heat of $Cr_2(SO_4)_35H_2O$. There is, however, not sufficient chromium sulfate in chrome leather to reduce the

TABLE 4. *Calculation of apparent specific heat of water at 25° C in leather assuming that specific heat of leather is same as for dry material*

No.	Material (conditioned)	Material (dry)	Water	Heat absorbed by dry material	Specific heat	Heat absorbed by conditioned material	Heat absorbed by water	Apparent specific heat of water
				Collagen				
	g	*g*	*g*	*cal/deg* C	*cal/g/deg* C	*cal/deg* C	*cal/deg* C	*cal/g/deg* C
1	27.6561	23.6313	4.0248	8.7979	0.3723	11.8368	3.0389	0.7550
2	25.1661	23.6313	1.5348	8.7979	.3723	10.2199	1.4220	.9265
3	24.7080	23.6313	1.0767	8.7979	.3723	9.9178	1.1199	1.0401
4	24.0947	23.6313	0.4634	8.7979	.3723	8.8163	0.0184	0.0397
5	23.8733	23.6313	.2420	8.7979	.3723	8.3318	−.4661	−1.9260
6	23.6313	23.6313	0	8.7979	.3723	8.7979	0	0
				Chrome-retanned leather				
1	25.7699	23.1547	2.6152	7.8819	0.3404	9.2926	1.4107	0.5394
2	25.2911	23.1547	2.1364	7.8819	.3404	8.7861	0.9042	.4232
3	24.8295	23.1547	1.6748	7.8819	.3404	8.5860	.7041	.4204
4	24.1352	23.1547	0.9805	7.8819	.3404	8.3218	.4399	.4486
5	23.6451	23.1547	.4904	7.8819	.3404	7.7215	−.1604	−.3271
6	23.5058	23.1547	.3511	7.8819	.3404	7.7264	−.1555	−.4429
7	23.1547	23.1547	0	7.8819	.3404	7.8819	0	0
				Vegetable-tanned leather				
1	26.9572	24.3265	2.6307	8.1103	0.3334	11.1302	3.0199	1.1479
2	26.5916	24.3265	2.2651	8.1103	.3334	10.2212	2.1109	0.9319
3	26.2307	24.3265	1.9042	8.1103	.3334	10.0596	1.9493	1.0237
4	25.8336	24.3265	1.5071	8.1103	.3334	9.6354	1.5251	1.0119
5	25.2632	24.3265	0.9367	8.1103	.3334	9.7112	1.6009	1.7091
6	24.8566	24.3265	.6301	8.1103	.3334	8.1861	0.0758	.1203
7	24.6467	24.3265	.3202	8.1103	.3334	8.0699	−.0404	−.1262
8	24.6065	24.3265	.2800	8.1103	.3334	7.8780	−.2323	−.2986
9	24.3265	24.3265	0	8.1103	.3334	8.1103	0	0
				Chrome-tanned leather				
1	27.5517	23.9660	3.5857	7.2973	0.3045	11.2918	3.9945	1.1140
2	27.1922	23.9660	3.2262	7.2973	.3045	10.4434	3.1461	0.9752
3	26.6188	23.9660	2.6528	7.2973	.3045	10.3626	3.0653	1.1555
4	26.2176	23.9660	2.2516	7.2973	.3045	9.7970	2.4997	1.1102
5	25.7848	23.9660	1.8188	7.2973	.3045	9.2213	1.9240	1.0578
6	24.8509	23.9660	0.8849	7.2973	.3045	9.0244	1.7271	1.9517
7	24.4395	23.9660	.4735	7.2973	.3045	7.1306	−0.1667	−0.3521
8	23.9660	23.9660	0	7.2973	.3045	7.2973	0	0

specific heat to the value found, if the values are assumed to be additive. It is probable that the chromium sulfate reduces the vibrational activity by forming cross links in the collagen molecule. The formation of cross links is in accordance with the most widely accepted theory of chrome tanning [10].

The comparatively high specific heats of the lubricating materials (table 3) used in leather, diminish the comfort of the leather in cold weather by accelerating the removal of heat from the body. Greases and oils are not firmly adsorbed by the leather. They adhere to the leather by filling the pores, and form an intimate mixture. It is, therefore, expected that the specific heats of leather and the lubricating materials would be additive, and that the combination of the two would have a higher specific heat than that of leather alone. It has also been shown that both moisture and grease increase the heat conductivity of the leather [11]. The combination of these factors would, therefore, further diminish the comfort of the leather containing lubricating materials.

The author wishes to express his appreciation to Edwin S. Newman for permission to use the calorimetric equipment, and for his interest in the work, and to R. R. Stromberg, T. J. Carter, and C. E. Weir for assistance in operating the equipment.

5. References

[1] J. R. Kanagy, J. Am. Leather Chemists' Assoc. **49,** 646 (1954).
[2] A. Cheshire and N. L. Holmes, J. Intern. Soc. Leather Trades' Chemists **26,** 237 (1942).
[3] Handbook of Chemistry and Physics 35th ed., p. 2103 (Chemical Publishing Co., Cleveland, Ohio, 1953–1954).
[4] W. F. Hampton and J. H. Mennie, Can. J. Research **10,** 452 (1934).
[5] E. Newman and L. Wells, J. Research NBS **20,** 825 (1938) RP1107.
[6] J. R. Kanagy, J. Research NBS **44,** 31 (1950) RP2056.
[7] C. E. Weir, J. Am. Leather Chemists' Assoc. **47,** 711 (1952).
[8] J. J. Windle and T. M. Shaw, J. Chem. Phys. **22,** 1752 (1954).
[9] L. Pauling, J. Am. Chem. Soc. **67, 555** (1945).
[10] G. D. McLaughlin and E. R. Theis, The Chemistry of Leather Manufacture (Reinhold Publishing Corp., New York, N. Y., 1945).
[11] N. W. McLachlan, H. Goodfellow, and H. C. Cushnie, J. Intern. Soc. Leather Trades Chemists **26,** 23 (1942).
[12] E. B. Randall, T. J. Carter, T. J. Kilduff, C. W. Mann, and J. R. Kanagy, J. Am. Leather Chemists' Assoc. **47,** 404 (1952).

Washington, March 23, 1955.

Journal of Research of the National Bureau of Standards Vol. 55, No. 4, October 1955 Research Paper 2619

*p*H Values of the Clark and Lubs Buffer Solutions at 25° C

Vincent E. Bower and Roger G. Bates

The *p*H values of the well-known Clark and Lubs buffer solutions have been determined at 25° C on the conventional activity *p*H scale defined by the NBS standards. These solutions, which are useful for *p*H control in the range 1 to 10, are readily prepared by combining portions of four stock solutions with standard solutions of hydrochloric acid or sodium hydroxide. The four stock solutions contain potassium chloride, potassium hydrogen phthalate, potassium dihydrogen phosphate, or boric acid and potassium chloride. The compositions and buffer values of the solutions are listed at intervals of 0.1 *p*H. The estimated accuracy is ±0.02 *p*H unit.

1. Introduction

Among the best known series of buffer solutions for *p*H control are those of Sørensen [1] [1]; Palitzsch [2]; Clark and Lubs [3]; McIlvaine [4]; and Cohn, Heyroth, and Menkin [5]. Of these, perhaps the most widely used, particularly as standards in colorimetric *p*H determinations, are the solutions of Clark and Lubs. These are prepared by addition of standard solutions of hydrochloric acid or sodium hydroxide to portions of four stock solutions, followed by suitable dilution with water. In this way, buffer solutions of a predetermined *p*H value from 1 to 10 can be made.

The compositions and *p*H ranges of the solutions are as follows:[2]

*p*H 1.0 to 2.2: 25 ml 0.2 *M* KCl+*x* ml 0.2 *M* HCl, diluted to 100 ml.

*p*H 2.2 to 3.8: 50 ml 0.1 *M* KH phthalate+*x* ml 0.1 *M* HCl, diluted to 100 ml.

*p*H 4.0 to 6.2: 50 ml 0.1 *M* KH phthalate+*x* ml 0.1 *M* NaOH, diluted to 100 ml.

*p*H 5.8 to 8.0: 50 ml 0.1 *M* KH_2PO_4+*x* ml 0.1 *M* NaOH, diluted to 100 ml.

*p*H 7.8 to 10.0: 50 ml of a solution 0.1 *M* in both H_3BO_3 and KCl+*x* ml 0.1 *M* NaOH, diluted to 100 ml.

The exact compositions of solutions whose Sørensen *p*H values at 20° C vary in steps of 0.2 unit are to be found in monographs on *p*H measurement and in chemical handbooks.

In recent years there has been a gradual shift from the *p*H scale set forth by Sørensen to a conventional activity scale defined in such a way that measured *p*H values are consistent with the thermodynamic dissociation constants of the weak acids and bases that fix the *p*H [6]. The *p*H values assigned by Clark and Lubs to their buffer solutions are based on the earlier, virtually outmoded, scale. They are, therefore, about 0.04 unit lower between *p*H 3 and 11 than the values that would be assigned today. Near the ends of the *p*H scale the difference may be considerably greater.

Moreover, the *p*H values of these buffer solutions were determined by Clark and Lubs at 20° C rather than at 25° C, the temperature preferred for most experiments today. For these reasons, the *p*H of these useful buffers has been redetermined on the new scale at 25° C.

[1] Figures in brackets indicate the literature references at the end of this paper.

[2] In his monograph [3], Clark proposed a series of hydrochloric acid-potassium chloride mixtures of constant ionic strength 0.1 to replace the above series for the *p*H range 1.0 to 2.2.

2. Method

The *p*H was calculated from the electromotive force, *E*, of cells of the type,

$$\mathrm{Pt;\ H_2\ (g)\ solution\ X\ |\ KCl\ (satd.)\ |\ solution\ S,\ H_2\ (g);\ Pt.} \quad \text{(I)}$$

at 25° according to the relation

$$pH_X = pH_S + \frac{E}{0.059156}, \quad (1)$$

In cell I, solution X is the "unknown" buffer solution and solution S one of the NBS *p*H standards. In eq (1), 0.059156 is the value of 2.3026 RT/F at 25° C, if R is 8.31439 j deg^{-1} mole^{-1}, F is 96493.1 coulombs equiv.$^{-1}$, and T is 298.16° on the absolute temperature scale.

In accord with the usual convention, E was given the sign of the electrode on the right. It was thus positive when the *p*H of solution X exceeded that of solution S and negative when the *p*H of X exceeded that of S. Due to the symmetry of cell I, the value of E is unaffected by changes in the partial pressure of hydrogen, for equality of the latter at the two electrodes was maintained.

For a part of the measurements, the potentials of the two half-cells were measured separately with respect to a saturated calomel reference electrode that made electrolytic contact with the bridge solution of cell I. The *p*H of solution X was then calculated by eq (1), modified by the substitution of $E_X - E_S$ for E.

Four of the NBS standards were used in this study. In general, the standard with *p*H nearest that of the "unknowns" was selected for each particular series, as follows:

Series	Standard	pH_S at 25° C
HCl, KCl (pH_X 1.0 to 2.2)	0.05 *M* potassium tetroxalate	1.68
KH phthalate, HCl (pH_X 2.2 to 4.0)	0.05 *M* potassium hydrogen phthalate	4.01
KH phthalate, NaOH (pH_X 4.1 to 5.9)	0.05 *M* potassium hydrogen phthalate	4.01
KH_2PO_4, NaOH (pH_X 5.8 to 8.0)	0.025 *M* KH_2PO_4, 0.025 *M* Na_2HPO_4	6.86
H_3BO_3, KCl, NaOH (pH_X 8.0 to 10.2)	0.01 *M* borax	9.18

The four standard solutions were freshly prepared for each series of measurements and were intercompared occasionally in cells of type I. The differences of pH among the three standards of pH above 4 were always consistent with the values assigned to these solutions. Because of the residual liquid-junction potential, which becomes significant at low and high pH [7], the measured difference between one of these three standards and the tetroxalate standard is found to be too large by about 0.02 pH unit. Therefore, uncorrected pH measurements with cell I in the range between pH 1.68 and pH 4.01 may be considered to be in error by $\pm 0.02n/(4.01-1.68)=\pm 0.009n$, where n is the difference of pH between the unknown and the standard. In applying this correction, due regard must be given the sign. If the assembly is standardized at pH 4 or above, the correction is added to the measured pH; if it is standardized at pH 1.68, the correction is subtracted. This correction has been applied to the values reported in this paper.

3. Experimental Procedures

The cell vessel has been described elsewhere [7]. Fresh hydrogen electrodes were prepared daily. For use in the phthalate solutions, the platinum foil bases were coated with palladium black [8]; in the other solutions, a coating of platinum black was satisfactory. The deposits were formed by electrolysis for about 2 min at a current of 300 ma. The palladium and platinum solutions were prepared as described elsewhere [9]. About 1 hr after the cell was immersed in the constant-temperature water bath and the flow of hydrogen begun, the liquid junctions were formed. The emf was measured immediately after establishment of the junctions and was found to remain constant within ± 0.1 mv for one-half to one hour.

The potassium hydrogen phthalate and potassium dihydrogen phosphate were NBS Standard Samples 185a and 186Ib, respectively. Boric acid was recrystallized twice from water and was dried in air at room temperature. The potassium chloride was a purified fused sample prepared in a manner described previously [10]. The standard solutions of hydrochloric acid were prepared from a distilled sample and were standardized by the gravimetric silver-chloride procedure. The solution of carbonate-free sodium hydroxide was standardized against NBS Standard Sample potassium hydrogen phthalate using phenolphthalein as the indicator. The standard solutions were not exactly 0.1 M or 0.2 M, but the results have been expressed on this basis. Calibrated volumetric glassware was used.

4. Results

The pH values obtained were plotted as a function of the quantity of standard acid or alkali added. The amounts of reagent read from the smoothed large-scale plots at even intervals of 0.1 pH are listed in the accompanying tables. The estimated accuracy of the pH values is ± 0.02 unit. When corrections for the differences in temperature and scale of reference are applied, the results of Clark and Lubs for the phthalate, phosphate, and borate solutions are found to be entirely consistent with those given here. The discrepancy is greater with the acid-chloride mixtures, for which the residual liquid-junction potential is appreciable.

The Van Slyke buffer value, β, is defined as $db/dp\mathrm{H}$ [11]. The quantity db represents the number of moles of strong alkali which increase the pH of 1 liter of the buffer solution by the amount dpH. The values of β given in the last columns of the tables were computed from the data for a finite increment, $\Delta p\mathrm{H}=0.2$, by the relation $\beta \approx \Delta b/\Delta p\mathrm{H}$. In this formula, then, Δb was the number of moles of strong alkali needed to raise the pH of 1 liter of the buffer solution from 0.1 unit below the point in question to 0.1 unit above. Both Δb and ΔpH are negative for additions of strong acid.

The pH values of the acid-chloride mixtures given in table 1 agree closely with the pH computed from the molar concentration, c, of hydrochloric acid and the ionic strength, μ, by the formula

$$p\mathrm{H}=-\log c+\frac{0.509\sqrt{\mu}}{1+1.643\sqrt{\mu}}$$

in which the activity coefficient of hydrogen ion is expressed by the Debye-Hückel equation with ion size of 5 A. This formula has also been used to calculate the pH values of mixtures of a constant total molarity (and ionic strength) of 0.1, which Clark [3] preferred. The results are given in table 6.

The buffer solutions should be prepared with a good grade of distilled water. Water for the preparation of the alkaline solutions should be boiled and protected from carbon dioxide while cooling, or should be purged with carbon dioxide-free air. The solutions will usually show satisfactory stability over a period of several weeks.

TABLE 1. *Compositions and buffer values of solutions of* pH *1.0 to 2.2: 25 ml 0.2 M* KCl, x *ml 0.2 M* HCl, *diluted to 100 ml*

pH	x	Buffer value, β
1.00	67.0	0.31
1.10	52.8	.24
1.20	42.5	.19
1.30	33.6	.16
1.40	26.6	.13
1.50	20.7	.10
1.60	16.2	.077
1.70	13.0	.060
1.80	10.2	.049
1.90	8.1	.037
2.00	6.5	.030
2.10	5.1	.026
2.20	3.9	.022

TABLE 2. *Compositions and buffer values of buffer solutions of pH 2.2 to 4.0: 50 ml 0.1 M* KH *phthalate, x ml 0.1 M* HCl, *diluted to 100 ml*

*p*H	*x*	Buffer value, β
2.20	49.5	----------
2.30	45.8	0.036
2.40	42.2	.035
2.50	38.8	.034
2.60	35.4	.033
2.70	32.1	.032
2.80	28.9	.032
2.90	25.7	.033
3.00	22.3	.034
3.10	18.8	.033
3.20	15.7	.030
3.30	12.9	.026
3.40	10.4	.023
3.50	8.2	.020
3.60	6.3	.018
3.70	4.5	.017
3.80	2.9	.015
3.90	1.4	.014
4.00	0.1	.014

TABLE 3. *Compositions and buffer values of buffer solutions of pH 4.1 to 5.9: 50 ml 0.1 M* KH *phthalate, x ml 0.1 M* NaOH, *diluted to 100 ml*

*p*H	*x*	Buffer value, β
4.10	1.3	0.016
4.20	3.0	.017
4.30	4.7	.018
4.40	6.6	.020
4.50	8.7	.022
4.60	11.1	.025
4.70	13.6	.027
4.80	16.5	.029
4.90	19.4	.030
5.00	22.6	.031
5.10	25.5	.031
5.20	28.8	.030
5.30	31.6	.026
5.40	34.1	.025
5.50	36.6	.023
5.60	38.8	.020
5.70	40.6	.017
5.80	42.3	.015
5.90	43.7	.013

TABLE 4. *Compositions and buffer values of buffer solutions of pH 5.8 to 8.0: 50 ml 0.1 M* KH_2PO_4, *x ml 0.1 M* NaOH, *diluted to 100 ml*

*p*H	*x*	Buffer value, β
5.80	3.6	----------
5.90	4.6	0.010
6.00	5.6	.011
6.10	6.8	.012
6.20	8.1	.015
6.30	9.7	.017
6.40	11.6	.021
6.50	13.9	.024
6.60	16.4	.027
6.70	19.3	.030
6.80	22.4	.033
6.90	25.9	.033
7.00	29.1	.031
7.10	32.1	.028
7.20	34.7	.025
7.30	37.0	.022
7.40	39.1	.020
7.50	40.9	.016
7.60	42.4	.013
7.70	43.5	.011
7.80	44.5	.009
7.90	45.3	.008
8.00	46.1	----------

TABLE 5. *Compositions and buffer values of buffer solutions of pH 8.0 to 10.2: 50 ml of a mixture 0.1 M with respect to both* KCl *and* H_3BO_3, *x ml 0.1 M* NaOH, *diluted to 100 ml*

*p*H	*x*	Buffer value, β
8.00	3.9	----------
8.10	4.9	0.010
8.20	6.0	.011
8.30	7.2	.013
8.40	8.6	.015
8.50	10.1	.016
8.60	11.8	.018
8.70	13.7	.020
8.80	15.8	.022
8.90	18.1	.025
9.00	20.8	.027
9.10	23.6	.028
9.20	26.4	.029
9.30	29.3	.028
9.40	32.1	.027
9.50	34.6	.024
9.60	36.9	.022
9.70	38.9	.019
9.80	40.6	.016
9.90	42.2	.015
10.00	43.7	.014
10.10	45.0	.013
10.20	46.2	----------

TABLE 6. HCl–KCl *mixtures of constant ionic strength, $\mu=0.1$; compositions and buffer values of solutions of pH 1.0 to 2.2: x ml 0.2 M* HCl, *y ml 0.2 M* KCl, *diluted to 100 ml*

Molarity of HCl	Molarity of KCl	*p*H	Buffer value, β
0.10	0	1.11	0.23
.09	0.01	1.15	.21
.08	.02	1.20	.18
.07	.03	1.26	.16
.06	.04	1.33	.14
.05	.05	1.41	.12
.04	.06	1.50	.092
.03	.07	1.63	.069
.02	.08	1.80	.046
.01	.09	2.11	.023
.005	.095	2.41	.012
.002	.098	2.80	.004
.001	.099	3.11	.002

*p*H	*x*	*y*	Buffer value, β
[a](1.00)	67.0	0	0.31
[b](1.10)	51.2	0	.24
1.20	40.7	9.3	.19
1.30	32.3	17.7	.15
1.40	25.7	24.3	.12
1.50	20.1	29.9	.093
1.60	16.0	34.0	.074
1.70	12.8	37.2	.059
1.80	10.2	39.8	.047
1.90	8.1	41.9	.037
2.00	6.5	43.5	.030
2.10	5.2	44.8	.024
2.20	4.2	45.8	.019

[a] $\mu=0.134$.
[b] $\mu=0.102$.

5. References

[1] S. P. L. Sørensen, Ergeb. Physiol. **12,** 393 (1912).
[2] S. Palitzsch, Biochem. Z. **70,** 333 (1915).
[3] W. M. Clark and H. A. Lubs, J. Biol. Chem. **25,** 479 (1916); see also W. M. Clark, Determination of hydrogen ions, 3d ed, ch. 9 (The Williams and Wilkins Co., Baltimore, Md., 1928).
[4] T. C. McIlvaine, J. Biol. Chem. **49,** 183 (1921); see also C. J. Schollenberger, Chemist Analyst **19,** Nos. 3 and 8 (1930).
[5] E. J. Cohn, J. Am. Chem. Soc. **49,** 173 (1927); E. J. Cohn, F. F. Heyroth, and M. F. Menkin, J. Am. Chem. Soc. **50,** 696 (1928).
[6] See, for example, D. I. Hitchcock and A. C. Taylor, J. Am. Chem. Soc. **59,** 1812 (1937); **60,** 2710 (1938); D. A. MacInnes, D. Belcher, and T. Shedlovsky, J. Am. Chem. Soc. **60,** 1094 (1938).
[7] R. G. Bates, G. D. Pinching, and E. R. Smith, J. Research NBS **45,** 418 (1950) RP2153.
[8] W. J. Hamer and S. F. Acree, J. Research NBS **33,** 87 (1944) RP1598.
[9] R. G. Bates, Electrometric pH determinations, pp. 167–168 (John Wiley & Sons, Inc., New York, N. Y., 1954).
[10] G. D. Pinching and R. G. Bates, J. Research NBS **37,** 311 (1946) RP1749.
[11] D. D. Van Slyke, J. Biol. Chem. **52,** 525 (1922).

Washington, May 13, 1955.

Journal of Research of the National Bureau of Standards Vol. 55, No. 4, October 1955 Research Paper 2620

Heat Capacity; Heats of Fusion, Vaporization, and Transition; and Vapor Pressure of *N*-Dimethylaminodiborane, $(CH_3)_2NB_2H_5$

George T. Furukawa, Robert E. McCoskey, Martin L. Reilly, and Ann W. Harman

The heat capacity of *N*-dimethylaminodiborane was determined in the temperature range from 17° to 285°K by means of an adiabatic calorimeter. A first-order solid-solid transition was found at 199.9 ± 0.1°K, with a latent heat of 7794 abs j mole^{-1}. The triple-point temperature was found to be 218.4 ± 0.2°K, and the heat of fusion to be 1,408 ± 30 abs j mole^{-1}. The measurements of the heat of vaporization at 271.60°K (94.3 mm Hg) yielded 30,119 ± 30 abs j mole^{-1}. The results of the vapor-pressure measurements from 220° to 290°K can be represented by the equation

$$\log_{10} p_{\text{mm Hg}} = 406.5734/T + 5.2095614 \times 10^{-2} T + 1.01048 \times 10^{-5} T^2 - 1.390588 \times 10^{-7} T^3 - 11.63086.$$

The data were used to construct a table of smoothed values of heat capacity, enthalpy, entropy, and Gibbs free energy from 0° to 285°K. The entropy of *N*-dimethylaminodiborane in the ideal gas state at 1 atm and 271.60°K was computed from the data to be 302.3 ± 0.6 abs j deg^{-1} mole^{-1} (72.25 ± 0.14 cal deg^{-1} mole^{-1}).

1. Introduction

Many boron hydrides and other boron-containing compounds are relatively unstable and undergo various disproportionation reactions. These equilibria are complicated in many cases by the large number of different compounds produced in the reaction. The dearth of thermodynamic information regarding these substances prevents computation of the degree of thermal and chemical stability. Also, there is considerable interest in these materials from the standpoints of their structure and of practical applications. In view of these considerations, a program of thermodynamic study was initiated to aid in the better understanding of boron-containing compounds. This paper deals with the determination of heat capacity, heats of fusion, vaporization, and transition, and vapor pressure, and with the computation of the thermal properties of *N*-dimethylaminodiborane, $(CH_3)_2NB_2H_5$.

2. Apparatus and Method

Measurements of the heat capacity and the heats of fusion and transition were carried out in an adiabatic calorimeter similar in design to that described by Southard and Brickwedde [1][1]. The details of the design and operation of the calorimeter have been previously given by Scott et al. [2].

In the measurements of the gross (sample plus container) heat capacities at the lower temperatures, where the heat-capacity curve has a large curvature, the temperature interval of heating, ΔT, was made small in order to minimize the curvature correction; from 17° to 30°K ΔT was 1 to 3 deg, from 30° to 60°K it was increased from 3 to 5 deg, and above 60°K it was as much as 8 deg. Also, in the transition range (discussed in section 4 of this paper) ΔT was made small to obtain as closely as possible the shape of the heat-capacity curve, as well as to minimize the curvature correction. The curvature corrections [2] were made whenever significant using the relation

$$Z_{T_m} = \frac{Q}{\Delta T} - \left(\frac{\partial^2 Z}{\partial T^2}\right)_{T_m} \frac{(\Delta T)^2}{24} \cdots, \qquad (1)$$

where Z is the heat capacity, T_m the mean temperature of the temperature interval ΔT, and Q the energy input. The net heat capacities were obtained by subtracting the tare (empty container) heat capacities from the gross heat capacities after the necessary curvature corrections have been made. The tare heat capacities at the temperatures of the observed gross heat capacities were obtained by four-point Lagrangian interpolation [3] in a table of smoothed tare heat capacities given at 1-deg intervals.

At the higher temperatures, where the vapor pressure became significant, corrections were applied to the net heat capacities for the heat of vaporization and for the mass of vapor in the filling tube. The corrections were determined by using the following relation [4]

$$C_{\text{satd}} = M \frac{C_{\text{net}} - T_m \frac{d}{dT}\left\{\frac{dp}{dT}[V - (m - m_t)\, v_c]\right\} - l \frac{dm_t}{dT}}{m - m_t}, \qquad (2)$$

where C_{satd} is the molal heat capacity of the condensed phase at saturation pressure, M the molecular weight of the material, C_{net} the net heat capacity, p the vapor pressure at T_m, V the volume of the calo-

[1] Figures in brackets indicate the literature references at the end of this paper.

rimeter, m the total mass of sample, m_l the mass of vapor in the filling tube, v_ϵ the specific volume of the condensed phase, and l the heat of vaporization of unit mass of sample at T_m. This correction at the highest temperature (285°K) of the measurements amounted to 0.15 percent.

The heat-of-vaporization experiments were made in another adiabatic calorimeter similar in design to those described by Osborne and Ginnings [5] and by Aston et al. [6]. The details of the design and operation can be found in these references.

For the vapor-pressure measurements, the calorimeter used in the heat-capacity experiments was connected to a mercury manometer, which was read by means of a mirror-backed calibrated glass scale. The calorimeter served as a thermostated container, and the vapor-pressure measurements were generally made at successively higher temperatures. As no provision was made to stir the sample, several measurements were made at successively lower temperatures as a check on the equilibrium of the sample. These two series of results, one obtained going up and the other going down the temperature scale, did not differ significantly. The pressure readings were converted to standard mm Hg ($g=980.665$ cm sec^{-2}, temperature=0°C) on the basis that the local gravity is 980.076 cm sec^{-2}.

Temperatures above 90°K were determined in accordance with the International Temperature Scale [7]. Below 90°K, a provisional scale was used, which is based on a set of platinum resistance thermometers calibrated against a helium-gas thermometer [8]. All electrical instruments and accessory equipment were calibrated at the Bureau. The atomic weights used were based on the values given in the 1952 Report of the Committee on Atomic Weights of the American Chemical Society [9].

3. Sample and Its Purity and Heat of Fusion

About 200 ml of the material was originally received in a break-seal ampoule; after degassing, by repeated freezing, pumping, and melting, approximately one-half of this material was transferred by vacuum distillation into a weighing flask for calorimetric studies. The sample in the weighing flask was degassed further, first by pumping at about −70°C and later by freezing, pumping, and melting three times. Following this treatment the sample (59.0725 g) was transferred immediately into the calorimeter.

The purity of the sample was determined prior to the heat-capacity measurements from its equilibrium melting temperatures. In this method all the impurity is assumed to remain in the liquid phase and not to form a solid solution with *N*-dimethylaminodiborane, and Raoult's law of solution is assumed to be applicable throughout the whole range of impurity concentration. The observed equilibrium melting temperatures are plotted versus the reciprocal of the corresponding fractions of the material melted, $1/F$. The fraction melted is obtained from the energy input, heat capacity, and heat of fusion. The product of the cryscopic constant, $\Delta H_f/RT_{tp}^2$, and the slope of the temperature versus $1/F$ curve is the mole fraction impurity. In the cryscopic constant, ΔH_f is the heat of fusion, R the gas constant, and T_{tp} the triple-point temperature. The extrapolated temperature intercept (at $1/F=0$) of the temperature versus $1/F$ plot is taken as the triple-point temperature of the pure material. The results of the measurements and subsequent computation are summarized in table 1. The cryscopic constant used was 0.0036 deg^{-1}.

TABLE 1. *Equilibrium melting temperatures of N-dimethylaminodiborane*

Mole fraction impurity = 0.0036 ΔT, °K = °C + 273.16°

Reciprocal of fraction melted, $1/F$	T
	°K
7.50	[a]217.2538
4.89	217.5751
3.39	217.7886
2.51	217.9303
1.42	218.1683
0.00	[b]218.4
Triple-point temperature, 218.4±0.2° K. Purity, 99.9+ mole percent.	

[a] The temperatures given are accurate to 0.01° K. Whenever temperatures are expressed to the fourth decimal, the last two figures are significant only in the measurement of small temperature differences.
[b] Extrapolated.

The heat of fusion was determined in the usual manner by heating continuously from a temperature a few degrees below the triple-point temperature to just above it and by correcting for heat capacity and for premelting caused by the presence of impurity. (Certain amounts of material are already melted at temperatures just below the triple-point temperature. The amount melted is dependent upon the impurity content, the cryoscopic constant, and the closeness of the temperature to the triple-point temperature.) The experimental heat capacities in the region just below the triple-point temperature were found to have apparently high values caused by the premelting of the sample. The premelting corrections calculated from the impurity content did not seem to correct the observed heat capacities satisfactorily. The final values of heat capacity in this region (see table 6) were obtained after revising the observed values by a combination of premelting correction and extrapolation. These corrections were not particularly accurate, consequently the heat capacities are believed to have large errors, probably as much as several percent. The calculated value of the heat of fusion, which is relatively small, has a large percentage uncertainty resulting from the inaccuracies in the heat capacity and premelting corrections.

The results of the heat-of-fusion measurements and computations are summarized in table 2. Considering the various known sources of uncertainties, such as premelting and heat capacity corrections mentioned in the previous paragraph, energy measurements, heat leaks, and mass of sample, the heat of fusion is probably accurate to ±30 abs j mole^{-1}.

TABLE 2. *Molal heat of fusion of N-dimethylaminodiborane*

Molecular weight = 70.756, triple-point temperature = 218.4° K
°K = °C + 273.16°

Temperature interval	Heat input	Corrections		ΔH_f
		Heat capacity	Premelting	
K°	*abs j mole⁻¹*	*abs j mole⁻¹*	*abs j mole⁻¹*	*abs j mole⁻¹*
214.2928 to 221.3568 [a]	2298.1	−953.3	61.0	1405.8
215.1552 to 220.2458	2008.0	−685.4	77.2	1399.8
214.8542 to 221.2065	2210.0	−859.6	70.6	1421.0
213.7353 to 221.5915	2408.3	−1058.4	53.7	1403.6
Mean				1407.6
Standard deviation of the mean				±4.7 [b]
Estimated uncertainty				±30

[a] The temperatures given are accurate to ±0.01° K. Figures beyond the second decimal are significant only insofar as small temperature differences are concerned.

[b] Standard deviation of the mean as used here and in table 4 is defined as $[\Sigma d^2/n(n-1)]^{1/2}$, where d is the difference between a single observation and the mean, and n is the number of observations.

4. Heat Capacity and Heat of Transition

Measurements of the heat capacity were made from about 17° to 285° K; corrections for curvature (see eq 1) and vaporization (see eq 2) were applied to the observed values wherever significant. The equation for the liquid density reported by Burg and Randolph [10], based on their experimental measurements, was used in making the vaporization corrections. The density equation was extended below its experimental temperature range whenever required. As the corrections become smaller at lower temperatures (at the highest temperature of the measurements, 285° K, the vaporization correction was 0.15 percent of the net heat capacity), the error in the extrapolation is considered to have negligible effect on the final observed heat-capacity values given in table 3 and figure 1.

The values given in table 3, although corrected for vaporization and curvature wherever significant, have not been corrected for premelting in the region just below the triple-point temperature. As mentioned in section 3, considerable premelting effects were observed in the apparently high values of heat capacity. In calculating the final smoothed values of heat capacities given in table 6 of section 7, the observed values were first revised by a combination of premelting correction and extrapolation. The revisions made are believed to be highly inaccurate, consequently the uncertainty in the heat capacity of this region may be as high as several percent. At other regions of temperature, except below about 60° K, the heat capacity is probably accurate to ±0.2 percent. Below 60° K the probable error in the values is believed to increase to about 1 percent largely due the smaller temperature interval of heating, smaller energy input, and decreased sensitivity of the thermometer.

Because of the relatively low heat of fusion and the large premelting effect observed, the solid-solid transition occurring between 195° and 205° K was originally thought to arise from the melting of a eutectic mixture. A close examination of the heat capacity between 200° K and the triple-point tem-

TABLE 3. *Observed heat capacity of N-dimethylaminodiborane*

Molecular weight = 70.756, °K = °C + 273.16°

T_m [a]	$\lvert\Delta T$	$C_{sat'd}$
RUN 1		
°K	*°K*	*abs j deg⁻¹ mole⁻¹*
207.7381 [b]	1.6866	125.62
209.4220	1.6811	126.16
211.2787	2.0324	127.52
213.2921	2.0014	129.45
215.2246	1.8635	146.63
216.7813	1.2500	271.62 [c]
217.8016	0.7906	1080.6 [c]
219.7768	3.1599	260.51 [c]
222.8033	2.8930	142.60
225.6900	2.8803	143.31
RUN 2		
213.7044	2.9016	133.85
215.9800	1.6496	175.53
217.0293	0.4490	283.33 [c]
217.4144	.3213	435.26 [c]
217.6818	.2135	710.27 [c]
217.8594	.1417	1125.4 [c]
218.0493	.2380	1868.1 [c]
219.2070	2.0775	334.84 [c]
221.0258	1.5599	142.39
RUN 3		
221.4889	1.1212	142.48
222.6082	1.1173	142.79
225.4610	4.5204	143.45
230.2422	5.0420	144.64
235.2658	5.0053	145.84
240.2574	4.9779	147.10
245.2123	4.9318	148.45
250.1228	4.8891	149.76
254.9938	4.8530	151.13
RUN 4		
90.0286	2.1671	59.266
93.6566	5.0887	61.123
98.6392	4.8765	63.660
104.0464	4.5293	66.449
108.8120	5.0019	68.925
115.3404	8.0549	72.254
123.2074	7.6791	76.304
130.7321	7.3702	80.148
137.9640	7.0936	83.826
144.9421	6.8626	87.357
151.7720	6.7973	90.867
158.4743	6.6072	94.374
RUN 5		
160.7098	6.5065	95.657
167.1356	6.3451	99.198
173.3990	6.1939	102.63
179.5152	6.0384	106.54
185.4870	5.4870	110.43
191.3747	5.8702	115.28
196.9508	5.2820	138.82
199.7366	0.2896	4359.1 [c]
RUN 6		
189.8876	2.9971	113.53
194.2642	5.7560	118.91
198.4696	2.6549	379.67 [c]
199.8516	0.1089	11730 [c]
199.9228	.0337	38081 [c]
199.9497	.0200	96316 [c]
201.2234	2.5273	1155.1 [c]
203.3206	1.6672	124.69
RUN 7		
202.3303	1.6582	124.25
204.8100	3.3011	124.70
210.6664	8.3755	126.85
218.0304	6.3523	347.90 [c]
222.4840	2.5551	142.70

TABLE 3. *Observed heat capacity of N-dimethylaminodiborane*—Continued

Molecular weight = 70.756, °K = °C + 273.16°

T_m[a]	ΔT	$C_{sat'd}$
	RUN 8	
°K	°K	*abs j deg⁻¹ mole⁻¹*
190.2736	4.1895	113.94
194.4084	4.0799	119.06
199.1227	5.3488	1573.3 [c]
203.0568	2.5193	124.82
205.5710	2.5092	125.47
210.2804	6.9097	127.06
217.6634	7.8562	306.55[c]
	RUN 9	
17.5414	1.6646	7.864
19.0626	1.3777	9.434
20.3464	1.1901	10.821
21.7180	1.5530	12.282
23.1742	1.3594	13.830
24.4628	1.2179	15.269
26.4766	2.8095	17.414
29.3340	2.9055	20.328
32.3968	3.2200	23.325
35.7151	3.4166	26.400
39.4570	4.0671	29.444
44.5193	6.0576	33.154
50.1185	5.1408	36.970
55.5076	5.6373	40.288
61.3216	5.9089	43.719
67.0340	5.4338	47.017
73.2088	6.9159	50.598
79.8362	6.3387	53.844
86.2264	6.4418	57.397
93.0664	7.7382	60.922
	RUN 10	
247.2118	6.1379	149.19
252.7154	4.8691	150.72
257.5652	4.8305	152.10
263.5702	7.1796	153.73
270.7090	7.0979	155.98
277.8226	7.1295	158.20
284.9132	7.0515	160.74

[a] T_m is the mean temperature of the heating interval.
[b] The temperatures given are accurate to ±0.01° K. Figures beyond the second decimal are significant only insofar as small temperature differences are concerned.
[c] These are apparently high values obtained in the temperature region of the solid-solid transition and the triple point.

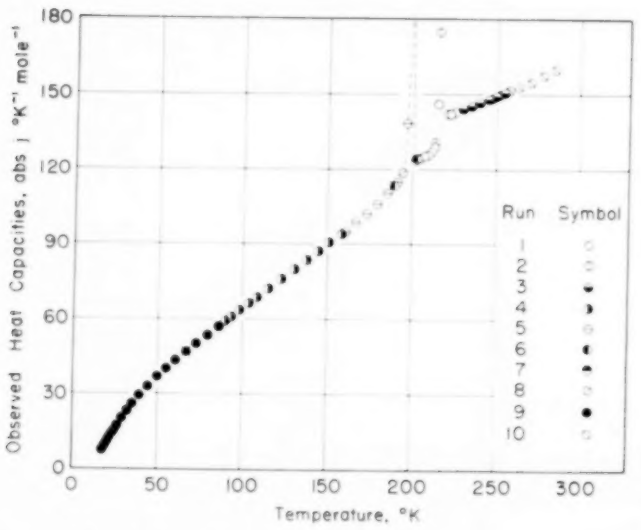

FIGURE 1. *Observed heat capacity of N-dimethylaminodiborane.*

perature suggested, however, that the discontinuity in the heat capacity is probably from a solid-solid transition. The transition was found to involve a large latent heat. The enthalpy change from 190° to 205° K was determined, in which two measurements from runs 6 and 8 (see tables 3 and 7) gave 9570.4 and 9573.8 abs j mole^{-1}, respectively. These values were obtained by summing the various input energies in this temperature range and by correcting to the even temperature interval. The results of the heat-capacity measurements (see table 3, runs 6 and 8) suggest that the peak or the transition temperature is 199.9 ±0.1° K. The latent heat associated with the transition was estimated from the enthalpy change from 190° to 205° K and the extrapolated heat capacity in this region to be 7794 abs j mole^{-1}.

5. Heat of Vaporization

The heat-of-vaporization experiments were made at 271.60° K (94.3 mm Hg). The experimentally determined quantity γ, the energy input per mole of sample collected [11], is related to the molal heat of vaporization ΔH_V, by the expression

$$\Delta H_V = \gamma - T\mathcal{V}\frac{dp}{dT} \qquad (3)$$

where $\mathcal{V}$ is the molal volume of the liquid, T the absolute temperature of vaporization, and p the vapor pressure. The molal volume of the liquid was obtained by extrapolating, a few degrees, the density equation (0° to 25° C) given by Burg and Randolph [10]. The temperature derivative of the vapor pressure, dp/dT, was obtained by differentiating with respect to temperature the vapor-pressure equation (eq 4). The results of the heat-of-vaporization measurements and computations are summarized in table 4. Considering various known sources of error and the precision of the measurements, a probable error of ±30 abs j mole^{-1} is assigned to the heat of vaporization.

TABLE 4. *Heat of vaporization of N-dimethylaminodiborane at 271.60° K*

Molecular weight = 70.756, pressure = 94.3 mm Hg
° K = ° C + 273.16°

γ	$T\mathcal{V}(dp/dT)$	ΔH_V
abs j mole⁻¹	*abs j mole⁻¹*	*abs j mole⁻¹*
30,144	18	30,126
30,127	18	30,109
30,141	18	30,123
Mean		30,119
Standard deviation of the mean		±5[a]
Estimated uncertainty		±30

[a] See footnote b, table 2.

The heat of vaporization computed in accordance with the Clapeyron equation gave 29,900 abs j mole^{-1}, which is in fair agreement with the experimental value obtained. In the computation the vapor was assumed to follow the Berthelot equation of state, the constants (T_c=485° K and p_c=36 atm) of which

were estimated according to $T_b=2/3T_c$ and the method described by Walden [12], respectively. The sources of the dp/dT and the molal volume of the liquid phase were those mentioned in the previous paragraph.

6. Vapor Pressure

The results of the vapor-pressure measurements, made from about 220° to 290°K, can be represented by the equation

$$\log_{10} p_{\text{mm Hg}}=406.5734/T+5.2095614\times10^{-2}T+1.01048\times10^{-5}T^2-1.390588\times10^{-7}T^3-11.63086. \quad (4)$$

The constants were determined by the method of least squares. In column 4 of table 5 are given the deviations of the observed values from the calculated values based on this equation. There are also given in this table the vapor-pressure results obtainable from the equation

$$\log_{10} p_{\text{mm Hg}}=-1727.64/T+1.75\log_{10} T-0.004661T+5.3370, \quad (5)$$

reported by Burg and Randolph [10] based on their experimental results from about −36° to 50° C.

Attempts were made to carry out vapor-pressure measurements at higher temperatures in an isoteniscope. However, it was found that even at 300°K the vapor pressure increased, presumably due to decomposition, over an extended time in the isoteniscope. The average increase over several days was about 0.01 mm Hg per hour at this temperature. Consequently, the results with the isoteniscope have not been considered in this paper.

TABLE 5. *Vapor pressure of N-dimethylaminodiborane*

°K=°C+273.16°

T	p, obs	p, calc[a]	Δp, obs-calc	p, [10]
		SERIES I		
°K	*mm* Hg	*mm* Hg	*mm* Hg	*mm* Hg
234.71	12.1	12.2	−0.1	10.7
237.51	14.8	14.5	+.3	13.0
242.75	19.8	19.8	0	18.3
245.57	23.8	23.3	+.5	21.9
249.29	29.0	28.9	+.1	27.5
256.48	43.2	43.1	+.1	41.8
261.95	57.7	57.8	−.1	56.6
264.86	67.3	67.2	+.1	66.1
268.89	82.4	82.5	−.1	81.4
271.33	92.8	93.1	−.3	92.0
273.50	103.5	103.5	0	102.4
283.22	162.5	162.4	+.1	161.5
287.18	193.3	193.0	+.3	192.4
		SERIES II		
219.79	4.8	4.8	0	3.6
227.78	7.8	8.0	−.2	6.6
236.55	13.5	13.7	−.2	12.2
248.82	28.4	28.1	+.3	26.7
255.98	41.6	41.8	−.3	40.7
258.91	49.0	49.1	−.1	47.8
260.53	53.8	53.6	+.2	52.4
266.54	73.0	73.2	−.2	72.1
		SERIES III		
218.28	4.4	4.4	0	3.2
226.05	7.3	7.2	+.1	5.8
245.19	22.5	22.8	−.3	21.4
260.15	52.3	52.5	−.2	51.3

[a] Equation (4).

7. Derived Thermal Properties

Empirical equations were fitted to the observed heat capacities and the deviations from the equa-

TABLE 6. *Heat capacity, enthalpy, entropy, and Gibbs free energy of N-dimethylaminodiborane*

Molecular weight=70.756, °K=°C+273.16°

T	C_{satd}	$(H_T-H_{0°K})_{\text{satd}}$	$(S_T-S_{0°K})_{\text{satd}}$	$-(F_T-H_{0°K})_{\text{satd}}$
°K	*abs j deg^{-1} mole^{-1}*	*abs j mole^{-1}*	*abs j deg^{-1} mole^{-1}*	*abs j mole^{-1}*
0	0	0	0	0
5	0.213	0.2671	0.0712	0.0890
10	1.701	.4268	.5692	1.424
15	5.332	20.96	1.874	7.145
20	10.43	60.00	4.081	21.63
25	15.86	125.7	6.990	49.02
30	20.99	218.0	10.34	92.24
35	25.77	335.1	13.94	152.9
40	29.86	474.4	17.66	231.9
45	33.50	632.9	21.39	329.5
50	36.90	809.0	25.09	445.7
55	40.08	1002	28.76	580.4
60	42.94	1209	32.37	733.3
65	45.84	1431	35.93	904.0
70	48.77	1668	39.43	1092
75	51.54	1919	42.89	1298
80	53.93	2182	46.29	1521
85	56.68	2459	49.64	1761
90	59.34	2749	52.96	2018
95	61.84	3052	56.24	2291
100	64.37	3367	59.47	2580
105	66.94	3696	62.67	2885
110	69.51	4037	65.85	3207
115	72.09	4391	68.99	3544
120	74.66	4758	72.12	3897
125	77.22	5137	75.22	4265
130	79.78	5530	78.30	4649
135	82.32	5935	81.35	5048
140	84.85	6353	84.39	5462
145	87.39	6784	87.42	5892
150	89.95	7227	90.42	6336
155	92.56	7683	93.41	6796
160	95.24	8153	96.39	7270
165	98.00	8636	99.37	7760
170	100.7	9132	102.33	8264
175	103.6	9643	105.29	8783
180	106.8	10169	108.26	9317
185	110.2	10711	111.23	9866
190	113.7	11272	114.21	10428
195	----------	----------	----------	----------
200	----------	----------	----------	----------
205	124.8	20842	162.14	12396
210	126.6	21477	165.20	13214
215	129.1	----------	----------	----------
218.4[a]	131.2	----------	----------	----------
		Liquid		
218.4[a]	141.9	----------	----------	----------
220	142.1	24133	177.46	14908
225	143.3	24847	180.67	15803
230	144.6	25566	183.83	16715
235	145.8	26292	186.95	17642
240	147.1	27025	190.04	18584
245	148.5	27764	193.08	19542
250	149.9	28510	196.10	20515
255	151.3	29263	199.08	21503
260	152.7	30023	202.03	22505
265	154.1	30790	204.95	23522
270	155.7	31565	207.85	24554
275	157.3	32347	210.72	25600
280	159.0	33138	213.57	26661
285	160.8	33938	216.40	27735

[a] Extrapolated.

tions were plotted on a large scale. The heat capacities given in table 6 at equally spaced integral temperatures were obtained by the combination of the approximate empirical equations and the large scale deviation curves. The heat-capacity values of table 6 below 17° K were obtained by extrapolation using a Debye function fitted to experimental values between 17° and 30° K.

The enthalpy, entropy, and Gibbs free energy values were obtained by evaluating, respectively, the thermodynamic relations

$$(H_T - H_{0°K})_{satd} = \int_0^T C_{satd}\, dT + \Delta H_{tr} + \Delta H_f + \int_0^T \mathcal{U}(dp/dT)_{satd}\, dT, \tag{6}$$

$$(S_T - S_{0°K})_{satd} = \int_0^T C_{satd}\, dT/T + \Delta H_{tr}/T_{tr} + \Delta H_f/T_{fp}, \tag{7}$$

and

$$(F_T - H_{0°K})_{satd} = -\int_0^T (S_T - S_{0°K})_{satd}\, dT + \int_0^T \mathcal{U}(dp/dT)_{satd}\, dT. \tag{8}$$

In these expressions ΔH_{tr} is the heat of transition, T_{tr} the temperature of transition, and $\mathcal{U}$ the molal volume of the condensed phase. Other symbols have the usual or previously defined significance. The equations were evaluated, except between 190° and 220° K, by numerical integration using four-point Lagrangian integration coefficients [3]. Between 190° and 220° K, the enthalpy change was obtained by summing the experimental input energies in runs that were made continuously through either or both of the two first-order transitions. This procedure was particularly necessary for evaluating the enthalpy change in the temperature region that included the triple-point temperature. As mentioned in section 3, the premelting corrections were highly uncertain and, although the measurements of the total energy involved were precise, the energy distribution between melting and heat capacity may be inaccurate. In the interval from 190° to 205° K, as given in table 7, the enthalpy changes for runs 6 and 8 were 9570.4 and 9573.8 abs j mole^{-1}, respectively. From 210° to 220° K, which includes the triple-point temperature, runs 1, 7, and 8 gave 2656.1, 2657.7, and 2660.3 abs j mole^{-1}, respectively, for the enthalpy change. In run 8, the heat-capacity experiments were made continuously from 188.1789° to 221.5915° K, which gave 12861.9 abs j mole^{-1} for the enthalpy change in the interval 190° to 220° K. Upon taking 9570.4 and 2656.1 abs j mole^{-1}, which have been obtained under optimum experimental conditions, for the enthalpy changes for the intervals 190° to 205° K and 210° to 220° K, respectively, the enthalpy change for the interval 205° to 210° K becomes 635.4 abs j mole^{-1}.

TABLE 7. *Molal enthalpy and entropy change of N-dimethylaminodiborane over various temperature intervals*

Molecular weight = 70.756, °K = °C + 273.16°

Run	Temperature interval	ΔH	ΔS
	°K	*abs j mole^{-1}*	*abs j deg^{-1} mole^{-1}*
6	190 to 205	9570.4	47.923
8	190 to 205	9573.8	48.154
1	210 to 220	2656.1	12.263
7	210 to 220	2657.7	12.274
8	210 to 220	2660.3	12.297
8	190 to 220	12861.9	
8	205 to 210	635.4	3.062

The entropy changes for the corresponding temperature intervals (see table 7) were obtained by summing the various $\Delta H/T_m$'s, where T_m is the mean temperature of the heating interval. In the interval 190° to 205° K, runs 6 and 8 gave 47.923 and 48.154 abs j deg^{-1} mole^{-1}, respectively. As ΔH and correspondingly the ΔT were smaller in run 6, the entropy change of this run was used in constructing table 6. For the interval 205° to 210° K, the entropy change was obtained by merely dividing the enthalpy change (635.4 abs j mole^{-1}) by the mean temperature (207.5°K). For the interval 210° to 220°K, runs 1, 7, and 8 gave 12.263, 12.274, and 12.297 abs j deg^{-1} mole^{-1}, respectively. The value 12.263 abs j deg^{-1} mole^{-1} of run 1 was selected for constructing the table.

The entropy of *N*-dimethylaminodiborane in the ideal gas state at 1 atm and 271.60°K was evaluated from the data, and the computations are summarized in table 8. To make the gas-imperfection correction, the *N*-dimethylaminodiborane vapor was assumed to follow the Berthelot equation of state. The uncertainty of ±0.6 abs j deg^{-1} mole^{-1} given for the entropy in the ideal-gas state was obtained by statistically combining the estimated uncertainties in the entropy of liquid *N*-dimethylaminodiborane at 271.60°K and in the entropy of vaporization. The uncertainty in the gas-imperfection correction was assumed negligible.

TABLE 8. *Summary of the experimental molal entropy calculated for N-dimethylaminodiborane*

Molecular weight = 70.756, °K = °C + 273.16°

	abs j deg^{-1} mole^{-1}
$S_{15°}$, Debye	1.9
$\Delta S_{15°-180°}$, solid	112.3
$\Delta S_{180°-220°}$, solid and liquid, including transitions	63.3
$\Delta S_{220°-271.60°}$, liquid	31.2
S of the liquid at 271.60° K	208.7±0.6
ΔS, vaporization, 30,119/271.60	110.9±0.1
ΔS, gas imperfection	0.1
ΔS, compression to 1 atm, R ln (94.3/760)	−17.4±0.0
S ideal gas at 1 atm and 271.60° K	302.3±0.6

8. References

[1] J. C. Southard and F. G. Brickwedde, J. Am. Chem. Soc. **55,** 4378 (1933).
[2] R. B. Scott, C. H. Meyers, R. D. Rands, Jr., F. G. Brickwedde, and N. Bekkedahl, J. Research NBS **35,** 39 (1945) RP1661.
[3] Tables of Lagrangian interpolation coefficients (Columbia University Press, New York, N. Y., 1944).
[4] H. J. Hoge, J. Research NBS **36,** 111 (1946) RP1693.
[5] N. S. Osborne and D. C. Ginnings, J. Research NBS **39,** 453, (1947) RP1841.
[6] J. G. Aston, H. L. Fink, G. J. Janz, and K. E. Russell, J. Am. Chem. Soc. **73,** 1939 (1951).
[7] H. F. Stimson, J. Research NBS **42,** 209 (1949) RP1962.
[8] H. J. Hoge and F. G. Brickwedde, J. Research NBS **22,** 351 (1939) RP1188.
[9] E. Wichers, J. Am. Chem. Soc. **74,** 2447 (1952).
[10] A. B. Burg and C. L. Randolph, Jr., J. Am. Chem. Soc. **71,** 3451 (1949).
[11] N. S. Osborne, BS J. Research **4,** 609 (1930) RP168.
[12] P. Walden, Z. physik. Chem. **66,** 385 (1909).

WASHINGTON, March 31, 1955.

Journal of Research of the National Bureau of Standards Vol. 55, No. 4, October 1955 Research Paper 2621

Phase Equilibrium Relations in the Systems Titania-Niobia and Zirconia-Niobia

R. S. Roth and L. W. Coughanour

The systems TiO_2-Nb_2O_5 and ZrO_2-Nb_2O_5 were studied by means of solid-state reactions and by observation of fusion characteristics. Two binary compounds, $TiO_2 \cdot Nb_2O_5$ and $TiO_2 \cdot 3Nb_2O_5$, were found to exist in the TiO_2-Nb_2O_5 system. One compound, $6ZrO_2 \cdot Nb_2O_5$, was found to exist in the ZrO_2-Nb_2O_5 system. This compound has been found to be essentially isostructural with $ZrO_2 \cdot TiO_2$ and has orthorhombic symmetry with the following unit cell parameters when quenched from 1,550° C: a=4.964 A, b=5.120 A, c=5.289 A. Solid-solution formation was observed in both systems. A probable equilibrium diagram is presented for each system.

1. Introduction

A study of phase relationships in the systems TiO_2-Nb_2O_5 and ZrO_2-Nb_2O_5 has been conducted as a part of a program of fundamental studies of ceramic dielectrics.[1] Some data for these systems have been reported by Durbin and Harman [1][2] and Durbin, Wagner, and Harman [2], although no phase diagrams were presented for either system.

X-ray diffraction data, together with the determination of the melting points of the compounds and of the solidus and liquidus temperatures at various compositions across the two systems, have supplied data from which equilibrium diagrams have been constructed. The phase equilibrium studies were of a preliminary nature, in an attempt to locate ceramic bodies of improved dielectric properties; consequently the conclusions should only be considered as tentative.

2. Sample Preparation and Test Methods

The following starting materials were used in the preparation of samples:

ZrO_2—Dense ZrO_2, nominal 99 percent purity, obtained from the Titanium Alloy Manufacturing Co.

TiO_2—Highly purified titania, over 99.9 percent, obtained from the Titanium Division of the National Lead Co.

Nb_2O_5—High-purity grade niobia, over 99.7 percent, obtained from the Fansteel Metallurgical Corp. The major impurity consisted of Ta_2O_5.

Calculations of weight composition were made to ±0.01 percent, no correction being made for the percentage purity of the raw materials.

The starting materials, in sufficient quantities to give a 10-g sample, were weighed to the nearest milligram. They were then mixed together with a binder of a 5-percent soluble-starch solution, and formed into 1-in.-diam disks at a pressure of 5,000 lb/in.^{2} The pressed disks were fired for 4 hr at 1,100° C on platinum foil in an air atmosphere, using an electrically-heated furnace wound with 80 percent Pt–20 percent Rh wire.

Following the preliminary heat treatment, the disks were ground, remixed with starch-solution binder, and new disks about ¼ in. high were formed at 15,000 lb/in.^{2} in a ½-in.-diam mold. Some of these disks were used for X-ray and petrographic studies, while others were used for the study of solidus and liquidus determinations. Those specimens selected for the X-ray study were refired at a temperature varying from 1,350° to 1,550° C for a time period of from 4 to 24 hr, in order to insure equilibrium conditions. X-ray powder diffraction patterns were made using a high-angle recording spectrometer and Cu$K\alpha$ radiation.

Specimens for solidus and liquidus determinations were ground in the form of small four-sided pyramids, grooved on each side, as described by Geller, et al. [3]. Tests at temperatures below 1,525° were made in the electrically heated furnace, using a Pt versus 90 Pt–10 Rh thermocouple for temperature measurements. The tests at temperatures above 1,525° were conducted in a thoria-resistor type furnace [4, 5]. The specimens rested on a disk of a platinum-rhodium alloy, which was on a support of ThO_2. The heating rate during the tests was about 4 deg C/min until the solidus temperature was approached, at which point it was reduced to about 2 deg C/min, or less. An oxidizing atmosphere existed in the furnace at all times. The temperature and fusion characteristics of the specimens were observed with an optical pyrometer calibrated by the Pyrometry Section of the Bureau. The solidus temperature was recorded as the first sign of liquid formation, as observed by rounding of the corners of the test pyramid. The temperature of complete melting, as observed by the formation of a flat button, was recorded as the liquidus temperature. In every case, several tests had to be made to determine these two values. The solidus and liquidus temperatures were arrived at by observations through the optical pyrometer and by visual inspection of the cooled specimen.

[1] This study was sponsored by the Office of Ordnance Research, Department of the Army.

[2] Figures in brackets indicate literature references at the end of this paper.

The method of determination of such temperatures is subject to a number of sources of error. Among these are the slight deviations from blackbody conditions, the introduction of small quantities of impurities into the specimens in the forming and grinding operations, the possibility of reduction of TiO_2 and Nb_2O_5 at high temperatures, and the inherent difficulty in the visual determination of the solidus and liquidus temperatures. It is believed that the temperatures as recorded are accurate to $\pm 10°$ C.

3. The TiO_2-Nb_2O_5 System

Brauer [6] reported three polymorphic forms of Nb_2O_5. The H-form, or high-temperature form, was reported as stable at temperatures above 1,200° to 1,250° C. In this study wherever free Nb_2O_5 was found, the high-temperature form was the one observed in the heated specimens, although the low-temperature form was used as the starting material.

Durbin and Harman [1] reported some fusion data for the system TiO_2-Nb_2O_5. All of the compositions between 1:4 and 4:1 were shown to begin melting between 1,440° and 1,500° C. One compound, $TiO_2 \cdot Nb_2O_5$, was observed. Durbin, Wagner, and Harman [2] reported that X-ray examination showed TiO_2:Nb_2O_5 to be a compound while $2TiO_2$:Nb_2O_5 was a mixture containing rutile.

Petrographic analyses in the present study were not relied upon, as all of the phases containing at least 50 percent Nb_2O_5 appeared very similar under the microscope. However, X-ray analyses succeeded in differentiating two compounds in the system TiO_2-Nb_2O_5. Figure 1 is a graphical representation of the X-ray diagrams for values of 2θ between 16° and 49° for compositions of the following molecular ratios: Nb_2O_5, TiO_2:$9Nb_2O_5$, TiO_2:$4Nb_2O_5$, TiO_2:$3Nb_2O_5$, TiO_2:$2Nb_2O_5$, $2TiO_2$:$3Nb_2O_5$, and TiO_2:Nb_2O_5. These compositions were heated at either 1,350° or 1,400° C for 3 hr and quenched

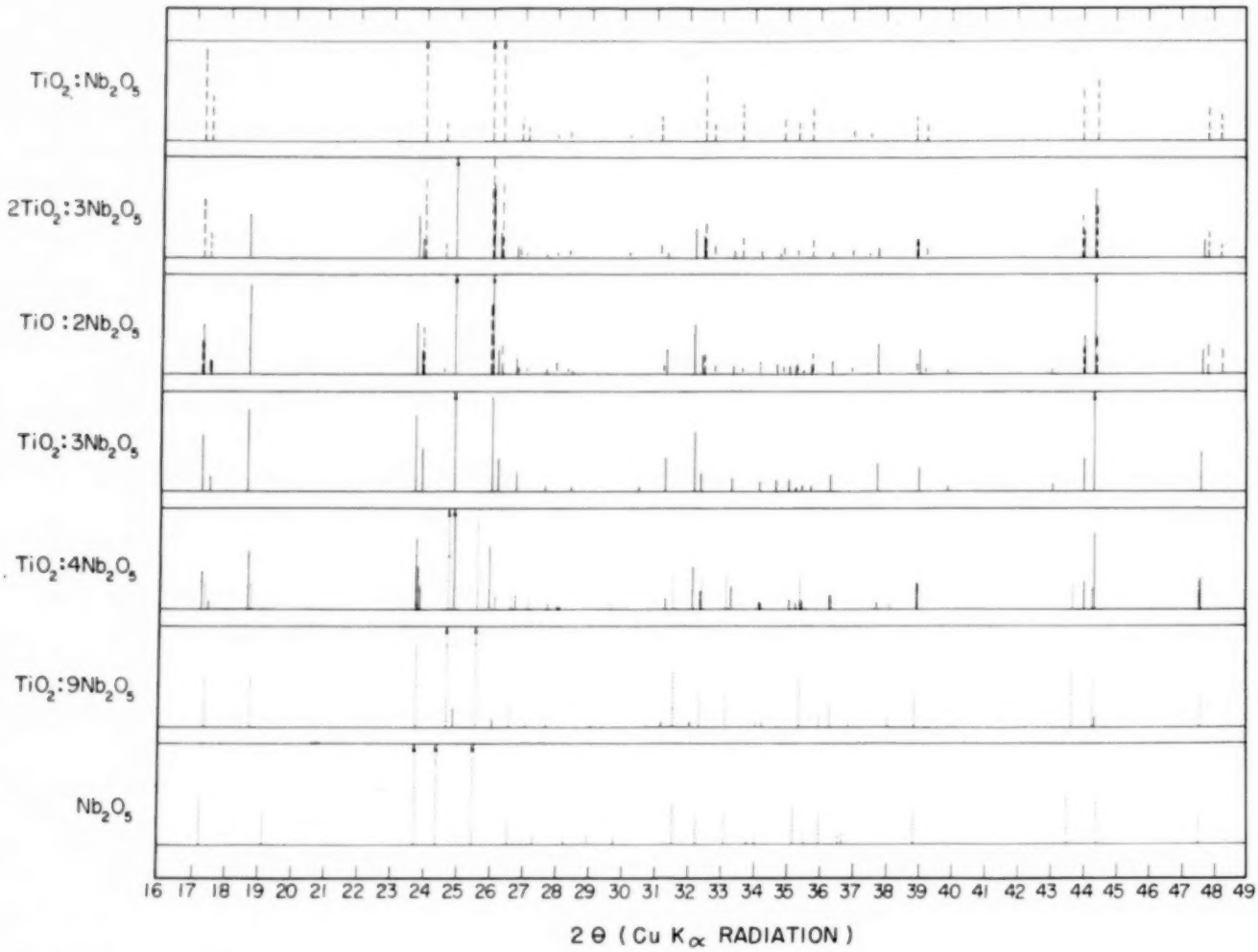

FIGURE 1. *Graphical representation of the X-ray powder diffraction patterns for the compositions* Nb_2O_5, TiO_2:$9Nb_2O_5$, TiO_2:$4Nb_2O_5$, TiO_2:$3Nb_2O_5$, TiO_2:$2Nb_2O_5$, $2TiO_2$:$3Nb_2O_5$, *and* TiO_2:Nb_2O_5 *from 16° 2θ to 49° 2θ.*

Interference maxima for Nb_2O_5 are shown as dotted lines, for TiO_2-$3Nb_2O_5$ as solid lines, and for TiO_2-Nb_2O_5 as dashed lines. Relative intensity is represented by the height of the lines. TiO_2-Nb_2O_5, TiO_2-$3Nb_2O_5$ and Nb_2O_5 are compounds while the others are mixtures of the conjugate phases.

in air. Although there are many overlapping lines in the diffraction pattern, it can be seen that TiO_2:$3Nb_2O_5$ and TiO_2:Nb_2O_5 are probably pure compounds, while the other diagrams are mixtures of the two conjugate phases. The X-ray diffraction data for $TiO_2 \cdot Nb_2O_5$ and $TiO_2 \cdot 3NbO_5$ are given in tables 1 and 2. It is possible that the compound designated $TiO_2 \cdot 3Nb_2O_5$ may actually be intermediate in composition between TiO_2:$3Nb_2O_5$ and TiO_2:$2Nb_2O_5$; however, the simple ratio of 1:3 is taken as the most logical composition for this compound.

The fusion-behavior data from which the equilibrium diagram is constructed are given in table 3, and the diagram is shown in figure 2. It may be seen that the compound $TiO_2 \cdot Nb_2O_5$ melts congruently at about 1,490° C and the compound $TiO_2 \cdot 3Nb_2O_5$ melts congruently at about 1,480 °C. At the eutectic temperature, 1,467° C and 21 mole percent TiO_2, 12 to 13 mole percent TiO_2 is accepted into solid solution by Nb_2O_5. At the eutectic temperature, 1,475° C and 58 mole percent TiO_2, about 17 mole percent Nb_2O_5 is found in solid solution in TiO_2. Both of the solid solutions decrease to slightly less than 10 percent at room temperature. The

TABLE 1. *X-ray powder diffraction data for the compound* $TiO_2 \cdot Nb_2O_5$, *furnace cooled from 1,400° C*

(CuKα1 radiation)

d	R. I.[a]	*d*	R. I.[a]	*d*	R. I.[a]
A		*A*		*A*	
10. 2	19	1. 884	18	1. 270	14
9. 4	16	1. 849	7		
5. 13	65	1. 778	6	1. 267	13
5. 06	43			1. 264	10
3. 71	100++[b]	1. 760	9	1. 224	6
		1. 740	9	1. 216	9
3. 61	18	1. 722	13	1. 208	7
3. 42	100+++[b]	1. 712	9		
3. 38	100+[b]	1. 698	9	1. 143	4
3. 31	22			1. 112	8
3. 28	17	1. 662	43	1. 085	8
		1. 652	11	1. 064	5
3. 14	6	1. 622	10	1. 057	5
2. 95	7	1. 579	8		
2. 87	23			1. 049	7
2. 75	53	1. 566	9	1. 035	5
2. 73	14	1. 556	14	1. 017	4
		1. 545	13	0. 9993	8
2. 66	25	1. 528	6	. 9502	17
2. 57	15	1. 518	18		
2. 54	13			. 9476	14
2. 51	22	1. 475	6	. 9393	6
		1. 469	12	. 9298	12
2. 42	17	1. 456	9	. 9209	6
2. 39	16	1. 438	7	. 9127	4
2. 31	18	1. 395	15		
2. 29	12			. 8536	4
2. 055	42	1. 389	17	. 8279	12
		1. 291	4	. 8019	11
2. 035	48	1. 285	9		
1. 899	26	1. 272	13		

[a] Relative intensity of diffraction peaks.
[b] These peaks were too strong to be completely recorded on the chart.

TABLE 2. *X-ray powder diffraction data for the compound* $TiO_2 \cdot 3Nb_2O_5$, *quenched from 1,400° C*

(CuKα1 radiation)

d	R. I.[a]	*d*	R. I.[a]
A		*A*	
14. 2	14	2. 090	5
9. 6	29	2. 053	29
7. 2	18	2. 039	100+[b]
5. 13	43	1. 907	31
4. 75	70	1. 785	21
3. 75	68	1. 752	11
3. 71	42	1. 697	10
3. 57	100++[b]	1. 682	15
3. 42	82	1. 677	29
3. 33	19	1. 663	25
2. 85	29	1. 574	22
2. 78	49	1. 551	9
2. 68	10	1. 448	8
2. 62	8	1. 398	8
2. 58	9	1. 394	9
2. 56	9	1. 298	36
2. 47	11	1. 135	21
2. 38	25	1. 051	11
2. 30	22		

[a] Relative intensity of diffraction peaks.
[b] These peaks were too strong to be completely recorded on the chart.

TABLE 3. *Fusion characteristics of compositions in the* TiO_2-Nb_2O_5 *system*

Composition mole percent		Temperature observed		X-ray examination of quenched samples [a]
TiO_2	Nb_2O_5	Solidus	Liquidus	
%	%	°C	°C	
95	5	1, 780	1, 800	
90	10	1, 510	.....	
85. 71	14. 29	1, 490	.....	
80	20	1, 475	.....	$TiO_2 \cdot Nb_2O_5$+TiO_2 solid solution.
75	25	1, 475	.....	Do.
67	33	1, 475	1, 500	Do.
60	40	1, 470	1, 480	
50	50	1, 490	1, 490	$TiO_2 \cdot Nb_2O_5$.
40	60	1, 465	1, 470	$TiO_2 \cdot 3Nb_2O_5$+$TiO_2 \cdot Nb_2O_5$.
33	67	1, 465	1, 475	Do.
25	75	1, 480	1, 480	$TiO_2 \cdot 3Nb_2O_5$.
20	80	1, 465	1, 470	Nb_2O_5 solid solution+$TiO_2 \cdot 3Nb_2O_5$.
16. 67	83. 33	.....	1, 475	
14. 29	85. 71	.....	.....	
10	90	1, 475	1, 485	Nb_2O_5 solid solution+$TiO_2 \cdot 3Nb_2O_5$.
5	95	1, 485	1, 495	
0	100	1, 500	1, 500	Nb_2O_5.

[a] Specimens for X-ray analyses were quenched, but compounds found may not have been those present at quenching temperature.

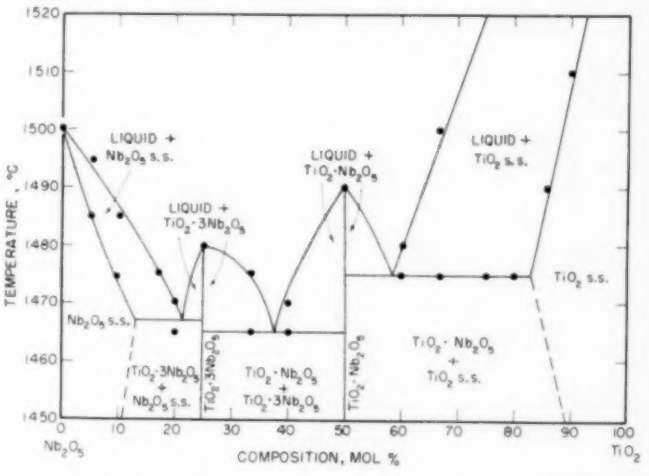

FIGURE 2. *Suggested equilibrium diagram for the system* TiO_2-Nb_2O_5.

(s. s. = solid solution)

eutectic between the two binary compounds occurs about 38 mole percent TiO_2 and 1,465° C. Neither of the two binary compounds shows solid solution.

4. The ZrO_2-Nb_2O_5 System

Durbin and Harman [1] reported some fusion data for the system ZrO_2–Nb_2O_5. Compositions high in Nb_2O_5 were reported as melting between about 1,400° and 1,450° C while mixtures higher in ZrO_2 melted between 1,450° and 1,550° C. Durbin, Wagner, and Harman [2] found solid solution of ZrO_2 in Nb_2O_5. These authors claimed that X-ray diffraction showed that cubic ZrO_2 was stabilized, indicating solid solution of Nb_2O_5 in ZrO_2. They report no compounds in this system.

In the present study, X-ray analyses have indicated the presence of a new compound, $6ZrO_2 \cdot Nb_2O_5$, in the system ZrO_2-Nb_2O_5. The X-ray pattern is very similar, both in *d* values and relative intensities, to that of the compound $ZrO_2 \cdot TiO_2$ [7]. The similarity between the compounds becomes apparent if the composition of the compound $6ZrO_2 \cdot Nb_2O_5$ is written as $Zr_4(Nb_2,Zr_2)O_{16}O$ and compared with $4ZrTiO_4$ or $Zr_4Ti_4O_{16}$. It seems possible that the structural arrangement of this compound may be capable of accommodating an additional one-fourth of an oxygen ion per formula unit. Because of the similarity of Nb_2O_5 and Ta_2O_5, a specimen of $6ZrO_2 \cdot Ta_2O_5$ was prepared and studied by X-ray diffraction. This composition proved to be isostructural with $6ZrO_2 \cdot Nb_2O_5$ and $ZrO_2 \cdot TiO_2$. All three compounds are orthorhombic with unit cell parameters as shown in table 4. The X-ray powder diagram for the compound $6ZrO_2 \cdot Nb_2O_5$ is given in table 5. Another possible interpretation of the structure occurring at the composition $6ZrO_2 \cdot Nb_2O_5$ is that of a solid solution of ZrO_2. This would be similar to the case of the cubic ZrO_2 solid solutions in the systems involving ZrO_2 and oxides of divalent ions like CaO, MgO, MnO, and TiO. However, the identity of $ZrO_2 \cdot TiO_2$ as a compound seems to be fully established [7,8]. The similarity of the structures of the two compositions justifies the assumption of $6ZrO_2 \cdot Nb_2O_5$ as a true compound. Apparently the cubic ZrO_2 solid solution reported by Durbin, et al. [2] in this system was actually the compound $6ZrO_2 \cdot Nb_2O_5$. Their interpretation may be explained by the fact that the strongest diffraction lines for the compound are close to what would be expected for a cubic ZrO_2 solid solution.

The equilibrium diagram for the ZrO_2-Nb_2O_5 system, as determined from the present study, is shown in figure 3 and the fusion-behavior data from

TABLE 4. *Unit cell parameters for the isostructural compounds,* $ZrO_2 \cdot TiO_2$, $6ZrO_2 \cdot Nb_2O_5$, *and* $6ZrO_2 \cdot Ta_2O_5$

Compound	$ZrO_2 \cdot TiO_2$	$6ZrO_2 \cdot Nb_2O_5$	$6ZrO_2 \cdot Ta_2O_5$
	A	A	A
a	4.892	4.964	4.961
b	5.034	5.120	5.117
c	5.483	5.289	5.278

TABLE 5. *X-ray powder diffraction data for the compound* $6ZrO_2 \cdot Nb_2O_5$, *quenched from 1,550° C*

[$CuK_{\alpha 1}$ radiation]

d	*hkl*	R. I.[a]	*d*	*hkl*	R. I.[a]
A			A		
4.92	100 (?)	1	1.138	------	9
3.61	101	9	1.125	------	2
2.95	111	100	1.118	------	3
2.64	002	17	1.098	------	3
2.56	020	18	1.092	------	4
2.48	200	12	1.062	------	3
2.35	012	6	1.046	------	6
2.31	021	2	1.034	------	3
2.244	201/210	1	1.030	------	4
2.179	112	1	1.014	------	3
2.091	121	6	0.9856	------	7
2.020	211	3	.9634	------	3
1.838	022	23	.9589	------	6
1.809	202	21	.9197	------	1
1.782	220	28	.8914	------	7
1.706	212	10	.8783	------	2
1.690	103	11	.8719	------	2
1.579	113	19	.8681	------	3
1.545	131	22	.8657	------	3
1.511	311	18	.8600	------	3
1.478	222	14	.8536	------	3
1.456	023	1	.8480	------	3
1.435	032	3	.8452	------	3
1.393	123	7	.8416	------	4
1.321	004	2	.8195	------	5
1.281	040/014	7	.8122	------	1
1.243	400	4	.8074	------	2
1.207	------	3	.8046	------	3
1.191	------	6	.7998	------	2
1.175	------	6	.7902	------	2
1.167	------	3	.7882	------	1
1.160	------	7	.7827	------	1
1.153	------	3	.7810	------	3

[a] R. I. is the intensity of each diffraction peak relative to the strongest peak.

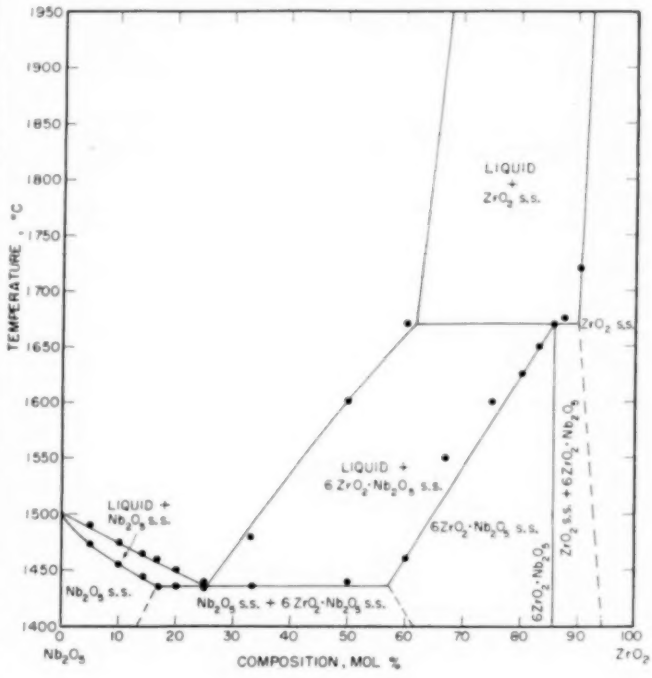

FIGURE 3. *Suggested equilibrium diagram for the system* ZrO_2-Nb_2O_5.

(s. s. = solid solution)

which the diagram was constructed are listed in table 6. It is seen that the compound $6ZrO_2 \cdot Nb_2O_5$ melts incongruently at about 1,670° C. The eutectic point for the system is located at about 25 mole percent ZrO_2 and 1,435° C. Rather extensive solid-solution formation is noted at the higher temperatures. Nb_2O_5 accepts about 16 percent ZrO_2 into solid solution at the eutectic temperature, and there is considerable solid solution between the $6ZrO_2 \cdot Nb_2O_5$ compound and Nb_2O_5. This solid solution is apparently not maintained by quenching, as X-ray patterns of compositions within this field show two phases. ZrO_2 apparently also accepts a small amount of Nb_2O_5 in solid solution at the higher temperatures, but loses most of it on cooling.

TABLE 6. *Fusion characteristics of compositions in the* ZrO_2–Nb_2O_5 *system*

Composition mole percent		Temperature observed		X-ray examination of quenched samples [a]
ZrO_2	Nb_2O_5	Solidus	Liquidus	
%	%	°C	°C	
95	5	>1,850	.....	
90	10	1,725	.....	$6ZrO_2 \cdot Nb_2O_5$+monoclinic ZrO_2.
87.50	12.50	1,675	.....	Do.
85.71	14.29	1,670	.....	$6ZrO_2 \cdot Nb_2O_5$.
83.33	16.67	1,650	.....	$6ZrO_2 \cdot Nb_2O_5$ solid solution.
80	20	1,625	.....	.....
75	25	1,600	.....	.....
67	33	1,550	.....	Nb_2O_5 solid solution+$6ZrO_2 \cdot Nb_2O_5$ solid solution.
60	40	1,460	1,670	.....
50	50	1,440	1,600	Nb_2O_5 solid solution+$6ZrO_2 \cdot Nb_2O_5$ solid solution.
40	60	.....	.....	.....
33	67	1,435	1,480	Nb_2O_5 solid solution+$6ZrO_2 \cdot Nb_2O_5$ solid solution.
25	75	1,435	1,440	
20	80	1,435	1,450	Nb_2O_5 solid solution+$6ZrO_2 \cdot Nb_2O_5$ solid solution.
16.67	83.33	1,435	1,460	
14.29	85.71	1,445	1,465	
10	90	1,455	1,475	
5	95	1,475	1,490	

[a] Specimens for X-ray analyses were quenched but compounds found may not have been those present at quenching temperature.

5. Summary

The systems TiO_2-Nb_2O_5 and ZrO_2-Nb_2O_5 were studied by means of solid-state reactions, fusion characteristics and X-ray diffraction data. The probable existence of two compounds in the TiO_2-Nb_2O_5 system was shown. They are $TiO_2 \cdot Nb_2O_5$ which melts congruently at about 1,490° C. and $TiO_2 \cdot 3Nb_2O_5$ which melts congruently at about 1,480° C. The three eutectic points are located as follows: 21 mole percent TiO_2 and 1,467° C., about 38 mole percent TiO_2 and 1,465° C, and about 58 mole percent TiO_2 and 1,475° C. Partial solid-solution formation was noted in this system.

One compound, $6ZrO_2 \cdot Nb_2O_5$, was found to occur in the ZrO_2-Nb_2O_5 system. The compound is essentially isostructural with $ZrO_2 \cdot TiO_2$ and melts incongruently at about 1,670° C. The eutectic point for the system was located at about 25 mole percent ZrO_2 and 1,435° C. Extensive solid-solution formation was noted.

6. References

[1] E. A. Durbin and C. G. Harman, Battelle Memorial Inst. **791** (Dec. 15, 1952).
[2] E. A. Durbin, H. E. Wagner, and C. G. Harman, BMI-**792** (Dec. 15, 1952).
[3] R. F. Geller, P. J. Yavorsky, B. L. Steierman, and A. S. Creamer, J. Research NBS **36,** 277 (1946) RP1703.
[4] R. F. Geller, J. Research NBS **27,** 555 (1941) RP1443.
[5] S. M. Lang and R. F. Geller, J. Am. Ceram. Soc. **34,** 193 (1951).
[6] G. Brauer, Z. anorg. u. allgem. Chem. **248,** 1–31 (1941).
[7] L. W. Coughanour, R. S. Roth, and V. A. DeProsse, J Research NBS **52,** 37 (1954) RP2470.
[8] F. H. Brown and P. Duwez, J. Am. Ceram. Soc. **37,** 129 (1954).

WASHINGTON, May 27, 1955.

Journal of Research of the National Bureau of Standards Vol. 55, No. 4, October 1955 Research Paper 2622

Synthesis of a Fluoro Talc and Attempted Synthesis of Fluoro Chrysotile and Fluoro Anthophyllite[1]

Alvin Van Valkenburg, Jr.

As part of a general study of the substitution of fluorine for hydroxyl in silicate structures, it was found that fluorine would partially substitute for hydroxyl in the talc structure. As a result of this substitution it was observed that the γ index of refraction was lowered by 0.01 and the temperature of thermal decomposition was raised about 180° C. Attempts to convert a fluoro talc to a fluoro anthophyllite hydrothermally were not successful. Also fluorine substitution for hydroxyl in chrysotile was not achieved hydrothermally.

1. Introduction

As part of a general study of the substitution of fluorine for hydroxyl in silicate structures, it was observed that talc ($3MgO{\cdot}4SiO_2{\cdot}H_2O$) readily formed as a reaction product while attempting to synthesize a chrysotile ($3MgO{\cdot}2SiO_2{\cdot}2H_2O$) containing fluorine. In those chrysotile experiments in which fluorine was absent from the batch ingredients only an occasional talc grain was detected in the reaction products and this suggested that fluorine might be aiding the formation of talc, possibly substituting for a hydroxyl. A review of the literature indicated that fluorine had never been reported in talc in significant amounts and most chemical analyses omit fluorine determinations entirely. In one reference [1][2] talc was found closely associated with a fluorine bearing hydroxyapatite, $3Ca_3P_2O_8{\cdot}Ca(OH,F)_2$. However, the chemical analysis showed only trace amounts of fluorine present and the authors concluded that hydroxyapatite had a greater affinity for fluorine than did talc.

The talc hydroxyl is structurally similar to the hydroxyl of the phlogopite micas, $K_2Mg_6Si_6Al_2O_{20}(F, OH)_4$. Both hydroxyls are located between layered sheets of SiO_4 groups and both are bonded to magnesium ions. The two minerals liberate their hydroxyls at temperatures of 800 to 900° C at 1 atm which indicates that the hydroxyl bonding energies are similar. Since the hydroxyls of the phlogopite micas can be substituted entirely by fluorine [2] it appeared reasonable that fluorine might enter the talc structure and a study was instigated to determine the nature of this possible substitution.

2. Experimental Procedure

The technique for synthesizing talc was essentially the same as that described by Bowen and Tuttle [3] in which stoichiometric proportions of MgO and SiO_2 were subjected to hydrothermal pressures obtained by using Morey-Ingerson type steel pressure bombs [4] or a Tuttle hydrothermal apparatus [5]. The inner walls of the bombs were lined with platinum to prevent contamination of the ingredients by steel and its alloys. In the Tuttle apparatus the batch ingredients were sealed in a platinum cylinder. Distilled water was added to the bombs and platinum cylinders in excess of that needed to satisfy the talc hydroxyl requirements. Batch samples were prepared by thoroughly grinding together the ingredients in a mechanical mortar to insure good mixing and to increase the reactivity of the ingredients by increasing the surface area. Calculated amounts of fluorine were added to the batch in the form of MgF_2 to give varying ratios of F:OH. The reaction products were examined by microscopic, X-ray, and differential thermal analysis techniques, and the data were compared with those of natural talcs. Careful examinations were made of the reaction products to detect the presence of MgF_2 as its presence in any appreciable amount would indicate that fluorine failed to enter the talc structure. MgF_2 has extremely low indices of refraction and can readily be detected microscopically in the presence of talc. The MgF_2 introduced into the raw batches had grains of irregular and indistinct outline. In comparison the MgF_2 observed in the reaction products of some experiments were well formed needles indicating they were formed as products of recrystallization. This eliminated the doubt that MgF_2 observed in reaction products might have resulted from incomplete reaction. Table 1 gives a list of experiments and their reaction products.

TABLE 1. *Hydrothermal fluoro-talc synthesis*

Experiment	F sub. for OH in batch	Temperature	Hydrothermal pressure	Time	Major phases
	%	°C	*psi*	*Hours*	
1	25	400	16,000	72	Talc [a]
2	40	400	20,000	16	Do.
3	40	500	18,000	72	Do.
4	40	600	18,000	72	Do.
5	40	700	20,000	16	Do.
6	50	400	18,000	72	Do.
7	50	706	16,000	1	Do.
8	50	808	16,000	5½	Do.
9	55	409	18,000	24	Talc+MgF_2+SiO_2
10	66	400	16,000	120	Do.
11	75	800	18,000	60	Do.
12	75	700	20,000	16	Do.
13	75	410	18,000	72	Do.
14	100	408	18,000	96	Do.
15	100	800	18,000	60	Do.

[a] In all cases, the talcs mentioned in this table contain fluorine.

[1] The program of fluorine substitution in hydrous silicates is sponsored by the Office of Naval Research.

[2] Figures in brackets indicate the literature references at the end of this paper.

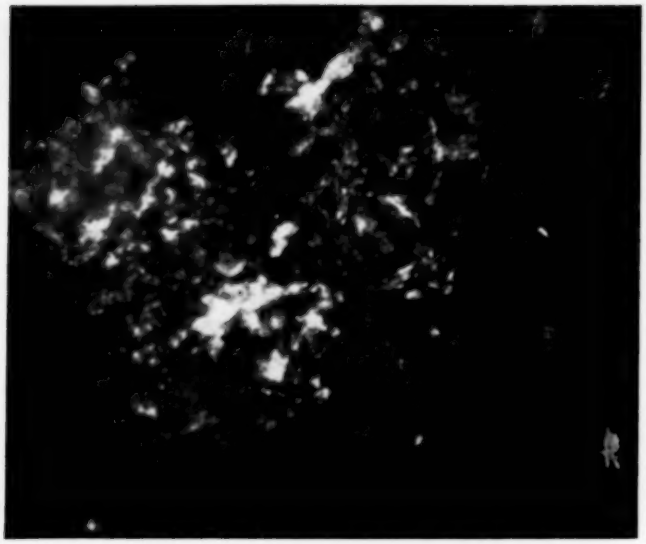

FIGURE 1. *Fluoro talc grains showing matted fibers in aggregate form.*

Crossed nicols, magnification, X 600.

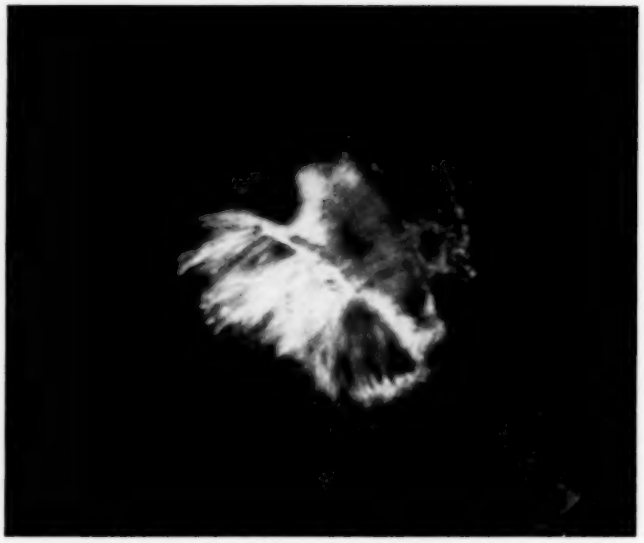

FIGURE 2. *Fluoro talc grain with fibers in parallel orientation.*

Crossed nicols, magnification, X 600.

Talc was the major phase observed in all the experiments prepared in the temperature range from 400° to 800° C and at 16,000 to 20,000 psi. Two general forms of talc were observed, one showing a matted fibrous aggregate in which the fibers appeared to be randomly oriented (fig. 1) and the second showing talc grains with fibers in parallel orientation (fig. 2). In both cases the fibers were extremely fine grained and it was difficult to obtain good optical data.

The refractive indices for pure synthetic hydroxyl-talc are approximately $\gamma=1.570$ and $\alpha=1.540$ which correspond to the observations of Yoder [6]. In comparison, the indices of the talcs containing the maximum fluorine content (experiments in which F:OH was 1:1 or greater) were approximately $\gamma=1.560$ and $\alpha=1.540$. As fluorine was substituted for hydroxyl there was a corresponding decrease in the γ indices of refraction. This lowering of the γ index indicates that fluorine is entering the talc structure. Previously, investigators [7] have established the fact that when fluorine substitutes for hydroxyl there is a lowering of the refractive indices and the amount of lowering is proportional to the fluorine present.

In those experiments where the calculated ratio of F:OH was 1:1 or less, the major phase was a fluoro talc with an occasional grain of quartz or MgF_2 present. However, when the ratio became greater than 1:1, MgF_2 was readily observed under the microscope in appreciable quantities. This would indicate that fluorine may be substituted for hydroxyl up to 50 mol percent.

The X-ray powder patterns of the synthetic fluoro talcs were identical to those of synthetic talcs without fluorine. Unfortunately the powder patterns of the synthetic talcs do not give sharp, clear reflections. The diffracted beams are broad and diffuse, characterizing poorly crystallized material.

Differential thermal/analysis studies were made on the fluoro talcs, and the results were compared to a synthetic talc without fluorine and to natural talcs. The apparatus used in these studies is similar to that used in other laboratories. A heating and cooling rate of about 12 deg/min was employed. Curve 1 (fig. 3) contains a typical endothermic reaction peak of a natural talc and it corresponds to the differential thermal analysis curves obtained by Pask and Warner [8]. The endothermic reaction peak at 970° C denotes the loss of hydroxyl in the talc. In comparison curve 2 is a typical differential thermal curve for a synthetic talc without fluorine. The general slopes of the two curves are essentially the same. However, their maximum endothermic peaks do not occur at the same temperature and it is believed that the thermal difference may be attributed to a difference in particle size of the two samples. The synthetic talc has extremely fine thread-like masses aggregated into grains and in comparison the natural talcs were artificially ground into a powder consisting of platy grains of uniform crystallinity. Curve 3 represents a differential thermal analysis of a synthetic fluoro talc in which the ratio of F:OH was calculated to be 1:1. The endothermic peak at 100° C is believed to be the result of interstitial or surface water escaping from the undried sample just removed from the hydrothermal bomb. The endothermic double peak with maximum intensities at 1,070° and 1,085° C probably represent reactions in which hydroxyl and possibly fluorine were released. The exothermic peak at 1,230° C may indicate a recrystallization phenomenon in which MgF_2, cristobalite and enstatite are forming. The endothermic peaks occurring at 1,250° and 1,290° C are similar to the endothermic peaks of curve 4 which

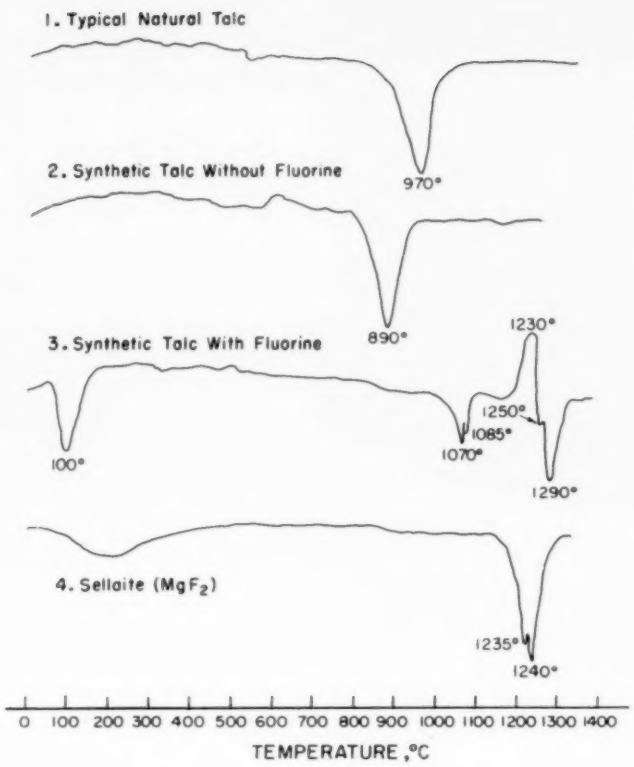

FIGURE 3. *Differential thermal curves.*

1, Typical natural talc; 2, synthetic talc without fluorine; 3, synthetic talc with fluorine; 4, sellaite (MgF_2).

represent a differential thermal curve for MgF_2. It is believed that these peaks represent the breakdown of MgF_2 with the release of fluorine. A comparison of the endothermic peaks of curves 2 and 3 shows that the fluoro talc has a higher thermal stability than does its hydroxyl analogue. Furthermore, the exothermic peak of curve 3 occurring at 1,230° C is lacking in curve 2, indicating that the presence of fluorine alters the course of reaction in the talcs.

Bowen and Tuttle [3] have shown that a synthetic anthophyllite $7MgO{\cdot}8SiO_2{\cdot}H_2O$ can be synthesized by heating a synthetic talc to 800° C with a hydrostatic pressure of 16,000 psi for a period of 1 hr. Longer heatings result in the breakdown of anthophyllite into enstatite and cristobalite. This was confirmed in the present investigation. Attempts to convert a fluoro talc into a fluoro anthophyllite were unsuccessful. Samples of fluoro talc were treated hydrothermally for 1 hr and 5½ hr at 800° C and 16,000 psi. The talc did not appear to have changed in either case as the X-ray and optical data were identical to those of the untreated material.

As stated in the beginning of this paper attempts were made to synthesize a fluoro chrysotile by a process essentially the same as that described for synthetic talc. Stoichiometric proportions of MgO and SiO_2 were sealed in a platinum container with water in excess of that required for formula proportions and a pressure of 16,000 psi and a temperature of 400° C were employed. These conditions are within the stability range for synthetic talc [3]. The chrysotile observed under the microscope consisted of irregular masses having low birefringence and a mean index of refraction of these masses was about 1.540. When fluorine in the form of MgF_2 was added stoichiometrically to the chrysotile batch there was no apparent lowering of the mean refractive index of the resulting chrysotile. Also the X-ray powder pattern of the chrysotile did not change. These two observations indicates that the hydroxyl in chrysotile does not favor substitution by fluorine.

The author gratefully acknowledges the assistance rendered by G. F. Rynders, R. G. Pike, and others who contributed their time to the project.

3. References

[1] L. Mitchell, G. T. Faust, S. B. Hendricks, and D. S. Reynolds, The mineralogy and genesis of hydroxyapatite, Am. Mineralogist **28,** 356 (1934).
[2] A. Van Valkenburg and R. G. Pike, The synthesis of mica, J. Research NBS **48,** 360 (1952) RP2323.
[3] N. L. Bowen and J. F. Tuttle, The system MgO-SiO_2-H_2O, Geol. Soc. Amer. **60,** 439 (1949).
[4] Morey and Ingerson, Alterations and synthesis of silicates, Econ. Geol. **32,** 607 (1937).
[5] John Van Den Heurk, Improved hydrothermal quenching apparatus, Bull. Geol. Soc. Amer. **64,** 993 (1953).
[6] American Journal of Science, Bowen Vol., 573 (1952).
[7] N. L. Bowen and J. F. Schairer, Grunerite from Rockport, Mass., and a series of synthetic fluo-amphiboles, Am. Mineralogist **20,** 543 (1935).
[8] J. A. Pask and M. F. Warner, J. Am. Ceram. Soc. **37,** 126 (1954).

WASHINGTON, May 2, 1955.

Journal of Research of the National Bureau of Standards Vol. 55, No. 4, October 1955 Research Paper 2623

Determination of Natural Rubber in GR-S—Natural Rubber Vulcanizates by Infrared Spectroscopy

Max Tryon, Emanuel Horowitz, and John Mandel

A rapid method for the estimation of natural rubber in vulcanizates of GR-S and natural rubber by means of infrared spectroscopy is reported. Samples were carefully prepared to contain known amounts of natural and GR-S rubber; the samples were vulcanized, extracted with acetone, and dried in a vacuum oven. Specimens from each sample were pyrolyzed in a combustion furnace at 550° C and the liquid pyrolyzates were analyzed by infrared absorption spectroscopy. An empirical relationship was developed in which the band intensities at 11.02 and 11.25 microns were related to natural rubber content. The experimental error of the method is characterized by a standard deviation of a single determination of 0.023, which represents approximately 3-percent natural rubber.

1. Introduction

Rubber chemists have long been aware of the limitations of current methods for the quantitative determination of rubber content of vulcanizates. For natural rubber, the direct method of analysis [1] [1] involves digestion of the sample with chromic acid, distillation of the acetic acid formed during oxidation, and titration of the distillate with standardized sodium hydroxide. This method requires considerable time and a large correction factor. In addition, unreliable results are often obtained for mixtures of natural and synthetic rubber. In the indirect method [2], all the constituents other than rubber hydrocarbon are determined, and the rubber content is calculated by difference. The procedures in this method are long and tedious, and the value obtained for rubber content reflects the cumulative error involved in the separate analyses for the nonrubber constituents. Synthetic rubber, whether alone or mixed with natural rubber, is not differentiated as such, but is merely determined as rubber hydrocarbon.

Burchfield [3] reported a qualitative method of analysis for natural and synthetic rubber in which the rubber vulcanizate is pyrolyzed, and the volatile products are collected in an indicating solution. The polymer type is then identified by the change in color of the solution. A superior method for the identification of natural and synthetic rubber was reported by Harms [4], in which the rubber is pyrolyzed in a test tube with a Bunsen burner and a portion of the decomposition products is analyzed by infrared spectroscopy. Bentley and Rappaport [5] applied a modification of Harms' method to the semiquantitative determination of nitrile rubber (Buna N) in mixtures with a phenolic resin.

The work described in this paper was undertaken in order to develop a rapid and reliable method for the quantitative estimation of natural and synthetic rubber in vulcanized rubber compounds. It was found in this work that most of the spectral absorption bands of pyrolysis products obtained from vulcanized samples of natural rubber, GR–S [2], and mixtures of these two polymers, are reproducible both in the wavelength of peak absorption and in relative intensity. Hence, the pyrolyzate lends itself to quantitative analysis for the original polymer.

In agreement with Harms [4], it was observed, early in this work, that the pyrolysis products of natural rubber showed a strong, distinct absorption band at 11.25 μ, while the products from GR–S showed a similar strong absorption band at 11.02 μ. The relative intensities of these two bands varied as the relative concentrations of the two rubbers were varied, in mixtures of the two materials. As these two bands are characteristic of the two polymers in question, and are adjacent to one another, allowing simple base line corrections and ratio measurements, the possibility of using the relative intensities of these bands as a measure of the natural rubber content was investigated. No attempt was made in this work to define the structures responsible for these bands. It was noted, however, that the band at 11.02 μ is also found in polybutadiene pyrolysis products. In qualitative analysis for GR–S, bands other than the 11.02 μ band are necessary to distinguish the material from polybutadiene. These bands in GR–S, as noted by Harms, are found at 6.22, 6.66, and 14.34 μ.

2. Method

Six samples of natural rubber, GR–S, and mixtures of these two polymers were prepared, according to the recipe given in table 1, using 100, 80, 60, 40, 20, and 0 percent of natural rubber. They were vulcanized at 140° C for one hr. The individual samples were then separately milled and extracted with acetone for 24 hr to remove soluble nonrubber constituents that might complicate the infrared spectra. The rubber samples were dried in a vacuum oven at 50° C for 2 hr to remove the solvent, and the samples were stored in an airtight container. The milling,

[1] Figures in brackets indicate the literature references at the end of this paper.

[2] GR–S is a synthetic rubber made by copolymerizing butadiene and styrene in the approximate proportion of 77 to 23 percent by weight, respectively. The GR–S sample used in this work contained 22.9 percent bound styrene. It is estimated, from work with similar mixtures of natural rubber and polybutadiene, that variations in the styrene content of GR–S of as much as 1-percent bound styrene in the polymer will not affect the calculated natural rubber content in a mixture by more than ±0.3-percent natural rubber.

TABLE 1. *Vulcanization recipe*

	Parts by weight
Total polymer	100
NBS standard channel black	40
Zinc oxide	5
Sulfur	2.5
Stearic acid	2
Altax (benzothiazyl disulfide)	1.5
Total compound	151.0

extraction, and vacuum drying are necessary steps in both of the usual chemical procedures [1, 2].

Four 0.5-gram specimens of each of the six rubber samples were weighed in 16×150-mm test tubes. The order of test of the specimens was according to a statistical design, that is discussed below in greater detail. Each specimen was pyrolyzed in a modified combustion tube furnace, figure 1, that was maintained at 550° C, and the liquid distillate was collected in a micro test tube. In a preliminary study, the temperature was varied between 400° and 550° C, and only a small effect on the analytical results was noted.

A portion of the pyrolyzate was placed between two sodium chloride windows, using a lead spacer 0.025 mm thick. The infrared spectrum was obtained for each of the pyrolyzates in the 10.0 to 12.0 μ region, using a Perkin-Elmer, model 21 recording spectrophotometer with sodium chloride optics.

Typical spectra for the pyrolyzates, obtained from the six samples of vulcanized rubber, are shown in figure 2. The time required for the six separate pyrolyses and infrared analyses is of the order of one hr.

An empirical relationship was developed for the quantitative estimation of percent natural rubber. Ratios of the transmittances at 11.02 and 11.25 μ wavelengths, corrected for background, were used to minimize variations in cell thickness from run to run. It was found that the logarithm of this ratio was very nearly a linear function of the concentration of natural rubber in the total polymer. This is demonstrated in figure 3. In order to avoid negative values, the ratios were multiplied by 10, prior to taking the common logarithm of the ratio.

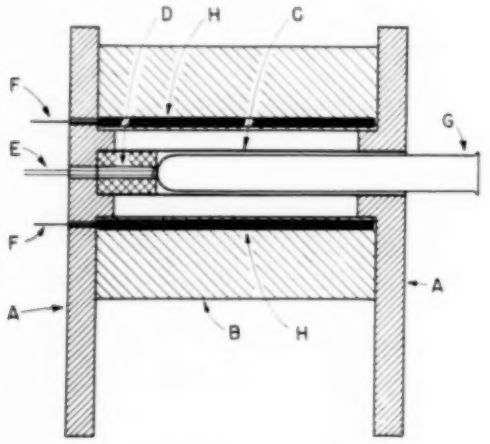

FIGURE 1. *Modified combustion-train furnace for pyrolysis of polymers.*

A, Transite sheet; B, furnace from combustion train; C, stainless steel tube; D, steel plug with hole for thermocouple; E, thermocouple; F, heater leads; G, test tube; H, heater coils.

Thermocouple and heater leads connect to some type of indicator-control device such as a Wheelco Capacitrol.

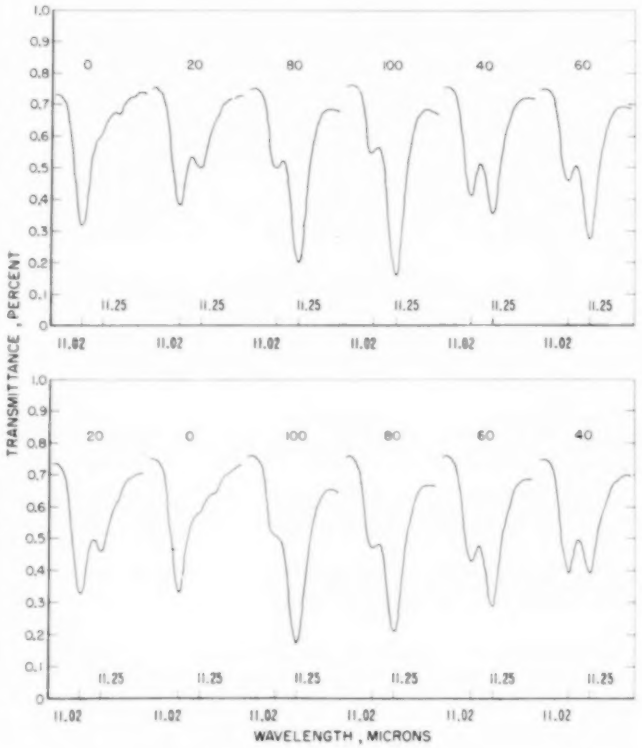

FIGURE 2. *Infrared spectra of a series of pyrolysates obtained from vulcanized mixtures of GR-S and natural rubber.*

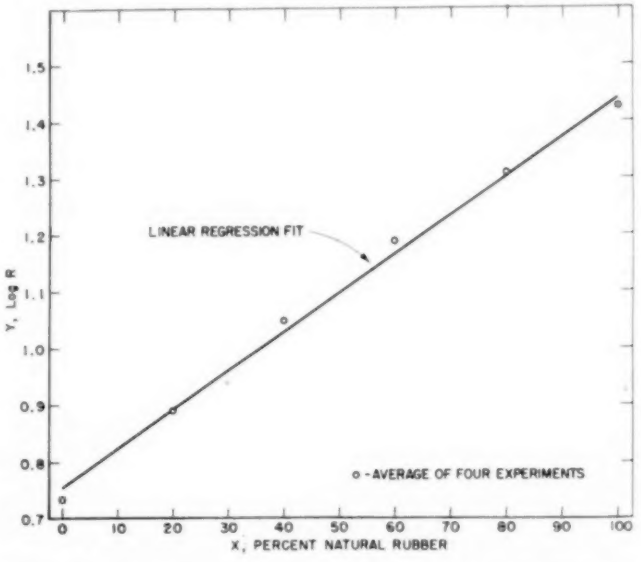

FIGURE 3. *Calibration curve relating log R to percent natural rubber in polymer.*

The data listed in table 4 for the 24 specimens furnish the basis for the calibration curve shown in figure 3, relating logarithm R to percent natural rubber, where

$$R=10\frac{T_{11.02}}{T_{11.25}}$$

and T is the transmittance at the designated wavelength, corrected for background.

3. Results and Discussion

The type of design used in this investigation is given in table 2 [6]. The six letters in the body of the table can be identified as the six concentrations of natural rubber. By letting each row represent a complete run in which the six determinations are made in a preassigned order, associated with the columns of the table, errors resulting from instrumental instability, or similar systematic sources, can be compensated. To eliminate bias, randomizations were carried out, and the actual sequence of the determinations is shown in table 3. The results are tabulated in table 4, in terms of logarithms of R, as previously defined.

A statistical analysis of the data revealed no detectable trend of the instrument within each run, but a small amount of instability was observed from one run to another. This small additional variability does not affect the precision of the results, as each run included a complete set of concentrations of natural rubber. The standard deviation of log R, reflecting the precision of a single random determination, was found to be 0.023, which corresponds to about 3-percent natural rubber. Thus, it can be stated with about 95 percent confidence, that a single measurement will not be in error by more than ± 6 percent.

TABLE 2. *Experimental design* [6]

Rows	Columns					
	1	2	3	4	5	6
1	a	b	c	d	e	f
2	b	a	d	c	f	e
3	e	f	a	b	c	d
4	f	e	b	a	d	c

TABLE 3. *Order of analyses* [a]

Run	Percent natural rubber					
	1	2	3	4	5	6
1	60	100	80	40	20	0
2	40	80	100	60	0	20
3	100	20	0	80	60	40
4	80	0	20	100	40	60

[a] The numbers in the body of the table represent the six concentrations of natural rubber, expressed as percent.

TABLE 4. *Experimental values for log* $_{10}$ R [a]

Natural rubber—percent					
0	20	40	60	80	100
0.727	0.884	1.073	1.194	1.350	1.442
.721	.880	1.050	1.184	1.291	1.369
.742	.885	1.045	1.205	1.291	1.458
.746	.890	1.033	1.180	1.323	1.459
Average 0.734	.885	1.050	1.191	1.314	1.432

[a] $R=10\frac{T_{11.02}}{T_{11.25}}$; T=transmittance at indicated wavelength in microns.

A calibration curve was obtained by plotting the average values, shown in table 4, corresponding to the various concentrations against the known concentrations. The data are represented satisfactorily by the following quadratic equation

$$Y=0.730+0.00851\ X-0.000015\ X^2 \qquad (1)$$

where X is the concentration of natural rubber in percent by weight, and Y is the logarithm of R, defined earlier. This equation fits the data within the experimental error.

If the slight curvature is neglected, the equation of the best straight line fitting the data is

$$Y=0.755+0.00692\ X. \qquad (2)$$

This fit is shown in figure 3.

The use of the linear equation introduces an additional error of a systematic type. This systematic error varies according to the natural rubber content. Averaged over the entire curve, it is of the order of ± 4 percent natural rubber. Unlike experimental random error, the systematic error cannot be reduced through repeated measurements on an unknown sample. If, in the analysis of such a sample, a total uncertainty [3] not exceeding ± 6 percent natural rubber is required, triplicate determinations are necessary when the linear relationship is used, while single determinations suffice when the quadratic form is employed. A comparison of the two methods of fit is shown in table 5.

TABLE 5. *Comparison of calibration functions*

Natural rubber concentration X	Y=log R		
	Observed value [a]	Straight line fit	Quadratic fit
0	0.734	0.750	0.730
20	.885	.891	.894
40	1.050	1.031	1.047
60	1.191	1.172	1.187
80	1.314	1.312	1.316
100	1.432	1.453	1.432

[a] Average of four determinations.

[3] Using a 95-percent confidence interval.

4. Conclusion

The method utilizing the infrared spectra of pyrolysis products to determine natural rubber and GR–S content, respectively, in their vulcanized mixture, has been found to be more rapid than existing methods, without appreciable loss in precision. It is entirely possible that refinement of the pyrolysis procedure and the use of a sealed absorption cell in the analysis, might lead to greatly improved precision of test. It should also be possible to develop a method in which the bound styrene content in the GR–S could be estimated at the same time by utilizing the band at 14.3 μ for styrene.

Acknowledgement is gratefully given to James Stewart of the Gas Chemistry Section, for his interest and assistance in obtaining the infrared data for this work.

5. References

[1] ASTM Book of Standards, pt. 6, D–833–46–T (American Society for Testing Materials, Philadelphia, Pa., May, 1951).
[2] Federal test method standard No. 601. Rubber sampling and testing, method 16111.
[3] H. P. Burchfield, Ind. Eng. Chem. **16,** 424–25 (1944); **17,** 806–10 (1945).
[4] D. L. Harms, Anal. Chem. **25,** 1140 (1953).
[5] F. F. Bentley and G. Rappaport, Anal. Chem. **26,** 1980–82 (1954).
[6] J. Mandel and M. Zelen, Annals of Mathematical Statistics **25,** No. 4, 807 (1954) (Abstract).

WASHINGTON, June 3, 1955.

Journal of Research of the National Bureau of Standards Vol. 55, No. 4, October 1955 Research Paper 2624

Thermal Degradation of Polychlorotrifluoroethylene, Poly-α,β,β-Trifluorostyrene, and Poly-*p*-Xylylene in a Vacuum [1]

S. L. Madorsky and S. Straus

Polychlorotrifluoroethylene (Kel-F) (I), poly-α,β,β-trifluorostyrene (II), and poly-*p*-xylylene (III) were pyrolyzed under conditions of molecular distillation, and some of the light volatile fractions analyzed in the mass spectrometer. The volatiles from (I) consisted of 27.9 weight percent monomeric fragments, mostly monomer, and 72.1 percent large fragments of average molecular weight 904. In the case of (II), the volatiles consisted of 73.6 percent monomeric fragments, almost all monomer, and 26.4 percent large fragments of average molecular weight 458. The volatiles from (III) consisted of 3.6 percent monomeric fragments, not containing any monomer, and 96.4 percent large fragments of average molecular weight 661. Rates of thermal degradation, in terms of rates of volatilization, were also investigated. The activation energies calculated from these rates are 66, 67, and 76 kilocalories per mole for (I), (II), and (III), respectively. The following order of thermal stability was found: (III)>(I)>(II).

1. Introduction

It was shown in a previous publication [1] [2] in the case of a number of simple polymers, that their thermal behavior in a vacuum, in the temperature range 250° to 550° C., is primarily a function of their molecular structure. In this paper a comparison is made between polymers that are similar to some of those previously studied, and yet differ from them in certain structural features. With this in view, the following polymers were selected for the present study:

1. Polychlorotrifluoroethylene (Kel-F)

This polymer differs in structure from tetrafluoroethylene in that one fluorine atom is replaced with a chlorine atom.

2. Poly-α,β,β-trifluorostyrene

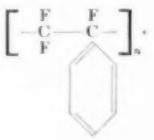

This polymer differs from polystyrene in that the hydrogen atoms in α,β,β-positions are replaced with fluorine atoms.

3. Poly-*p*-xylylene

This polymer differs from polybenzyl in that it contains two, instead of one, CH_2 groups between the phenyl groups in the chain. It is also isomeric with polystyrene; however, here the phenyl group is a part of the chain, while in polystyrene it is pending from every second carbon atom in the chain.

2. Apparatus and Experimental Procedure

The experimental work consisted of (1) a study of pyrolysis in a molecular still and a subsequent investigation of the decomposition products, and (2) measurements of rates of thermal degradation in a vacuum, as indicated by the loss in weight of a sample suspended from a spring balance.

In the pyrolysis study, samples weighing 15 to 30 mg were heated at various temperatures. In each case it took about 45 min to heat the sample to the required temperature, and this temperature was then maintained for 30 min. Four fractions were collected:

(I) Residue. This fraction was weighed on a semimicro balance, but was not investigated further.

(II) Heavy fraction, volatile at the temperature of pyrolysis, but not at room temperature. The weight of this fraction was calculated as the difference between the sum of the weights of the other three fractions and the original weight of the sample. The average molecular weight was determined by a microfreezing-point-lowering method.

(III) Light fraction volatile at room temperature, and containing monomer or monomer-size fragments. This fraction was weighed and then analyzed in the mass spectrometer.

(IV) Gaseous fraction, volatile at the temperature of liquid nitrogen. This fraction was also analyzed in the mass spectrometer and was found to consist of hydrogen. Its weight was calculated from its volume, pressure, and composition, and amounted to about 0.02 percent of the weight of the original

[1] This work was supported in part by the Ordnance Corps, Department of the Army, and in part by the Federal Facilities Corporation, Office of Synthetic Rubber. This paper was presented at the National Meeting of the American Chemical Society in Cincinnati, Ohio, March 29-April 7, 1955.

[2] Figures in brackets indicate the literature references at the end of this paper.

356420—55——4

sample. Details of apparatus and experimental procedure have been described previously [2, 3].

Rates of thermal degradation were determined for each polymer at several temperatures. A 5–7-mg sample of the polymer was placed in a platinum crucible suspended from a very sensitive tungsten helical spring balance, enclosed in a Pyrex glass housing, which could be evacuated to 10^{-5} to 10^{-6} mm Hg. An electric furnace was preheated to the temperature required for a particular run. The furnace was then placed in position to enclose that part of the glass apparatus that contained the crucible. It ordinarily required about 15 min from the time the furnace was placed in position, to the time at which the thermocouple under the crucible indicated the temperature required for the given experiment. There was some loss of weight of the sample by evaporation during this heating-up period. This loss was designated as the preliminary loss, and the zero time for any rate experiment was considered as the time when the thermocouple indicated that the operating temperature had been reached. The apparatus and experimental procedure have been described in detail in previous publications [1, 4, 5].

In all the rate experiments the percentage of the sample volatilized at any given temperature was plotted against time. These plots can be used as a basis for constructing graphs of logarithm of residue at time t versus time. For some polymers these graphs are straight lines, indicating a first-order reaction [6], and the slopes of these lines are the rate constants for the respective temperatures. For other polymers the reaction is not of first order, and the plots of logarithm of residue versus time are curved lines. The three polymers of this investigation belong to the second class. In this case, other methods of plotting the results were adopted: (1) K_1–rates, which are expressed in percent volatilized based on original sample per minute, at any given time t, were plotted against cumulative percentage volatilization at t. (2) K_2–rates, which are expressed in percent volatilized based on the residue at any time t, per minute, were plotted against cumulative percentage volatilization at t. Usually, one or the other, or both, sets of plots are straight lines in the range of about 10- to 80-percent volatilization.

It was not possible to make an accurate and detailed study of initial rates with the present experimental setup. It is planned to make such a study by degrading polymer samples by pyrolysis slowly at low temperatures, using automatic recording of the rates of volatilization. In the present work, the apparent initial rates were obtained by extrapolating the main parts of the rate plots to zero evaporation.

While the apparent initial rates can serve as a measure of thermal stability, it is perhaps more accurate, for the purpose of comparing thermal stability of various polymers, to use a value designated as T_s and defined as the temperature, in degrees centigrade, at which a sample of a given polymer loses half its weight by evaporation during 45 min of heating in a vacuum up to this temperature, followed by 30 min of heating at this temperature. Most of the weight loss takes place during the last 30 min.

3. Mechanism of Thermal Degradation of Polymers

A possible mechanism of thermal degradation through scissions has been described in a previous paper [1]. According to this mechanism, degradation by heat takes place through scissions of the polymer chain. In some cases the scissions are accompanied by transposition, as in polymethylene,

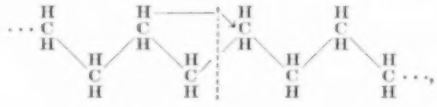

resulting in one olefin and one paraffin end. In other cases the scissions result in two free radical ends, as in polytetrafluoroethylene,

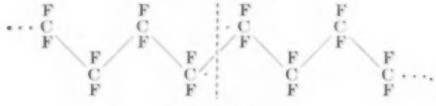

The free radicals then proceed to depolymerize into monomer by a chain reaction,

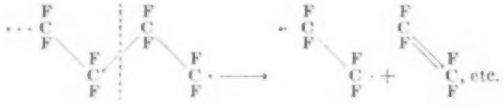

The difference in the behavior of the above two polymers can be ascribed to the difference in the C—H and C—F bond strengths, the latter being greater that the former. Although there is a great deal of disagreement among investigators in regard to numerical values of bond strengths, there seems to be a general agreement as to their relative strengths. Thus, in the case of bonds with which this investigation is concerned, the bonds can be arranged in the following order:

$$C-F > C-H > C-Cl > C-C.$$

In the case of polychlorotrifluoroethylene, as will be shown below, the volatiles consist partly of monomer and partly of large fragments. This is due to the weakness of the C—Cl bond, so that transposition of chlorine during scissions takes place. However, since there is only one chlorine atom on every second carbon, this transposition is limited. As a result, some scissions are accompanied by transposition,

without monomer formation, while other scissions result in formation of free radical ends, followed by monomer formation.

As to what happens to the residue during thermal degradation, some information is found in the literature on polystyrene [4, 7, 8], poly-α- and poly-β-deuterostyrene [7], polymethyl methacrylate [9], polyethylene [10], polymethylene [11], and polyisobutylene [12]. It was found, with all these polymers, that there is an initial rapid drop in molecular weight during the first few percent volatilization, or even before volatilization begins, followed by a much slower drop in molecular weight as volatilization proceeds. This rapid initial drop in molecular weight may be due to weak links [13] or to other causes. However, it is quite possible that the deviation of the initial rates from the linearity of the subsequent K_1- or K_2-rates is due, to a large extent, to this rapid initial drop in molecular weight. It was also found that additives, such as benzoyl peroxide, affect initial rates of thermal degradation, as was shown in the case of polymethyl methacrylate [14].

One should be able to find a difference in the shape of the curves for molecular weight of residue versus volatilization, beyond the first few percent volatilization, depending on whether the mechanism of degradation is of the polymethylene type or the polytetrafluoroethylene type. However, the literature data are inconclusive with regard to this point. While in the case of polymethyl methacrylate, which degrades by the same mechanism as polytetrafluoroethylene, degradation was carried out to about 90 percent loss of weight [9], polymethylene was degraded to only about 14 percent volatilization [11]. As for polyethylene, the investigation was made at a temperature below volatilization [10].

4. Results

4. 1. Polychlorotrifluoroethylene

This polymer[3] was in the form of a transparent sheet 0.2 mm thick. It contained no additives and had an average molecular weight of 100,000. Experimental conditions and results of pyrolysis are shown in table 1. The light fraction III is, on the average from three experiments, 27.9 percent of the total volatilized part, as compared with almost 100 percent in the case of polytetrafluoreothylene [5]. Mass spectrometer analysis of this fraction showed it to consist of about 90 to 95 mole percent monomer, the rest being a mixture of C_3F_5Cl and $C_3F_4Cl_2$. Thus, the yield of monomer was actually 26 to 27 percent of the total volatilized part, as compared with almost 100 percent for polytetrafluoroethylene. When pyrolyzed in bulk [15] in nitrogen at atmospheric pressure, polychlorotrifluoroethylene yields 67 percent monomer. Bulk pyrolysis gives similar results in the case of other polymers [16, 17].

[3] The authors are indebted to H. S. Kaufman of the W. M. Kellogg Co. for supplying this polymer.

In figure 1 the percent of polymer volatilized is plotted against temperature for the experiments shown in table 1. The value of T_h for polychloro-

TABLE 1. *Pyrolytic fractionation of polymers*

Experiment	Temperature	Fractions of original sample			Fraction III in percent of total volatilized part
		I Residue	II Nonvolatile at room temperature	III Volatile at room temperature	
Polychlorotrifluoroethylene (Kel-F)					
	°C	wt %	wt %	wt %	wt %
1	347	98.9			
2	380	47.5	37.5	15.0	28.6
3	401	1.2	71.5	27.3	27.6
4	418	0.6	70.0	27.4	27.6
Average					27.9±0.4
Poly-α, β, β-trifluorostyrene					
1	333	70.0	7.5	22.5	75.1
2	348	34.5	16.6	48.9	74.6
3	365	4.8	22.0	73.2	77.0
4	382	0.9	32.2	66.9	67.5
Average					73.6±1.5
Poly-*p*-xylylene					
1	419	85.7			
2	431	56.6	41.7	1.7	3.8
3	439	33.5	63.2	3.3	4.9
4	449	8.5	89.5	2.0	2.2
5	464	2.5	93.9	3.6	3.6
Average					3.6±0.7

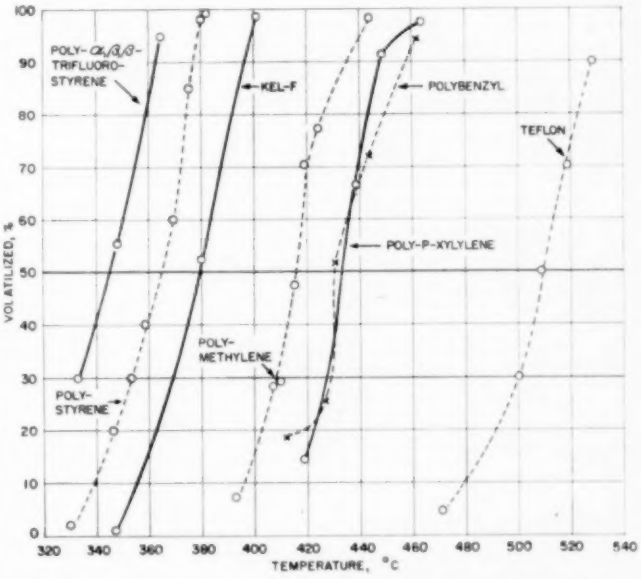

FIGURE 1. *Relative thermal stability of polychlorotrifluoroethylene (Kel-F), poly-α,β,β-trifluorostyrene and poly-p-xylylene.*

The other polymers are shown for comparison. In each experiment the sample was heated up to the required temperature in 45 min and then kept at this temperature for 30 min.

trifluoroethylene is about 380° C, as compared with 416° for polymethylene, and 509° for polytetrafluoroethylene.

The residue, fraction I, was a transparent glass. The heavy volatile fraction II had an average molecular weight of 904, as determined by the freezing-point lowering in camphor. This value is higher than those observed for other vinyl polymers, but fluorocarbon compounds are known to have higher vapor pressures than hydrocarbons.

The rates of thermal degradation of polychlorotrifluoroethylene were investigated at five temperatures. The experimental conditions and results are shown in table 2. In figure 2, percentage volatilization is plotted against time. It can be seen from this figure that the preliminary losses by volatilization are from 0 to 3 percent. The K_2-rates, in percent volatilized based on the residue per minute, are shown plotted in figure 3. These plots are straight lines above 10 to 20 percent volatilization, and the apparent initial rates are obtained by extrapolation to zero volatilization. The values of these initial rates are shown in table 2. The activation energy, as calculated from these initial rates, using Arrhenius' equation, is 66 kcal/mole. The apparent initial rate of thermal degradation of polymers at 350° C, $K_{350°}$ was selected for the purpose of comparing thermal stability of polymers [1]. If this rate is not conveniently determined experimentally, it can be calculated from a given rate at a given temperature by means of a modified Arrhenius' equation:

$$\log_{10} K_{350°C} = \frac{E\left(1.605\times10^{-3}-\frac{1}{T_1}\right)}{2.303\ R}+\log_{10} K_{T_1}$$

where K_1 is the rate corresponding to the absolute temperature, T_1, and R is the gas constant. For polychlorotrifluoroethylene, this rate is 0.044 percent per min, as compared with 0.000002 percent for polytetrafluoroethylene.

TABLE 2. *Rates of thermal degradation of polymers*

Polymer	Temperature	Duration of experiment	Total volatilized	Initial rate of volatilization	Activation energy
	°C	min	%	%/min K_2	kcal
Polychlorotrifluoroethylene $\left[-\underset{F}{\overset{F}{C}}-\underset{F}{\overset{Cl}{C}}-\right]_n$	365	400	78.1	0.20	
	370	300	82.9	.28	
	375	200	75.0	.42	
	380	160	82.3	.58	
	385	130	83.2	.84	66
Poly-α, β, β-trifluorostyrene $\left[-\underset{F}{\overset{F}{C}}-\underset{F}{\overset{F}{C}}-\right]_n$				K_1	
	325	360	59.7	0.27	
	330	410	72.1	.43	
	335	200	64.3	.60	
	340	200	79.9	1.02	67
Poly-p-xylylene $\left[-CH_2-C_6H_4-CH_2-\right]_n$				K_2	
	415	230	80.4	0.06	
	420	170	88.9	.10	
	425	110	91.6	.16	
	430	80	93.3	.23	76

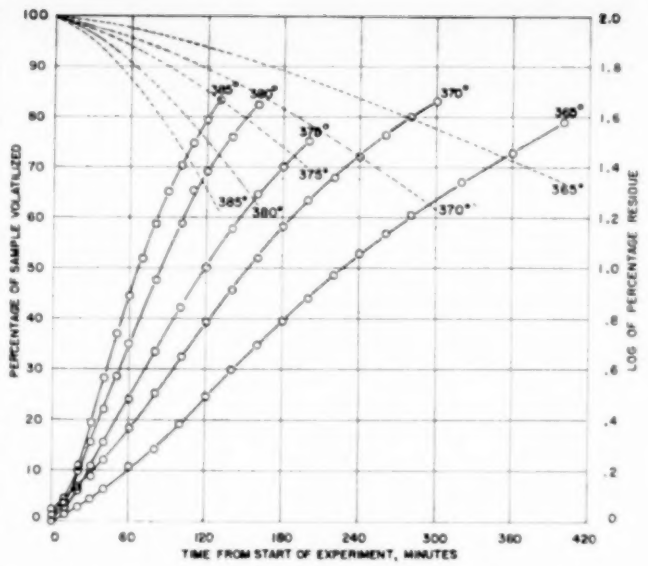

FIGURE 2. *Thermal degradation of polychlorotrifluoroethylene.*
———, Percentage of sample volatilized versus time; ·····, logarithm 10 of percentage residue versus time.

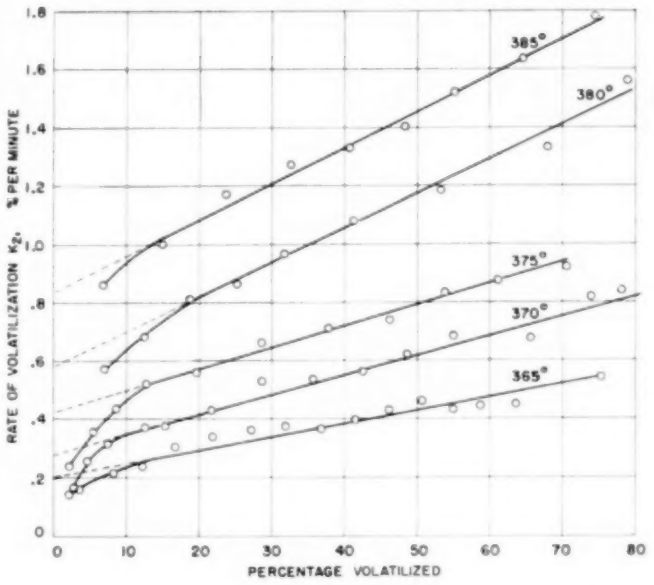

FIGURE 3. *Rates of volatilization of polychlorotrifluoroethylene in percent of residue per minute, as a function of percentage volatilization.*

4.2. Poly-α, β, β-trifluorostyrene

This polymer,[4] in the form of white light flakes, was prepared by R. S. Corley, of Polaroid Corp., from the monomer at 50° C, using a small amount of dodecylamine as emulsifier. The emulsion was coagulated by the addition of 1-percent sodium sulfate. The product was purified by washing thoroughly with ethanol to remove the emulsifier, dimer, and alcohol-

[4] The authors are indebted to the Signal Corps Engineering Laboratory, Fort Monmouth, N. J., for supplying this polymer.

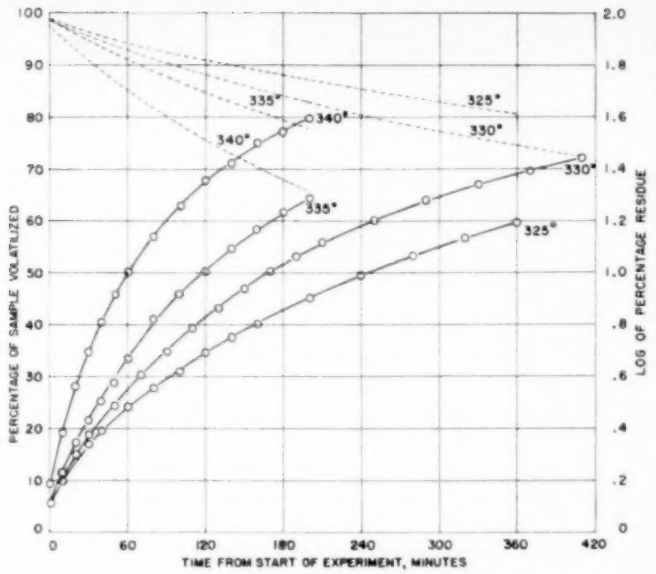

FIGURE 4. *Thermal degradation of poly-α,β,β-trifluorostyrene.*

———, Percentage of sample volatilized versus time; ·····, logarithm 10 of percentage residue versus time.

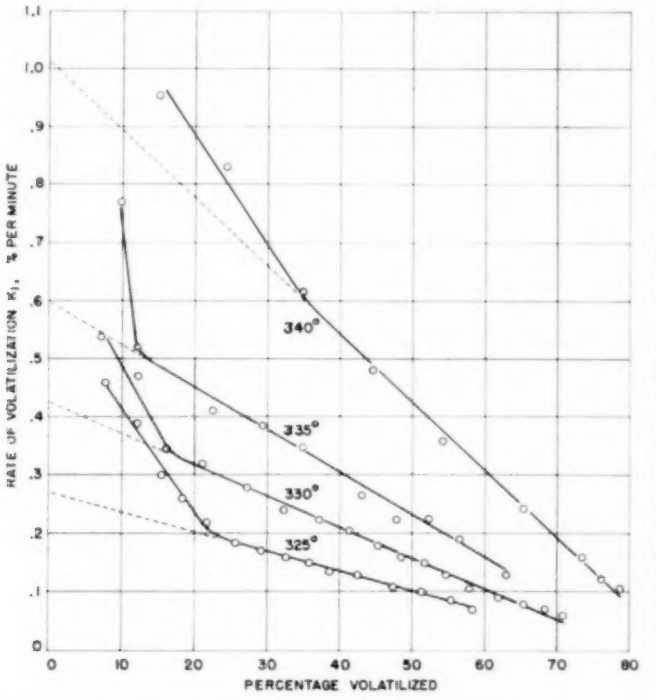

FIGURE 5. *Rates of volatilization of poly-α,β,β-trifluorostyrene in percent of original sample per minute, as a function of percentage volatilization.*

soluble low polymers, and was then vacuum dried. Preliminary experiments on pyrolysis and rate of degradation showed that the polymer contained a considerable amount of short-chain molecules. A 2-g sample was fractionated by dissolving at room temperature in 100 ml benzene and precipitating with 35 ml methanol. About 1 g of heavy fraction was thus obtained. This operation was repeated on the heavy fraction, resulting in 0.5 g of a still heavier fraction. This last fraction was freeze-dried and used in the experiments described here. On the basis of information with regard to the molecular weight by osmotic determination of the original material, the weight average molecular weight of the twice-fractionated 0.5 g heavy fraction was estimated to be at least 300,000.

Experimental conditions and results of pyrolysis of poly-α, β, β-trifluorostyrene at four temperatures are shown in table 1. The amount of fraction III in percent of total volatilized part is about 74 percent, as compared with 42 percent for ordinary polystyrene [1]. Temperature of 50 percent volatilization, T_h, as seen from figure 1, is 342° C, as compared with 364° for ordinary polystyrene [18]. There does not seem to be any satisfactory explanation at present for the greater stability of polystyrene as compared with poly-α, β, β-trifluorostyrene.

Mass spectrometer analysis showed fraction III to consist almost entirely of the monomer. Judging from the large monomer yield in the pyrolysis of poly-α, β, β-trifluorostyrene, the mechanism of degradation consists mainly of scissions without transposition, resulting in two free radicals:

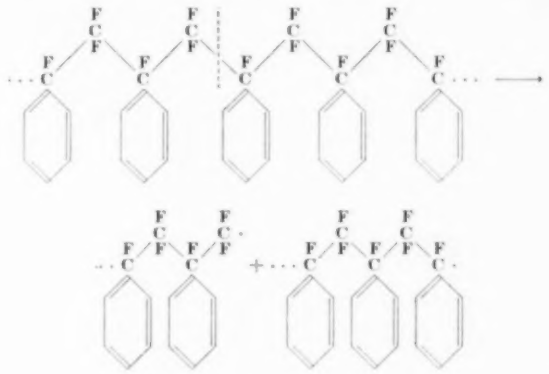

These free radicals then break up into monomers by a chain reaction (unzipping). The lack of transposition of fluorine here could be ascribed to the high C—F bond strength.

The heavy fraction II had an average molecular weight of 458, as determined by the freezing-point-lowering method in benzene. This molecular weight corresponds to a trimer, and could consist of a mixture of dimer, trimer, and tetramer, as in the case of polystyrene, poly-α and poly-β-deuterostyrenes, and poly-*m*-methylstyrene [14]. While the weight ratio of fractions II and III in poly-α, β, β-trifluorostyrene is 74:26, the mole ratio is 89:11, so that only a few large molecules have evaporated. The residue, fraction I, was glassy and light brown in color.

Measurements of rates of degradation were carried out at four temperatures. Experimental conditions and results are shown in table 2. Cumulative percentage volatilization is plotted against time in figure 4. A preliminary loss of weight of 6 to 10 percent is shown. Rates K_1, in percent volatilized based on original sample per min, are shown in figure 5. The initial rates were obtained by extra-

polation to zero time, and are shown numerically in table 2. The activation energy based on these rates is 67 kcal/mole, as compared with 58–59 determined previously for polystyrenes [14]. Rate, $K_{350°}$, of thermal degradation at 350°, calculated as in the case of polychlorotrifluoroethylene, is 2.4, as compared with 0.14, 0.24, 0.27, and 0.90 determined previously [4, 14] for poly-β-deuterostyrene, polystyrene, poly-α-deuterostyrene, and poly-*m*-methylstyrene, respectively.

4.3. Poly-*p*-xylylene

This polymer[5] was prepared by the Szwarc pyrolysis method, and is the same as the one used by the Polaroid investigators in their work [19] on poly-*p*-xylylene. It is a light-yellow powder and is described by Livingston [20] as "apparently all crosslinked." Its molecular weight was unknown, but must be quite high, judging from the fact that on pyrolysis the initial rate was not excessive, as is the case with low molecular weight polymers.

Szwarc's method [21, 22] for the preparation of poly-*p*-xylylene consists of heating gaseous *p*-xylene at about 800° C. At this temperature, *p*-xylene loses hydrogen to form 3,6-dimethylene-1,4-cyclohexadiene,

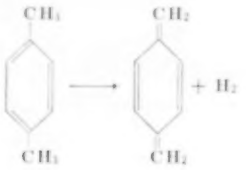

which is stable in the gaseous phase, but is labile in the condensed phase, and polymerizes at about 0°C. to form poly-*p*-xylylene. On the basis of X-ray analysis and energy of formation of this polymer, Szwarc assumes that it has a linear structure with

as the repeating unit. However, other investigators [19, 23, 24], on the basis of high crystallinity, infusibility, insolubility in most of the ordinary solvents, and of other chemical, as well as physical, properties of poly-*p*-xylylene, came to the conclusion that this polymer is highly cross-linked.

Results of pyrolysis experiments are shown in table 1 and figure 1. Fraction III, in percent of the total volatilized part, is 3.6. Mass spectrometer analysis of this fraction is shown in table 3. As seen from this table, the monomer,

does not appear at all in fraction III. Fraction II was found by the freezing-point-lowering method in camphor to have an average molecular weight of 661. The residue was light brown. The T_k value, as seen from figure 1, is 432, as compared with 430 for poly-

[5] The authors are indebted to the Polaroid Corp. for supplying them with this polymer.

TABLE 3. *Mass-spectrometer analysis of fraction III collected at room temperature in the pyrolysis of poly-p-xylylene*

Component	Temperature of pyrolysis, °C			Average
	419	431	464	
	Mole %	*Mole %*	*Mole %*	*Mole %*
Methyl-ethyl-benzene (C_9H_{12})	7.5	7.0	6.0	6.8
Methyl-styrene	5.7	2.9	3.2	3.9
Xylene	68.0	83.1	84.5	78.6
Toluene	12.2	5.6	6.3	8.0
Benzene	6.6	1.4		2.7
Total	100.0	103.0	100.0	103.0

benzyl and 364 for polystyrene. Thus, polybenzyl and poly-*p*-xylylene approach polytetrafluoroethylene, with a T_k of 509 [5] in thermal stability. This is most likely due to the fact that the highly resonating benzene ring forms a part of the polymer backbone in these two polymers. On the other hand, styrene, which is isomeric with poly-*p*-xylylene, but has the benzene ring pending from every second carbon in the polymer backbone, is less thermally stable than polybenzyl or poly-*p*-xylylene.

Results of rate measurements are shown in table 2. Percentage volatilization versus time is shown in figure 6. As seen from this figure, the preliminary losses vary from about 3 to 5 percent volatilization. The K_2 rate curves are plotted as solid lines in figure 7. These curves, when extrapolated to zero volatilization, run close together, and the rates are subject to considerable error. The initial K_2-rates are shown in table 2. The activation energy calculated on the basis of these rates is 76 kcal, as compared with 53 for polybenzyl [1]. As a check on the accuracy of the activation energy for poly-*p*-xylylene, the K_1-rates are shown plotted as interrupted lines in figure 7. The K_1-rates at the position of maxima are shown in table 4, and the activation energy calculated on the basis of these maximum K_1-rates is about the same as that calculated from the initial K_2-rates. A surprising similarity to polystyrene [4], with regard to the mechanism of thermal degradation, is the shape of the K_1 and K_2-rate curves for poly-*p*-xylylene, which point to a reaction intermediate between a first and a zero order, the same as in polystyrene.

TABLE 4. *Maxima on K_1 rate-curves for poly-p-xylylene*

Temperature	Maxima
°C	%/min
415	0.50
420	.76
425	1.26
430	1.76

The $K_{350°}$ initial rate calculated from K_2-rates is 0.002, as compared with 0.006 percent for polybenzyl [1] and 0.24 percent per minute for polystyrene [4].

Even if we assume that poly-*p*-xylylene has a highly cross-linked structure, some parts of the

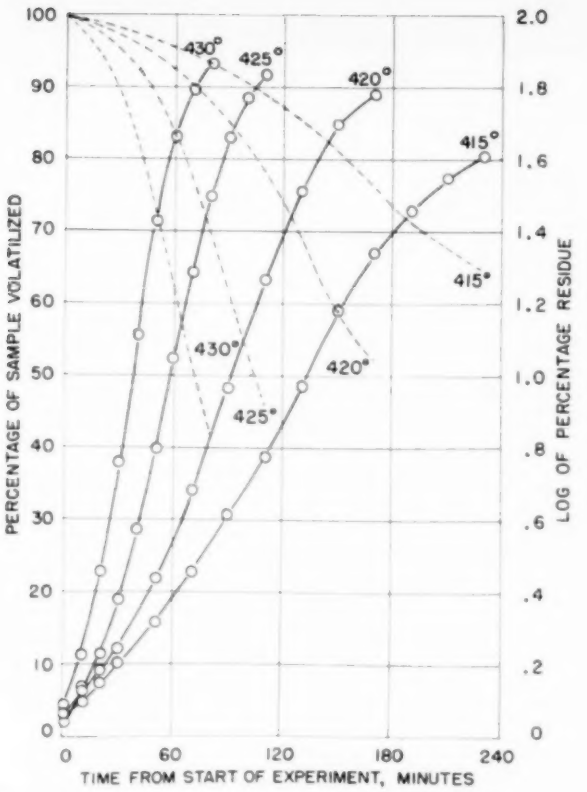

FIGURE 6. *Thermal degradation of poly-p-xylylene.*

———, Percentage of sample volatilized versus time; ·····, logarithm$_{10}$ of percentage residue versus time.

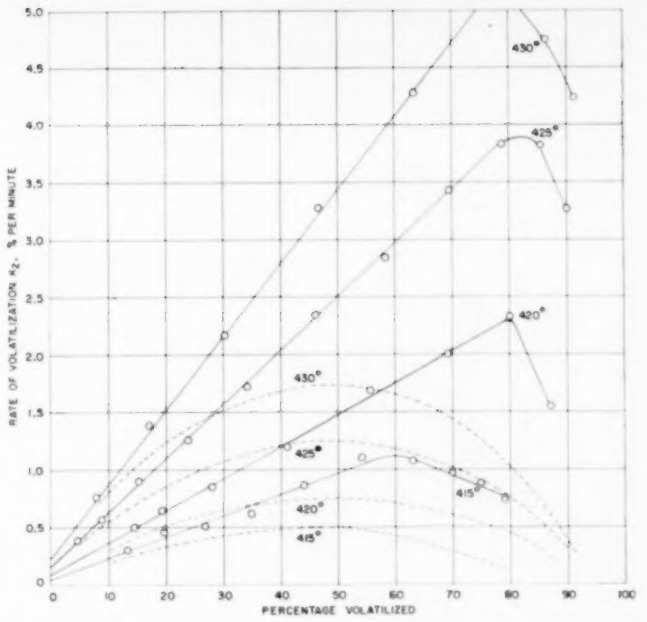

FIGURE 7. *Rates of volatilization of poly-p-xylylene, residue per minute as a function of percentage volatilization.*

The interrupted lines represent K_1-rates, in percent volatilized based on original sample per minute.

polymer would be linear. It was shown by Szwarc that the monomer, 3,6-dimethylene-1,4-cyclohexadiene,

is stable in the gaseous phase. This monomer can be expected to form as part of the volatile product and remain stable while in the gaseous state. The mechanism of monomer formation could be as follows: A thermal scission occurs at the —CH_2—CH_2— bond, which is in β-position to double bonds in benzene rings on both sides. This scission takes place without hydrogen transposition and results in two free radicals:

These radicals could then unzip into monomers:

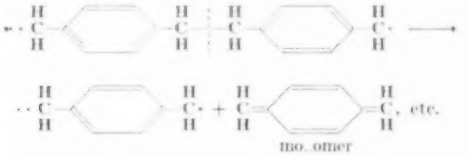

mo. omer

In order to check on the existence of the monomer in the pyrolysis of poly-*p*-xylylene, a sample of the polymer was pyrolyzed directly into the ionizing chamber of the mass spectrometer [6] by a method developed by Bradt, Dibeler, and Mohler [25]. The mass spectrogram consists of a series of peaks of formulae $nX+1$ and $nX-1$, where X is the monomer unit CH_2:C_6H_4:CH_2, molecular weight 104. With increase of n from 2 to 8, the intensity decreases from 1,000 to 10 (on an arbitrary scale), as shown in table 5. There are also smaller peaks with one or two CH_2 radicals taken from or added to $nX+1$. The amount of monomer, 3,6-dimethylene-1,4-cyclohexadiene, could not be determined quantitavely, in view of unknown contributions from the dimer, trimer, tetramer, etc., to the 104 peak. However, this amount is estimated as considerably less than 10 mole percent. Xylene, molecular weight 106, is present to the extent of about 1 mole percent. The highest peak is for m/e=105. This peak could be due chiefly to contributions from the larger ions which are multiples of X. Peaks at 207 and 209 are due to dimer, those at 311 and 313 to trimer, etc. These results are in general agreement with those obtained from pyrolysis, where the bulk of the vola-

[6] The authors are indebted to Paul Bradt and F. L. Mohler, of the Mass Spectrometry Section, for carrying out this experiment and interpreting the results.

TABLE 5.[a] *Mass spectrograph of poly-p-xylylene pyrolyzed directly into the ionizing chamber of the mass spectrometer at 381° C.*

(Only the more conspicuous peaks are shown.)

m/e	Peaks on the basis of 105 m/e = 1,000	Monomer multiple ±1
103	16	X−1 monomer
104	135	X
105	1,000	X+1
106	95	xylene
207	334	2X−1 dimer
209	204	2X+1
311	84	3X−1 trimer
313	42	3X+1
415	22	4X−1 tetramer
416	23	4X
417	19	4X+1
519	19	5X−1 pentamer
521	19	5X+1
623	24	6X−1 hexamer
727	20	7X−1 heptamer
831	10	8X−1 octamer

[a] This table is from a paper now in preparation by Paul Bradt and F. L. Mohler.

tiles consisted of fraction II, having an average molecular weight of 661, while fraction III consists mainly of xylene.

Poly-*p*-xylylene and polybenzyl are two examples of polymers in which the phenyl group constitutes a part of the chain backbone. Both polymers are thermally stable, and do not yield the monomer unit as part of the volatile products. It was shown in the case of polybenzyl [1] that the configuration of the chain is such that monomer formation by unzipping is not to be expected. However, in the case of poly-*p*-xylylene, one could expect a considerable amount of monomer instead of the small amount actually found, which should be stable in the gaseous phase, according to the work of Szware. The absence of a large amount of monomer in the volatiles in the gaseous state could be explained on the basis of resonance in the poly-*p*-xylylene, which prevents the free radical end of the chain from unzipping in the same manner as in the case, for example, of polytetrafluoroethylene, polychlorotrifluoroethylene, and other polymers.

5. Comparative Thermal Stability of Polymers

It was pointed out above that a comparison of thermal stability of polymers can be made on the basis of their initial rates of volatilization. These initial rates were not determined experimentally, but were obtained by extrapolating to zero volatilization the main parts of the rate curve extending from about 10 to 80 percent volatilization. In making this comparison, the rates $K_{350°}$ of all the polymers are calculated to 350° C. Perhaps a more accurate comparison can be made on the basis of the T_h values of polymers. This value was defined as the temperature at which a polymer sample will lose half its weight when heated in a vacuum for 30 min at this temperature, preceded by a 45-min heating-up period to this temperature. Table 6 shows a comparison of thermal stability of 16 polymers on the basis of $K_{350°}$ and T_h. With a few slight deviations, the two comparisons run parallel.

TABLE 6. *Relative stability of polymers*

Polymer	$K_{350°}$-rates		T_h	
	Percent per min	Reference	°C	Reference
Polytetrafluoroethylene	0.0000002	[5]	509	[5]
Poly-*p*-xylene	.002		432	
Polybenzyl	.006	[1]	430	[1]
Polymethylene	.004	[1]	407	[1]
Polyethylene	.008	[4]	404	[11]
Polypropylene	.060		387	
Polychlorotrifluoroethylene	.044	[1]	380	[1]
Poly-β-deuterostyrene	.14	[1]	372	[1]
Polyvinylcyclohexane	.45	[17]	369	[18]
Polystyrene	.24	[4]	364	[18]
Poly-α-deuterostyrene	.27	[17]	362	[18]
Poly-*m*-methylstyrene	.90	[17]	358	[18]
Polyisobutylene	2.4	[1]	348	[1]
Poly-α,β,β-trifluorostyrene	2.4		342	
Polymethylmethacrylate	5.2	[17]	327	[18]
Poly-α-methylstyrene	230	[17]	278	[18]

6. References

[1] S. L. Madorsky and S. Straus, J. Research NBS **53,** 361 (1954) RP2553; also, Ricerca sci. (1955).
[2] S. L. Madorsky and S. Straus, J. Research NBS **40,** 417 (1948) RP1886.
[3] S. L. Madorsky, S. Straus, D. Thompson, and L. Williamson, J. Research NBS **42,** 499 (1949) RP1989.
[4] S. L. Madorsky, J. Polymer Sci. **9,** 133 (1952).
[5] S. L. Madorsky, V. E. Hart, S. Straus, ad V. A. Sedlak, J. Research NBS **51,** 327 (1953) RP2461.
[6] S. Glasstone, Textbook of Physical Chemistry, 2d ed. p. 1046 (D. Van Nostrand Co., New York, N. Y., 1946).
[7] L. A. Wall, D. W. Brown, and V. E. Hart, J. Polymer **15,** 157 (1955).
[8] H. H. G. Jellinek, J. Polymer Sci. **4,** 13 (1949).
[9] V. E. Hart, (unpublished work.)
[10] W. G. Oakes and R. B. Richards, J. Chem. Soc. (London) **619,** 2929 (1949).
[11] L. A. Wall, S. L. Madorsky, W. D. Brown, S. Straus, and R. Simha, J. Am. Chem. Soc. **76,** 3430 (1954).
[12] V. A. Golubtzov, Doklady Akad. Nauk S.S.S.R. **84,** 701 (1952).
[13] H. H. G. Jellinek, J. Polymer Sci. **3,** 850 (1948).
[14] S. L. Madorsky, J. Polymer Sci. **11,** 491 (1953).
[15] E. L. Kropa and J. J. Padbury, U. S. Patent 2,543,530 (February 27, 1951).
[16] H. Staudinger and A. Steinhofer, Ann. Chem. Justus Liebigs **517,** 35 (1935).
[17] B. B. S. T. Boonstra and G. J. van Amerongen, Ind. Eng. Chem. **41,** 161 (1949).
[18] S. Straus and S. L. Madorsky, J. Research NBS **50,** 165 (1953) RP2405.
[19] R. S. Corley, H. C. Haas, M. W. Kane, and D. I. Livingston, J. Polymer Sci. **13,** 137 (1954).
[20] D. I. Livingston (private communication).
[21] M. Szware, J. Chem. Phys. **16,** 128 (1948).
[22] M. Szware, J. Polymer Sci. **6,** 319 (1951).
[23] L. A. Auspos, C. W. Burnam, L. A. R. Hall, J. K. Hubbard, W. Kirk, J. R. Schaefgan, and S. B. Speck, J. Polymer Sci. **15,** 19 (1955).
[24] P. O. Powers and A. E. Austin, J. Polymer Sci. **6,** 575 (1951).
[25] Paul Bradt, V. H. Dibeler, and F. L. Mohler, J. Research NBS **50,** 201 (1953) RP2410.

WASHINGTON, April 28, 1955.

Journal of Research of the National Bureau of Standards Vol. 55, No. 4, October 1955 Research Paper 2625

Infrared Transmittance of Some Calcium Aluminate and Germanate Glasses[1,2]

Jack M. Florence,[3] Francis W. Glaze, and Mason H. Black

The infrared transmittance of some calcium aluminate and germanate glasses has been measured out to 6 microns. The range of compositions of the calcium aluminate glasses was CaO, 26.7 to 52.0 percent, and Al_2O_3, 28.2 to 49.6 percent. Barium oxide, BeO, Bi_2O_3, La_2O_3, MgO, and PbO were added in varying amounts up to a maximum of 36.0 percent for any one constituent. These calcium aluminate glasses are good infrared transmitters, but show a prominent water absorption band at 2.9 to 3.0 microns. This absorption can be decreased somewhat by means of a dry air treatment of the melt. These glasses have a strong tendency toward devitrification.

Germanium oxide is a good glass-former. Its glasses have about the same infrared transmittance as the calcium aluminate glasses in the absence of oxides such as SiO_2 and BeO, which absorb in the 4.5- to 5.5-micron region.

1. Introduction

The study of the transmittance of infrared energy by glass [1, 2, 3][4] at the National Bureau of Standards has resulted in the preparation of glasses departing from the ordinary glass compositions. The common glass-forming oxides are B_2O_3, P_2O_5, and SiO_2. Samples of glasses, 2 mm thick, prepared with B_2O_3 and P_2O_5 transmit very little infrared energy beyond the water absorption band at 2.9 μ. Silica is the best of the ordinary glass-formers as far as the transmittance of infrared energy is concerned. However, silicate glasses in 2-mm thicknesses do not transmit much energy of wavelengths beyond approximately 4.5 μ because of the absorption by Si–O bond at 4.45 μ. Other compounds considered to be glass-formers are GeO_2, Al_2O_3, BeF_2, Sb_2O_3, V_2O_5, and Bi_2O_3. Only those compositions which showed promise of being able to produce glass blanks of appreciable size, and which could be melted in platimun, were investigated. They contained $CaO+Al_2O_3$, GeO_2, or BeF_2.

Some BeF_2 glasses, similar to those reported by Heyne [4], were prepared free from visible crystallization only by incorporating ammonium acid fluoride in the batch. These glasses were found to be readily attacked by water, as reported by Heyne, hence were given no further consideration.

GeO_2 glasses are interesting, but, unfortunately, the cost of germanium is high and the material is in great demand in the electronics field. However, a limited number of compositions were studied.

The glass-forming ability of Al_2O_3 has been in controversy since the beginning of the century. The earliest reported aluminate glass was by Shepherd, Rankin, and Wright [5], from the study of the $MgO–CaO–Al_2O_3$ system. Bussem and Eitel [6] found that the composition 52.2 percent Al_2O_3 and 47.8 percent CaO could be quenched to glass. Stevels [7] and Safford and Silverman [8] regard it as improbable that such a glass could be formed. Further phase-equilibria studies of the calcium aluminates with a third component have indicated the ability of aluminum atoms to assume the fourfold coordination said to be necessary for glass formation [9]. Sun [9, 10] has published and patented a series of aluminate and beryllo-aluminate glasses. Sun [11, 12] and Stanworth [12, 13] published a series of notes on the aluminate glasses. Weyl [14] states that "Al_2O_3 can play the role of glass-forming oxide only in combination with CaO, the only example of a pure aluminate glass being the vitreous calcium aluminate."

2. Preparation of the Glasses

The procedure for the preparation of the glasses and for the transmittance measurements has been given in previous publications [1, 2]. During the fining of several of the glasses, dry air was introduced into the bottom of the melt by means of a platinum tube for 2 hr. This procedure is referred to, for brevity, as the "dry-air treatment" [3]. With some glasses of low viscosity, this treatment is very effective in removing water vapor and possibly other soluble gases.

Both anhydrous and hydrated alumina, as indicated in table 1, were used in the batches as the source of Al_2O_3.

3. Calcium Aluminate Glasses

The base glasses for this phase of the work were the low silica eutectic composition from the $CaO–Al_2O_3–SiO_2$ phase diagram and another glass of very similar composition [15, 16]. Glass C–1458 (fig. 1) is the ternary eutectic composition. The other glass (C–1474, fig. 2) is very similar to one mentioned by Dusing in U. S. Patent No. 2,252,495, covering a series of infrared transmitting glasses. Dusing reports that a glass of composition, SiO_2, 6.9 percent, CaO, 49.7 percent, and Al_2O_3, 43.4 percent, transmits infrared energy beyond 6 μ for a sample 1

[1] Presented at the Fifty-Seventh Annual Meeting of the American Ceramic Society, Cincinnati, Ohio, April 27, 1955.
[2] This project was supported by the Department of the Navy, Bureau of Ships.
[3] Present address, Kimble Glass Co., Toledo, Ohio.
[4] Figures in brackets indicate the literature references at the end of this paper.

TABLE 1. *Glass compositions*

Figure No.	Glass No.	Composition in weight percent										Remarks
		SiO_2	Al_2O_3	CaO	MgO	GeO_2	BaO	BeO	La_2O_3	PbO	Bi_2O_3	
1 & 22	C–1458	6.8	41.2	52.0	.....	.....	.....	.....	.....	.....	.....	Anhydrous Al_2O_3
2	C–1474	6.8	43.7	49.5	.....	.....	.....	.....	.....	.....	.....	Do.
3	2–51	5.0	41.5	48.5	5.0	.....	.....	.....	.....	.....	.....	Hydrated Al_2O_3
4	C–1540	.....	49.6	45.4	.....	.....	.....	5.0	.....	.....	.....	Hydrated Al_2O_3, dry-air treatment.
5	C–1532	.....	47.0	43.0	.....	.....	10.0	.....	.....	.....	.....	Hydrated Al_2O_3
6	C–1461	.....	41.2	42.0	.....	.....	16.8	.....	.....	.....	.....	Do.
7	C–1479	.....	41.2	42.0	.....	.....	16.8	.....	.....	.....	.....	Anhydrous Al_2O_3
8	C–1528	.....	41.7	38.3	.....	.....	20.0	.....	.....	.....	.....	Do.
9	C–1464	.....	38.7	39.5	.....	.....	21.8	.....	.....	.....	.....	Hydrated Al_2O_3
10	C–1466	.....	38.7	30.0	.....	.....	21.8	.....	9.5	.....	.....	Do.
11	C–1529	.....	36.5	33.5	.....	.....	20.0	10.0	.....	.....	.....	Anhydrous Al_2O_3
12	C–1569	.....	47.0	43.0	.....	.....	5.0	5.0	.....	.....	.....	Hydrated Al_2O_3
13	C–1468	.....	41.2	42.0	.....	.....	6.8	5.0	5.0	.....	.....	Do.
14	C–1478	.....	41.2	42.0	.....	.....	6.8	5.0	5.0	.....	.....	Hydrated Al_2O_3, dry-air treatment.
15	C–1605	.....	37.2	34.2	.....	.....	14.3	9.5	.....	4.8	.....	Hydrated Al_2O_3
16	C–1624	.....	34.0	31.2	.....	.....	13.1	8.7	.....	13.0	.....	Do.
17	C–1668	.....	39.1	30.9	.....	.....	15.0	10.0	.....	.....	5.0	Do.
18	C–1661	.....	31.3	28.7	.....	.....	12.0	8.0	.....	.....	20.0	Do.
19	C–1660	.....	31.3	28.7	.....	.....	12.0	8.0	.....	.....	20.0	Hydrated Al_2O_3, dry-air treatment.
20	C–1654	.....	28.9	26.7	.....	.....	11.1	7.4	.....	.....	25.9	Hydrated Al_2O_3
10	C–1442	.....	28.2	35.6	.....	.....	.....	.....	.....	.....	36.2	Do.
21	C–1284	30.0	.....	.....	.....	.....	.....	.....	.....	70.0	.....	Dry-air treatment
21	C–1526	.....	.....	.....	.....	42.7	.....	.....	.....	57.3	.....	Do.
22	C–1434	.....	39.2	49.5	.....	11.3	.....	.....	.....	.....	.....	
23	C–1534	.....	.....	.....	.....	53.7	37.2	1.4	.....	7.7	.....	Do.
23	C–1223	40.0	.....	.....	.....	.....	48.2	1.8	.....	10.0	.....	

mm thick. The batch compositions of glasses C–1458 and C–1474, as well as those for the other glasses reported in the paper, are given in table 1.

The main difficulty, in the preparation of this family of glasses, is their high melting temperature and their tendency toward devitrification when poured in thick slabs. The melting temperature required is about 1,550° C, measured by means of an optical pyrometer sighted on the surface of the glass. They also show appreciable color, amber to brown, which does not seem to affect their infrared transmittance. This color is probably due to platinum dissolved from the crucibles in which they were melted.

Glasses C–1458 and C–1474, with a silica content of 6.8 percent, have some transmittance out to 6 μ in 2-mm thicknesses. Previously reported glasses with higher silica content cut off between 5.0 and 5.5 μ [2]. A reduction in silica content also materially increased the transmittance of the glass beyond 3.25 μ [3]. Figure 3 shows the transmittance curve for a low silica eutectic glass, reported by McMurdie and Insley [17], melt 2–51.[5]

The substitution of other oxides for silica was tried, leaving only the CaO–Al_2O_3 group as the glass-former. One in which BeO was substituted for silica gave a glass of satisfactory quality, free from crystallization. This was glass C–1540, the transmittance curve of which is shown in figure 4. This glass shows improved transmittance between 2.8 to 3.8 μ, but decreased transmittance from 3.8 to 5+ μ, in comparison with the CaO–Al_2O_3–SiO_2 glasses. This glass was given the dry-air treatment.

[5] In the discussion of the individual glasses, the original melt numbers are used. Consequently, the order has been jumbled to obtain a proper continuity in this paper.

In the CaO–Al_2O_3–BaO system, glasses were formed in a wide range of composition: CaO, 38 to 42 percent; Al_2O_3, 39 to 47 percent; BaO, 10 to 22 percent. The best glass, as far as ease of production is concerned, is C–1532 (fig. 5), with C–1461 (fig. 6) a close second. To determine the effect of H_2O in the batch materials, glasses C–1479 and C–1528 (figs. 7 and 8) were made with anhydrous aluminum oxide as the source of alumina; glasses C–1461 and C–1464 (figs. 6 and 9) were made with hydrated alumina. Those made with hydrated alumina show a slightly more prominent absorption band at 2.9 to 3.0 μ than those made with anhydrous alumina.

Glass C–1466 (fig. 10) is of the same composition as glass C–1464 (fig. 9), with the exception of 9.5 percent of La_2O_3 in place of CaO. This substitution had practically no effect on the transmittance.

A comparison of figures 5 to 9 shows that the substitution of BaO for CaO and Al_2O_3 has no effect on the infrared transmittance of the glasses. However, comparison of figure 8 with 11 shows that the substitution of BeO for CaO and Al_2O_3 substantially decreases the transmittance beyond 4.5 μ, acting similarly to SiO_2 in this respect, a fact also indicated by figure 12. It also seems to increase the transmittance at 2.9 to 3.0 μ, but less effectively than the dry-air treatment.

Modification of some glasses prepared by Sun [6] gave a five-component glass CaO–Al_2O_3–BaO–BeO–La_2O_3 that could be prepared without too much difficulty. Glass C–1468 (fig. 13) was prepared in the usual manner, whereas glass C–1478 (fig. 14) of the same composition was given the dry-air treat-

ment. Both melts were made with hydrated alumina. Glass C–1478 shows superior transmittance between 2.8 and 4.75 μ. Note in figure 13 that the decrease in the 2.9- to 3.0-μ absorption due to BeO, observed in figures 11 and 12, does not persist, while the absorption beyond 4.5 μ does persist.

Transmittance curves for glass C–1605, containing 4.8 percent PbO, is shown in figure 15 and for glass C–1624, containing 13.0 percent PbO, in figure 16. The curves for these glasses are quite similar, except that the glass with the larger PbO content shows a slightly more prominent absorption band at 2.9 to 3.0 μ.

In the hope of lowering the melting temperature of the calcium aluminate glasses, four melts containing Al_2O_3, CaO, BaO, BeO, and varying amounts of Bi_2O_3 (figs. 17, 18, 19, and 20) and one containing only Al_2O_3, CaO, and Bi_2O_3 (glass C–1442 in fig. 10) were made. The hope of a low melting temperature was, however, a false one. Examination of figures 17, 18, and 20 shows that the absorption caused by water at 2.9 μ is not affected by the Bi_2O_3 content, while figure 19 shows that the dry-air treatment can materially decrease this absorption. A comparison of figures 17 and 20 shows that increasing the Bi_2O_3 from 5 to 26 percent, with BeO present, does not increase the transmittance beyond 4.5 μ. Nor does the addition of Bi_2O_3 up to 36.2 percent (glass C–1442) have any significant effect on the transmittance in comparison with the barium oxide glass C–1464 in the absence of BeO (figs. 9 and 10). The increased transmittance, beyond 4.5 μ shown in the latter pair of figures, in comparison with figures 11, and 17 to 20, is evidently due to the fact that BeO is absent.

It seems apparent from the representative glasses given in this paper that, although novel compositions for glasses have been found among the calcium aluminates, their application to the transmittance of infrared energy is limited for certain uses because of the high water absorption. This is indicated by the absorption bands at 2.9 and 4.7 μ. However, this difficulty can be somewhat overcome by means of the dry-air treatment.

The usefulness of glass for many applications is often determined, not only by transmittance, but also by other physical properties as well. The unusually high value of Young's modulus for one calcium aluminate composition is reported here since it may be of practical, as well as theoretical, interest. Glass C–1461 has a Young's modulus of 1,052 kilobars (15,230,000 psi) at 20° C. This is in comparison to that for fused silica of 730 kilobars (10,590,000 psi) and for most commercial glasses of 540 to 805 kilobars (7,830,000 to 11,680,000 psi) [18]. In table 2, the values for Young's and shear moduli and Poisson's ratio for this glass are given for various temperatures from 20° to 750° C.

Coefficients of expansion of five calcium aluminate glasses (C–1461, C–1468, C–1529, C–1532, and C–1654) varied from 9.0×10^{-6} to 11.1×10^{-6}/° C, with C–1654 giving the lowest and C–1461 the highest value. The deformation points[6] of these same glasses varied from 671° to 835° C, with C–1529 having the lowest, and C–1532 the highest, value.

TABLE 2. *Young's and shear moduli and Poisson's ratio versus temperature for calcium aluminate glass C–1,461*

Temperature	Young's modulus (E)	Shear modulus (G)	Poisson's ratio
°C	*Kilobars*	*Kilobars*	
20	1052	408.0	0.289
65	1045	405.9	.287
110	1041	403.9	.289
210	1028	397.6	.293
300	1017	393.5	.292
410	999.5	387.1	.291
500	989.1	382.8	.292
600	974.7	376.7	.294
700	956.0	368.8	.296
730	952.4	366.5	.299
750	934.0	359.8	.298

4. Germanate Glasses

The great advantage of the dry-air treatment to glasses has been shown in a previous paper [3]. Figure 21 compares the transmittance of a lead silicate glass C–1284 with that for the molar equivalent lead germanate glass C–1526. Both were given the dry-air treatment.[7] Had glass C–1284 not been given the dry-air treatment, its transmittance at 2.9 to 3.0 μ would only have been 30 to 40 percent [3]. Out to 3.6 μ, the silicate glass C–1284 has the higher transmittance; beyond 3.6 μ the germanate glass C–1526 has the superior transmittance. The lower transmittance of the germanate glass below 3.6 μ is probably due to its higher index of refraction, hence higher reflectance. Also, the range of transparency in the infrared is increased about 1.2 μ in the case of the germanate glass, in line with the respective vibration frequencies: for Si–O, 1,242.03 cm^{-1} (8.05 μ); and for Ge–O, 985.7 cm^{-1} (10.15 μ) [19].

Glass C–1,434 (fig. 22) is the $CaO–Al_2O_3–GeO_2$ glass equivalent, in mole percent, to $CaO–Al_2O_3–SiO_2$ glass C–1458 (fig. 1). In this case, the silicate glass C–1434 has slightly higher transmittance out to 4.6 μ. Beyond 4.6 μ, the germanate glass C–1,434 is definitely the better.

In figure 23, glass C–1534, a $BaO–PbO–BeO–GeO_2$ glass, is compared in transmittance with molar equivalent $BaO–PbO–BeO–SiO_2$ glass C–1223. Although glass C–1534 was given the dry-air treatment and glass C–1223 was not, the latter is the better

[6] "The temperature observed during the measurement of expansivity by the interferometer method at which viscous flow exactly counteracts thermal expansion. The deformation point generally corresponds to a viscosity in the range from 10^{11} to 10^{12} poises". Terms relating to glass and glass products, ASTM Designation: C–162–49 T.

[7] About 6 years ago we made 30 double-convex lenses of glass C–1284, 4½ in. in diameter and 1 in. thick at the center, for the Department of the Navy, Bureau of Aeronautics. As far as we know, they are still giving satisfaction, which speaks well for the permanence of the effect of the dry-air treatment.

transmitter out to 4.1 μ. Glass C–1534 does not have as good transmittance beyond 2.8 μ as glass C–1526, which contains only PbO and GeO_2.

5. Summary

Calcium aluminate glasses should find wide use for infrared transmission in applications where their prominent water absorption band at 2.9 to 3.0 μ is not detrimental. Where it is detrimental, its magnitude can be decreased somewhat by means of the dry-air treatment. One of the calcium aluminate glasses had a very high Young's modulus—1,052 kilobars or 15,230,000 psi, and it may find special applications for this reason. It has been found that BeO has a detrimental effect on the transmittance of calcium aluminate glasses beyond 4.5 μ.

The dry-air treatment of a lead germanate glass melt produced one of the best oxide glasses for the transmittance of infrared energy to come to our attention, especially for wavelengths beyond 3.6 μ. However, the high cost and short supply of GeO_2 will limit application of germanate glasses.

To our present knowledge, the transmittance of oxide glasses for infrared energy seems limited to about 6 μ for 2-mm thicknesses. Since it has been found that the use of higher atomic weight elements in general extends the region of infrared transmittance, the best possibility of increasing this region is by replacing oxygen by heavier elements such as sulfur, selenium, etc.

The authors are indebted to Marshall Anderson and Nicolo Acquista, of the Radiometry Section, for supplying the data on the transmittance of these glasses.

6. References

[1] J. M. Florence, F. W. Glaze, C. H. Hahner, and R. Stair, Transmittance of near-infrared energy by binary glasses, J. Am. Ceramic Soc. **30**, 328 (1948); J. Research NBS **41**, 623 (1948) RP1945.

[2] J. M. Florence, C. C. Allshouse, F. W. Glaze, and C. H. Hahner, The absorption of near-infrared energy by certain glasses, J. Research NBS **45**, 121 (1950) RP2118.

[3] J. M. Florence, F. W. Glaze, and M. H. Black, Transmission of near-infrared energy by some two- and three-component glasses, J. Research NBS **50**, 187 (1953) RP2408.

[4] G. Heyne, The preparation and properties of some beryllium flouride glasses, Angew, Chem. **46**, 473 (1933).

[5] E. S. Shepherd, G. A. Rankin, and F. E. Wright, The binary systems of alumina with silica, lime, and magnesia, Am. J. Sci. [4] **28**, 293 (1909).

[6] W. Büssem and A. Eitel, The structure of pentacalcium trialuminate, Z. Krist. **95**, 175 (1936).

[7] J. M. Stevels, The physical properties of glass in relation to its structure, J. Soc. Glass Tech. **30**, 31 T (1946).

[8] Hurd W. Safford and Alexander Silverman, Alumina-silica relationship in glass, J. Am. Ceramic Soc. **30**, 203 (1947).

[9] K. Sun, Glass-forming substances, Glass Ind. **27**, 552 (1946).

[10] K. Sun, Aluminate glasses, Glass Ind. **30**, 199 (1949).

[11] K. Sun, A note on aluminate glass, Glass Ind. **32**, 82 (1951).

[12] J. E. Stanworth, K. Sun, More about aluminate glasses, Glass Ind. **32**, 296 (1951).

[13] J. E. Stanworth, On the structure of glass, J. Soc. Glass Tech. **32**, 154 T (1948).

[14] W. A. Weyl, Coloured glasses, J. Soc. Glass Tech. **27**, 133 (1943).

[15] G. A. Rankin and F. E. Wright, The ternary system: $CaO–Al_2O_3–SiO_2$, Am. J. Sci. [4] **39**, 52 (1915).

[16] J. W. Greig, Immiscibility of silicate melts, Am. J. Sci. [5] **13**, 41 (1927).

[17] H. F. McMurdie and H. Insley, Studies on the quaternary system $CaO–MgO–2CaO.SiO_2–5CaO.3Al_2O_3$, J. Research NBS **16**, 467 (1936) RP884.

[18] Sam Spinner, Elastic moduli of glasses by a dynamic method, J. Am. Ceramic Soc. **37**, 229 (1954).

[19] Gerhard Herzberg, Molecular spectra and molecular structure I. Spectra of diatomic molecules, 2nd ed., table 39 (D. Van Nostrand Co., Inc., New York, N. Y., 1951).

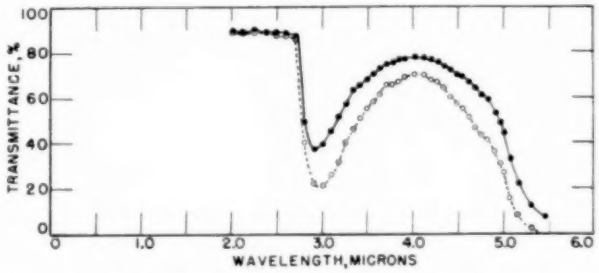

FIGURE 1. *Infrared transmittances of* $CaO–Al_2O_3–SiO_2$ *glass C–1,458.*

●, T = 2.18 mm; ○, T = 4.10 mm.

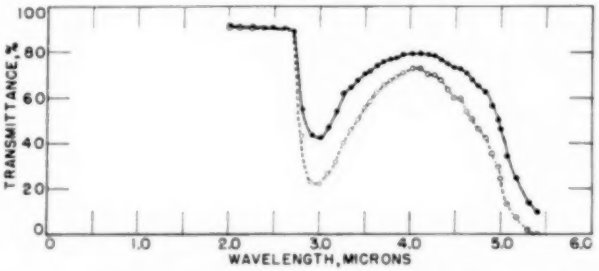

FIGURE 2. *Infrared transmittances of* $CaO–Al_2O_3–SiO_2$ *glass C–1,474.*

●, T = 2.02 mm; ○, T = 4.16 mm.

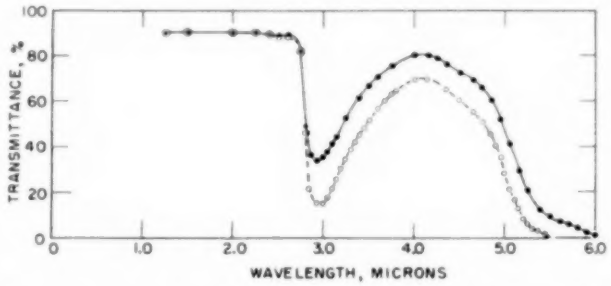

FIGURE 3. *Infrared transmittances of* $CaO–Al_2O_3–MgO–SiO_2$ *glass 2–51.*

● T = 2.00 mm; ○, T = 3.96 mm.

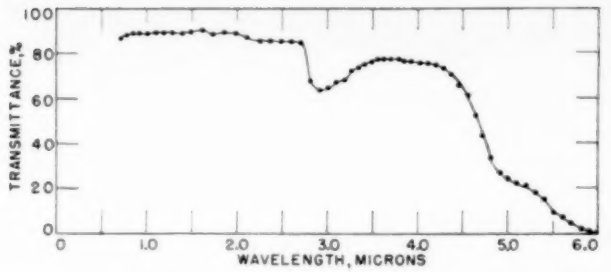

FIGURE 4. *Infrared transmittances of* $CaO–Al_2O_3–BeO$ *glass C–1,540.*

This glass was given the dry-air treatment.
T = 2.02 mm.

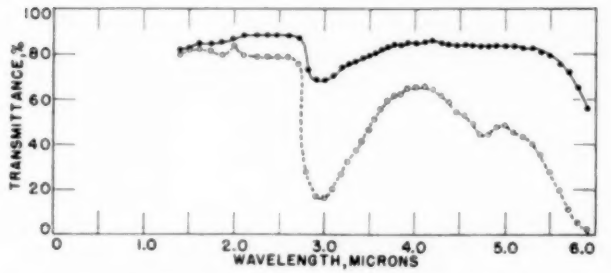

FIGURE 5. *Infrared transmittances of* $CaO–Al_2O_3–BaO$ *glass C–1,532.*

●, T = 0.39 mm; ○, T = 3.56 mm.

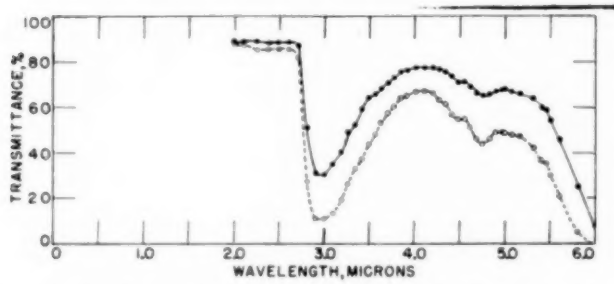

FIGURE 6. *Infrared transmittances of* $CaO–Al_2O_3–BaO$ *glass C–1,461 (hydrated* Al_2O_3*).*

●, T = 1.72 mm; ○, T = 3.50 mm.

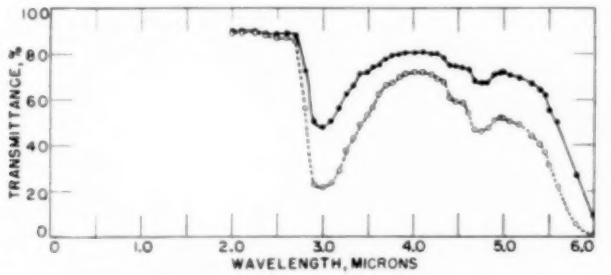

FIGURE 7. *Infrared transmittances of* $CaO–Al_2O_3–BaO$ *glass C–1,479 (anhydrous* Al_2O_3*).*

●, T = 1.71 mm; ○, T = 3.99 mm.

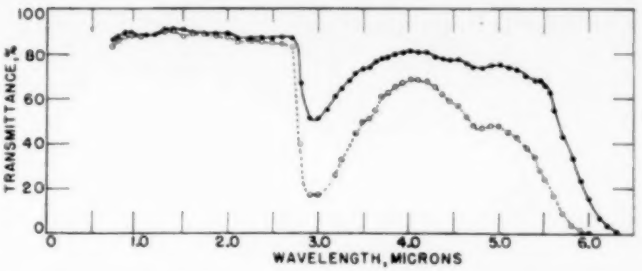

FIGURE 8. *Infrared transmittances of* $CaO–Al_2O_3–BaO$ *glass C–1,528.*

●, T = 1.11 mm; ○, T = 3.81 mm.

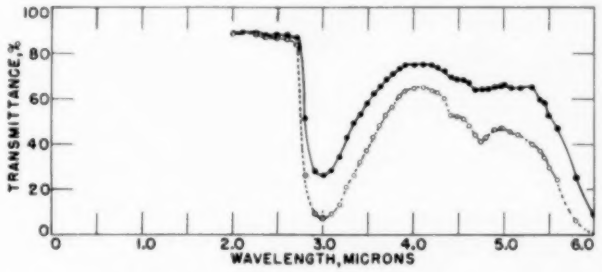

FIGURE 9. *Infrared transmittances of* $CaO–Al_2O_3–BaO$ *glass C–1,464.*

●, T = 1.78 mm; ○, T = 3.81 mm.

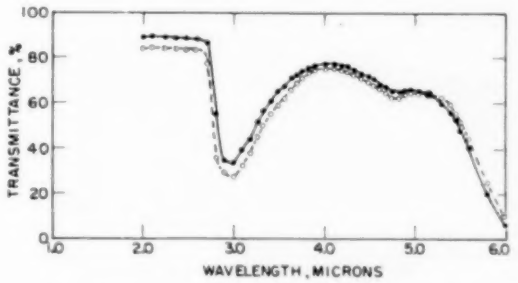

FIGURE 10. *Infrared transmittances of* $CaO–Al_2O_3–BaO–La_2O_3$ *glass C–1,466 and* $CaO–Al_2O_3–Bi_2O_3$ *glass C–1442.*

●, Glass C-1,466, T = 1.98 mm; ○, Glass C-1,442, T = 1.82 mm.

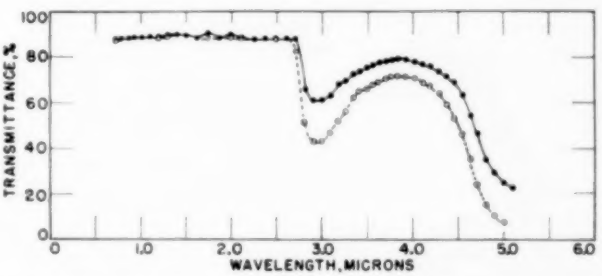

FIGURE 11. *Infrared transmittances of* $CaO–Al_2O_3–BaO–BeO$ *glass C–1,529.*

●, T = 1.07 mm; ○, T = 2.04 mm.

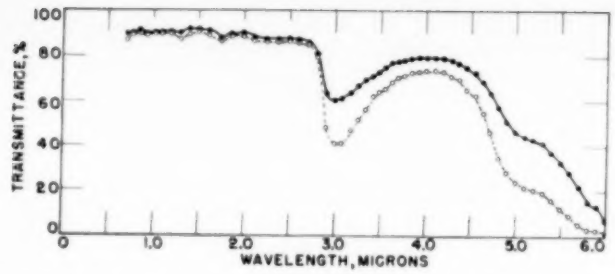

FIGURE 12. *Infrared transmittances of* $CaO–Al_2O_3–BaO–BeO$ *glass C–1,569.*

●, T = 0.95 mm; ○, T = 1.96 mm.

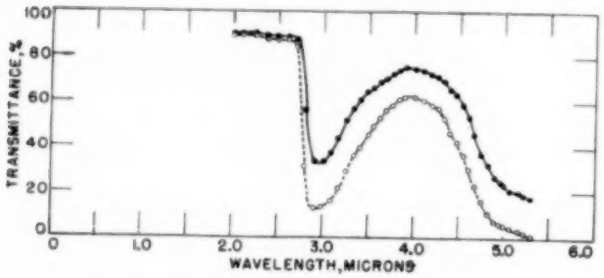

FIGURE 13. *Infrared transmittances of* $CaO–Al_2O_3–BaO–BeO–La_2O_3$ *glass C–1,468.*

●, T = 2.04 mm; ○, T = 4.16 mm.

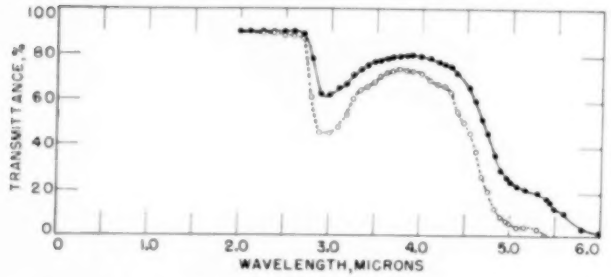

FIGURE 14. *Infrared transmittances of glass C–1,478 (glass C–1,468 given the dry-air treatment).*

●, T = 2.05 mm; ○, T = 4.16 mm.

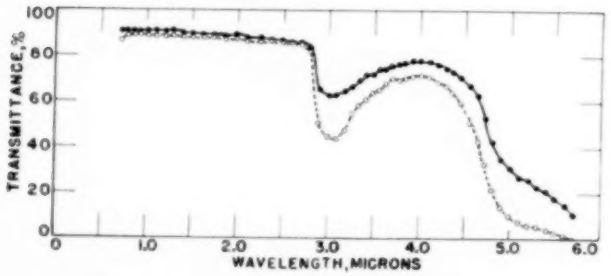

FIGURE 15. *Infrared transmittances of* $CaO–Al_2O_3–BaO–BeO–PbO$ *glass C–1,605*

●, T = 0.97 mm; ○, T = 1.98 mm.

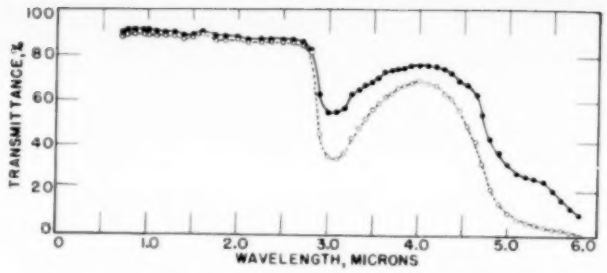

FIGURE 16. *Infrared transmittances of* $CaO–Al_2O_3–BaO–BeO–PbO$ *glass C–1,624.*

●, T = 0.91 mm; ○, T = 1.97 mm.

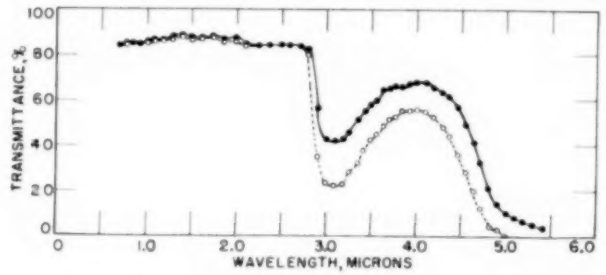

FIGURE 17. *Infrared transmittances of* $CaO–Al_2O_3–BaO–BeO–Bi_2O_3$ *glass C–1,668.*

●, T = 1.96 mm; ○, T = 3.98 mm.

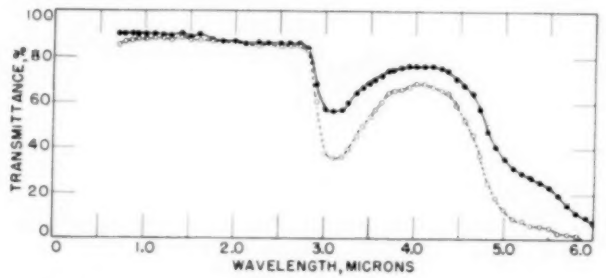

FIGURE 18. *Infrared transmittances of* $CaO–Al_2O_3–BaO–BeO–Bi_2O_3$ *glass C–1,661.*

●, T = 0.90 mm; ○, T = 1.97 mm.

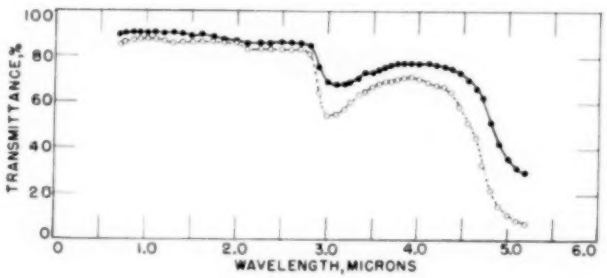

FIGURE 19. *Infrared transmittances of glass C–1,660 (glass C–1,661 given the dry-air treatment).*

●, T = 0.90 mm; ○, T = 2.01 mm.

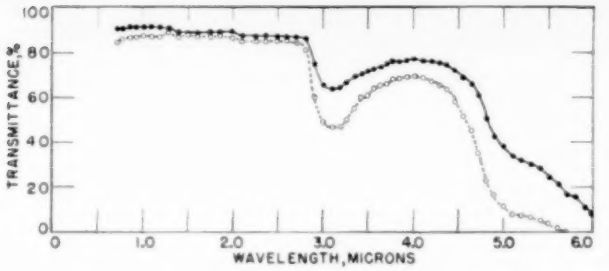

FIGURE 20. *Infrared transmittances of* $CaO–Al_2O_3–BaO–BeO–Bi_2O_3$ *glass C–1,654.*

●, T = 0.88 mm; ○, T = 2.02 mm.

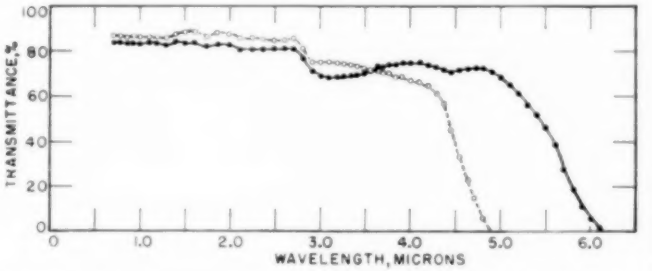

FIGURE 21. *Infrared transmittances of* $PbO–SiO_2$ *glass C–1,284 and the equivalent* $PbO–GeO_2$ *glass C–1,526, both given the dry-air treatment.*

●, Glass C–1,526, T = 2.07 mm; ○, Glass C–1,284, T = 1.90 mm.

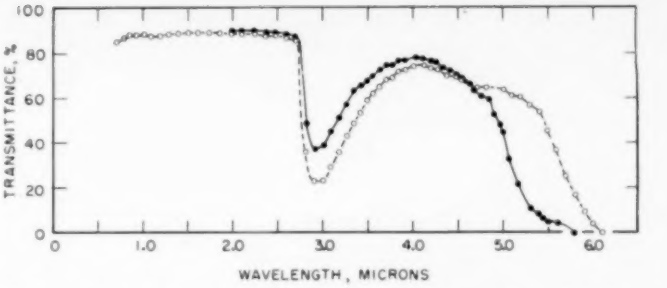

FIGURE 22. *Infrared transmittances of* $CaO–Al_2O_3–SiO_2$ *glass C–1,458 and the equivalent* $CaO–Al_2O_3–GeO_2$ *glass C–1,434.*

○, Glass C–1,458, T = 2.18 mm; ●, Glass C–1,434, T = 2.00 mm.

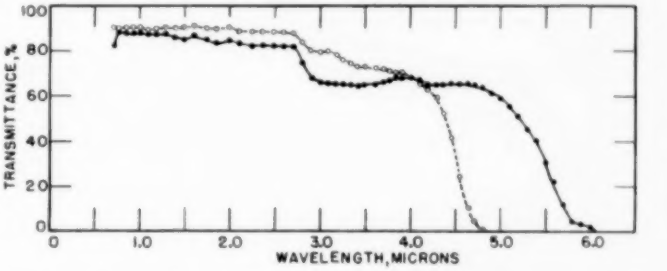

FIGURE 23. *Infrared transmittances of* $BaO–PbO–BeO–SiO_2$ *glass C–1,223 and the equivalent* GeO_2 *glass C–1,534, latter with dry-air treatment.*

○, Glass C–1,223, T = 1.96 mm; ●, Glass C–1,534, T = 1.75 mm.

WASHINGTON, June 22, 1955.

U. S. GOVERNMENT PRINTING OFFICE: 1955